Analysis of *Arabidopsis thaliana* glucosinolate profiles in response to a native root fungal endophyte

Inaugural-Dissertation

zur
Erlangung des Doktorgrades
der Mathematisch-Naturwissenschaftlichen Fakultät

der Universität zu Köln

vorgelegt von

Charles Uhlmann

aus Annecy, Frankreich

Köln, 2022

Die vorliegende Arbeit wurde am Max Planck Institut für Pflanzenzüchtungsforschung in Köln in der Abteilung für Pflanze-Mikroben Interaktionen (Direktor: Prof. Dr. Paul Schulze-Lefert), Arbeitsgruppe Prof. Dr. Jane Parker durchgeführt.

The work described in this thesis was conducted under the supervision of Prof. Dr. Jane Parker at the Max Planck Institute for Plant Breeding Research (Department of Plant-microbe interactions, Director: Prof. Dr. P. Schulze-Lefert)

MAX-PLANCK-GESELLSCHAFT

Max Planck Institute for
Plant Breeding Research

Berichterstatter: Prof. Dr. Jane Parker

Prof. Dr. Gunther Doehlemann

Prof. Dr. Meike Burow

Prüfungsvorsitzender: Prof. Dr. Bart Thomma

Tag der Disputation: 27. Februar 2023

Summary

Plants host communities of microbes termed the microbiota, which contributes to plant nutrition and stress relief, notably in roots. With diverse microbiota fungi, plants can accept invasive hyphal growth inside their cells. Which immune signaling pathways regulate colonization of root tissues and cells by fungal endophytes is unclear. However, at the metabolite level, Tryptophan (Trp)-derived compounds, including indolic-glucosinolates (GLS), prevent excessive fungal endophyte growth and associated harm in roots of *Arabidopsis thaliana* (Arabidopsis). This PhD thesis aims to provide i) knowledge on immune pathways relevant to general fungal colonization and ii) insights into the regulation of aliphatic- and indolic-GLS by phosphate (Pi). In the first chapter, I explored whether the broad host range Sebacinales fungi showed enhanced or reduced growth in roots of diverse established Arabidopsis immunity mutants but detected no differences compared to wild-type Col-0 plants. In the second chapter, I investigated whether the Phosphate Starvation Response (PSR) system modulates aliphatic- and indolic-GLS accumulation as important immune metabolic outputs. As fungal endophyte test organism, I selected a strain of *Truncatella angustata* (F73) isolated from Arabidopsis roots in nature and known to relieve long-term Pi limitation stress in an agar-based system. Using confocal microscopy, I determined that the root differentiation zone is more permissive to rapid F73 intracellular colonization, compared to the root apical meristem or the elongation zone. A fluorescent transcriptional reporter of the Trp-derived metabolites pathway showed increased signal width in the differentiation zone upon F73 inoculation, suggesting Arabidopsis responds to fungal colonization by spatially expanding Trp-derived metabolite production. I then performed time course RNA-seq and GLS quantification experiments to reveal how Pi and immune signaling are integrated at the transcriptional and metabolomics levels. Pi availability did not impact GLS-related gene expression but governed the number of F73-responsive genes in Col-0 in a temporal manner, suggesting that the PSR regulates general immune dynamics. Yet, amounts of long chained aliphatic-GLS in roots and shoots were constitutively higher at low Pi. Furthermore, F73 induced greater accumulation of most GLS at high Pi, hinting at PSR-dependent modulation of GLS synthesis. F73 displayed hallmarks of increased growth rate and virulence at a transcriptional level, but not deleterious infection, in the *cyp79b2/b3* mutant depleted in Trp-derived metabolites. Altogether, my work provides spatio-temporal insights into how Pi stress influences interactions with fungi and suggests that the PSR fine-tunes aliphatic- and indolic-GLS accumulation. This hypothesis warrants further exploration using PSR mutants.

Zusammenfassung

Pflanzen beherbergen Gemeinschaften von Mikroben, die so genannte Mikrobiota, die zur Ernährung der Pflanzen und zum Stressabbau beitragen, insbesondere in den Wurzeln. Verschiedene Pflanzen-assoziierte Pilze können Pflanzenzellen invasiv mit ihren Hyphen besiedeln. Welche Immunsignalwege die Besiedlung von Wurzelgeweben und -zellen durch Pilzendophyten regulieren, ist unklar. Auf der Metabolitebene, verhindern Tryptophan (Trp)-abgeleitete Verbindungen, darunter Indol-Glucosinolate (GLS), ein übermäßiges Wachstum von Pilz-Endophyten und damit verbundene Schäden in den Wurzeln von Arabidopsis thaliana (Arabidopsis). Ziel dieser Dissertation ist es, i) Erkenntnisse über Immunsignalwege zu gewinnen, die für die Pilzbesiedlung relevant sind, und ii) Einblicke in die Regulierung von aliphatischen und indolischen GLS zu gewinnen. Ich untersuchte, ob Pilze der Ordnung Sebacinales, welche durch ein breites Wirtsspektrum gekennzeichnet sind, in den Wurzeln verschiedener etablierter Arabidopsis-Immunitätsmutanten ein verstärktes oder reduziertes Wachstum zeigten, konnte jedoch keine Unterschiede im Vergleich zu Wildtyp-Pflanzen des Ecotyps Col-0 feststellen. Anschließend untersuchte ich, ob das Phosphatmangel-Reaktions (PSR) System des Wirtes die Akkumulation von aliphatischen und indolischen GLS als wichtige immunologische Stoffwechselprodukte moduliert. Als Pilz-Endophyt-Testorganismus wählte ich einen Stamm von Truncatella angustata (F73), der in der Natur aus Arabidopsis-Wurzeln isoliert wurde und dafür bekannt ist, dass er in einem agarbasierten System langfristigen Phosphat-(Pi)-Limitierungsstress beseitigt. Mit Hilfe der konfokalen Mikroskopie habe ich festgestellt, dass die Wurzeldifferenzierungszone für eine schnelle intrazelluläre Besiedlung durch F73 durchlässiger ist als das Wurzelapikalmeristem oder die Streckungszone. Als nächstes zeigte ein fluoreszierender Transkriptionsreporter des Trp-Stoffwechselwegs eine erhöhte Signalbreite in der Differenzierungszone bei F73-Inokulation, was darauf hindeutet, dass Arabidopsis auf die Pilzbesiedlung mit einer räumlichen Ausweitung der Produktion von Trp-Stoffwechselprodukten reagiert. Anschließend führte ich Zeitverlaufs-RNA-seq- und GLS-Quantifizierungsexperimente durch, um herauszufinden, wie Pi und die Immunsignalisierung auf der Transkriptions- und Metabolomebene integriert sind. Die Pi-Verfügbarkeit wirkte sich nicht auf die GLS-bezogene Genexpression aus, steuerte aber die Anzahl der auf F73 reagierenden Gene in Col-0 in zeitlicher Abhängigkeit, was darauf hindeutet, dass die PSR die allgemeine Immundynamik reguliert. Die GLS-Quantifizierung zeigte dennoch, dass die Mengen an langkettigen aliphatischen GLS in Wurzeln und Sprossen bei niedrigem Pi

konstitutiv höher waren. Darüber hinaus induzierte F73 eine stärkere Akkumulation der meisten GLS bei hohem Pi, was auf eine PSR-abhängige Modulation der GLS-Synthese hindeutet. F73 zeigte in der cyp79b2/b3-Mutante, welche durch eine gestörte Produktion von Trp-abgeleiteten Metaboliten charakterisiert ist, Merkmale einer erhöhten Wachstumsrate und Virulenz auf transkriptioneller Ebene, aber keine schädliche Infektion des Wirtes. Insgesamt bietet meine Arbeit räumlich-zeitliche Einblicke in die Art und Weise, wie Pi-Stress die pflanzliche Interaktionen mit Pilzen beeinflusst, und legt nahe, dass die PSR die Akkumulation aliphatischer und indolischer GLS moduliert. Diese Hypothese sollte mit Hilfe von PSR-Mutanten weiter erforscht werden.

Table of Contents

Acknowledgments

I would like to thank first and foremost Prof. Dr. Jane E. Parker and Prof. Dr. Alga Zuccaro for having recruited me to work in the DECRyPT consortium, funded by the Deutsche Forschungsgemeinschaft. Over the years, I had the opportunity to see that I can learn a lot of skills and also develop critical thinking — both of these things are priceless — thank you Alga and Jane for that.

I would like to thank Prof. Dr. Gunther Doehlemann for support and for being a member of my Thesis Advisory Committee. Thank you Dr. Tonni Grube Andersen for giving a new direction to my PhD and for teaching me microscopy. I am also grateful to have been able to benefit from metabolite quantification facilities of Prof. Dr. Meike Burow, without which this thesis would not have the depth it has.

I want to thank all the members of my group over the years for their patience, the nice working atmosphere and group gatherings. Thanks again Jane, for selecting great people to assemble the JP group. Special thanks go to Dr. Anthony Piro and Dr. Dmitry Lapin for "hands-on" supervision and answering my questions in the lab. The award of the most appreciated genius goes to Noah Kürtös, for the design and manufacture of 3D-printed 12-well plates strainers that facilitated tremendously the staining of plant material for microscopy. While we are on that topic, thanks a lot to Ton Timmers that came up with the solution to image very fragile tissues (see methods!). Thanks also to Fantin Mesny for performing the fungal RNA-seq analysis part (see results!) 1 month before submission. Distinguished recognition goes out to the right honourable gentleman Eddie Francis Trew Seabrook for having rightly noted that it makes no bloody sense to pronounce "fungi" fʌnd͡ʒaɪ when one pronounces "fungus" fʌŋ.ɡəs rather than fʌŋʒəs. Therefore, let us be consistent and pronounce fʌŋ.ɡaɪ.

I am particularly grateful to have been able to do my PhD in the Max Planck Institute for Plant Breeding research, in which the scientific staff benefits from numerous and significant yet often hidden or not recognized advantages such as: media and autoclave kitchen staff, greenhouse staff, technical services, IT department and administration. I was also very pleased to have been able to regularly attend the Wednesday-seminars given by excellent scientists. Most notably, my PhD experience at the MPI benefited critically from the care and attention of Dr. Stephan Wagner, as Graduate School coordinator, without which I would probably not have been able to finish this thesis.

Many scientists start a PhD with such passion that the scientific work encroaches on personal life; we can see this repeatedly. Therefore, at least in my case, the PhD time results in

many lessons that are not about science. I thank as honestly as I can M.G. for space, time and an infectious patience. My gratitude goes to Tanja Düttra, my yoga teacher, who taught me to "relax" while in twisted positions (literally) — which is quite the analogy about trying to do a PhD on a background of pandemic, nascent World War III and catastrophic global climate disruption. Sincerely, I thank R.D. for heart-breaking comfort and for an unrivalled blend of warmth, humour and honesty. Thanks also to Terence McKenna, for your eloquence and for preaching what you called "the redemption of the human spirit". And of course, I am grateful to *Pc* and *Cp* for a glimpse of iridescence.

Last but not least, I thank my friends: Joram, Annabel, Lucas, Anniek, Milena, Jana, Felix, Noah, Blanca, Nora, Nela, Alessandro, Rinat, Robert, Eddie, María, Rigel, Jozefien, Marco and Camille. Without all of you, especially Alessandro, Nora, Nela and Camille, I would not be so strong. You inspire me every day to be better, not because you suck (you do, a bit, like me), but because without you, all of this would not have been worth it.

"Nature loves courage. You make the commitment and nature will respond to that commitment by removing impossible obstacles. Dream the impossible dream and the world will not grind you under, it will lift you up. This is the trick. This is what all these teachers and philosophers who really counted, who really touched the alchemical gold, this is what they understood. This is the shamanic dance in the waterfall. This is how magic is done. By hurling yourself into the abyss and discovering it's a feather bed."

Terence McKenna

Abbreviations

2PE	2-phenylethyl
3BZO	3-benzoyloxylpropyl
3OHP	3-hydroxypropyl
3MTP	3-methylthiopropyl
3MSP	3-methylsulfinylpropyl
4-OH-ICN	4-hydroxyindole-3-carbonyl nitrile
4BZO	4-benzoyloxylpropyl
4MOI3M	4-hydroxy-3-indolylmethyl
4OHB	4-hydroxypropyl
4MTB	4-methylbutyl
4MSB	4-methylsulfinylbutyl
5MSP	5-methylsulfinylpentyl
7MTH	7-methylthioheptyl
7MSH	7-methylsulfinylheptyl
8MTO	8-methylthiooctyl
8MSO	8-methylsulfinyloctyl
ALMT1	*ALUMINIUM ACTIVATE MALATE TRANSPORTER 1*
AM	Arbuscular mycorrhizal
ANOVA	Analysis of Variance
AOC2	*ALLENE OXIDE CYCLASE 2*
Arabidopsis	*Arabidopsis thaliana*
BAK1	*BRI ASSOCIATED KINASE 1*
BKK1	*BAK1-LIKE KINASE1*
CAZymes	Carbohydrate active enzymes
CCaMK	*CALCIUM AND CALMODULIN DEPENDENT KINASE 1*
CERK1	*CHITIN ELICTOR RECEPTOR KINASE 1*
COI1	*CORONATINE INSENSITIVE 1*
CYP	*CYTOCHROME P450*
DAMP	Danger associated molecular pattern
dde2	*DELAYED DEHISCENCE 2*
DMI1	*DOES NOT MAKE INFECTIONS 1*
DNA	Desoxyribonucleic acid

dpi	days post inoculation
DEG	Differentially expressed genes
DZ	Differentiation zone
EIN2	*ETHYLENE INSENSITIVE 2*
et al.	et alia
ETI	Effector triggered immunity
ETH	Ethylene
EZ	Elongation zone
F134	*Neonectria radicicola*
F34	*Paraphoma chrysanthemicola*
F73	*Truncatella angustata*
flg22	Flagellin
FOX1	*FAD-LINKED OXIDOREDUCTASE*
g	gram
GLS	Glucosinolates
GTR	*GLUCOSINOLATE TRANSPORTER*
IPS1	*INDUCED BY PHOSPHATE STARVATION 1*
IGMT	*INDOLE GLUCOSINOLATE O-METHYLTRANSFERASE*
JA	Jasmonic Acid
JAZ	*JASMONATE ZIM DOMAIN*
l	liter
LCOs	Lipochitooligosaccharide
MAMP	Microbe associated molecular pattern
mg	milligram
ml	milliliter
MPIPZ	Max Planck Institut für Pflanzenzüchtungsforschung
MS	Murashige & Skoog
NLR	nucleotide-binding/leucine-rich-repeats receptors
NMOI3M	N-hydroxy-3-indolylmethyl
NmrA	*NITROGEN METABOLITE REPRESSION*
NPR1	*NON-EXPRESSOR OF PR PROTEINS*
pad/PAD	*PHYTOALEXIN DEFICIENT*
PCA	Principal Component Analysis
PCR	Polymerase Chain reaction

PERMANOVA	Analysis of variance by permutations
PHO1&2	*PHOSPHATE1&2*
PHT	*PHOSPHATE TRANSPORTER*
PHF	*PHOSPHATE TRANSPORTER TRAFFIC FACILITATOR*
Pi	Inorganic Phosphate
PNM	Plant Nutrition Media
PR	*PATHOGENESIS RELATED*
PRR	Pattern recognition receptor
PSR	Phosphate starvation response
PTI	Pattern triggered immunity
qRT-PCR	Quantitative real time PCR
RAM	Root apical meristem
RNA	Ribonucleic acid
RNA-seq	Ribonucleic acid sequencing
SA	Salicylic acid
STOP1	*SENSITIVE TO PROTON TOXICITY1*
Si	*Serendipita indica*
sid2	*SALICYLIC ACID INDUCTION DEFICIENT 2*
SPX	*SYG1/Pho81/XPR1*
Sv	*Serendipita vermifera*
Trp	Tryptophan
TN	TOLL-INTERLEUKIN RECEPTOR NUCLEOTIDE-BINDING
VSP2	*VEGETATIVE STORAGE PROTEIN 2*
WAK	*WALL ASSOCIATED KINASE*
WGA	Wheat Germ Agglutinin
µl	microliter
µM	micromolar
µm	micrometre

Introduction

Land plants emergence on the earth's surface (*i.e.* "terrestrialization") was a formative event that provided the basis for terrestrial ecosystems. Terrestrialization required that plants concomitantly cope with nutrient scarcity and the presence of microbes already established on land (Retallack, 1992; Redecker, 2000; Gan *et al*, 2021). Plants overcame these challenges by evolving new traits, notably symbiotic interactions and an immune system, both in part elaborated from ancestral genes and characteristics (Delaux *et al*, 2015; Nishiyama *et al*, 2018). Plants existing today are usually healthy whilst hosting complex communities of bacteria, fungi and oomycetes, termed the "microbiota" (Hassani *et al*, 2018). However, it is largely unknown how plants recruit specific microbes to assemble the microbiota.

Interactions with some filamentous fungi occupy a particular position within the microbiota due to the capacity of plant tissues and cells to accommodate intracellularly the invasive growth of hyphae (Koh *et al*, 2005; O'Connell & Panstruga, 2006; Lo Presti *et al*, 2015; Bozkurt & Kamoun, 2020; Ivanov *et al*, 2019; Qin *et al*, 2020). Hence, with many fungi, direct plant-hyphae interfaces for nutrient and signal exchanges are formed. Because these interfaces occurred in plant fossils (Krings *et al*, 2007; Remy *et al*, 1994) and now within the modern parasitism-mutualism continuum (Lo Presti *et al*, 2015; Bozkurt & Kamoun, 2020), whether hyphae accommodation is a single and ancient trait or evolved multiple times is a standing mystery.

In contemporary situations, it was repeatedly shown that microbe effects exerted on plant health, including hyphae accommodation, depend on plant nutritional status (Maciá-Vicente *et al*, 2022; Mesny *et al*, 2021; Harbort *et al*, 2020; Yu *et al*, 2021). Specifically, the Phosphate Starvation Response (PSR), a nutrient stress pathway which pre-dates terrestrialization (Rubio *et al*, 2001; Rico-Reséndiz *et al*, 2020), can strongly impact the outcomes of plant-microbe interactions (Hiruma *et al*, 2016; Frerigmann *et al*, 2021; Castrillo *et al*, 2017). However, whether the PSR directly or indirectly influences plant immune pathways is unclear. Investigations into the genetic basis of hyphae accommodation and mapping the PSR control over the immunity-fungi dialogue will deepen our understanding of plant-microbiota homeostasis.

Plant symbiotic and immune signaling

To understand the processes underlying plant-microbiota interactions, including hyphae accommodation or the PSR, it is informative to turn first to the immunity and symbiosis research fields. Historically, these fields were studied separately, immunity mostly in

Arabidopsis thaliana (hereafter Arabidopsis) leaves facing pathogens and beneficial symbioses mostly in legume (*Medicago truncatula* and *Lotus japonicus*) roots. Recently, both fields have undergone their own substantial advancements and immunity-symbiosis intersections are being discovered. This is important because immunity was strictly interpreted as defense but it might serve broader roles in plant-microbe interactions (Liang *et al*, 2013; Feng *et al*, 2019).

Plants evolved diverse immune systems from a common foundation

The activation of plant immunity is the result of microbe sensing. By monitoring their immediate environment using cell surface receptors, plants establish a first layer of microbe perception and signaling. Receptor-like kinases and receptor-like proteins (RLKs/RLPs) are anchored to the plasma membrane and extend an extracellular domain involved in directly binding microbial associated molecular patterns (MAMPs). Therefore, immune RLKs and RLPs are also called pattern recognition receptors (PRRs) and their activation leads to pattern triggered immunity (PTI) (Zhou *et al*, 2019b). For instance, N-acetyl chitooligosaccharides MAMPs derived from chitin present in fungal-cell walls are perceived by the PRR *CHITIN ELICTOR RECEPTOR KINASE 1* (*CERK1*) (Miya *et al*, 2007; Cao *et al*, 2014; Liu *et al*, 2012), a gene co-incident with terrestrialization (Fig. 1) (Nishiyama *et al*, 2018). Damage or injury induce the release of endogenous molecules that trigger PTI, such as the plant peptides Pep1 and 2 perceived by *PEPR1* and *2* (Yamaguchi *et al*, 2010). PTI activation relies on PRR forming heterodimers, of which the ancient common co-receptor *BAK1* (Fig. 1) notably stands out by perceiving Pep1 and 2 and the bacterial MAMPs flg22 (flagellin derived) and elf18 (elongation factor EF-Tu derived) (Schwessinger *et al*, 2011; Roux *et al*, 2011; Yamada *et al*, 2016). However, pathogens can evade or dampen PTI via secretion of extra- or intra-cellular molecules termed "effectors" (Deslandes & Rivas, 2012; Redkar *et al*, 2022a, 2022b).

The second layer of microbe perception relies on the recognition of intra-cellular effectors via nucleotide-binding/leucine-rich-repeats receptors (NLRs) which often culminate in localized cell-death (Cui *et al*, 2015). PRRs and NLRs operate in distinct cellular compartments but share outputs and similarities. These include cytoplasmic Ca^{2+} influx, a burst of reactive oxygen species in the apoplast, phytohormone signaling and transcriptional reprogramming for activation of pathogen responsive genes and metabolites (Cui *et al*, 2015; Kadota *et al*, 2019; Lu & Tsuda, 2021). Both PTI and ETI induce the phytohormones Salicylic Acid (SA), Jasmonic Acid (JA) and ethylene (ETH) (Liu *et al*, 2016; Zhang & Li, 2019; Albert *et al*, 2015; Guan *et al*, 2015), for which some signaling machineries components co-occur with terrestrialization (Fig. 1) (Nishiyama *et al*, 2018). Combined knock-out mutations in *dde2* (JA biosynthesis), *ein2* (ETH responses), *pad4* (SA-dependent and -independent responses) and *sid2* (SA

biosynthesis) account for up to 80% reduction in functional outputs of PTI and ETI depending on the trigger (Tsuda *et al*, 2009). Therefore, immune pathways operate in parallel for quantitative outputs (Tsuda *et al*, 2009). Pathogen colonization of host tissues, including fungal hyphae accommodation, is prevented if a successful PTI or ETI is mounted (Bhandari *et al*, 2019; Lipka *et al*, 2005). It was recently shown that PTI and ETI mutually potentiate each other in Arabidopsis (Ngou *et al*, 2021; Pruitt *et al*, 2021) but not in *Nicotiana benthamiana* (Zönnchen *et al*, 2022), hinting at variation in immune network connectivity in distinct plant species.

Immune repertoires, including PRRs, NLRs and downstream components, change within (Clark *et al*, 2007) and across species (Baggs *et al*, 2020; Zipfel & Oldroyd, 2017). Prime examples of such diversity are the sulfur-rich thioglucoside-based glucosinolates (GLS) in the order Brassicales (Mithen *et al*, 2010). Aliphatic-GLS and indolic-GLS were sequentially acquired during evolution, therefore short chained- and long-chained aliphatic-GLS as well as indolic-GLS are present in Arabidopsis (Fig. 1) (Mithen *et al*, 2010). GLS are constitutively accumulated but also induced upon attack by herbivores or microbes (Wittstock & Gershenzon, 2002). Active GLS products (isothiocyanates) are formed upon cleavage of the glucose moiety by β-glucosidases and can be further specified into nitriles and epithionitriles by specifier enzymes (Wittstock & Burow, 2010; Kuchernig *et al*, 2012). In Arabidopsis, aliphatic-GLS are derived from methionine whilst indolic-GLS are derived from tryptophan (Trp). In parallel pathways using the same first enzymes, CYP79B2 and CYP79B3, Trp is also the precursor for the antimicrobial compounds camalexin and 4-hydroxyindole-3-carbonyl nitril (4-OH-ICN) and one of the precursors for auxin (Zhao *et al*, 2002; Rajniak *et al*, 2015; Tsuji *et al*, 1992). Arabidopsis *cyp79b2/b3* double mutants depleted in Trp-derived metabolites consistently show increased vulnerability to pathogens (Hiruma *et al*, 2013; Frerigmann *et al*, 2016). Intriguingly, model beneficial or neutral microbes such as the broad host-range *Serendipita indica* and *Serendipita vermifera* (order Sebacinales) fungi become detrimental in the absence of Trp-derived metabolites (Fig. 2A) (Nongbri *et al*, 2012; Lahrmann *et al*, 2015). Therefore, immune innovations can participate not only in deterring pathogens but also in harnessing non-pathogenic microbes. Overall, immunity is built on ancestral genes and principles that are core to land plants, but immune systems considerably diversified during evolution.

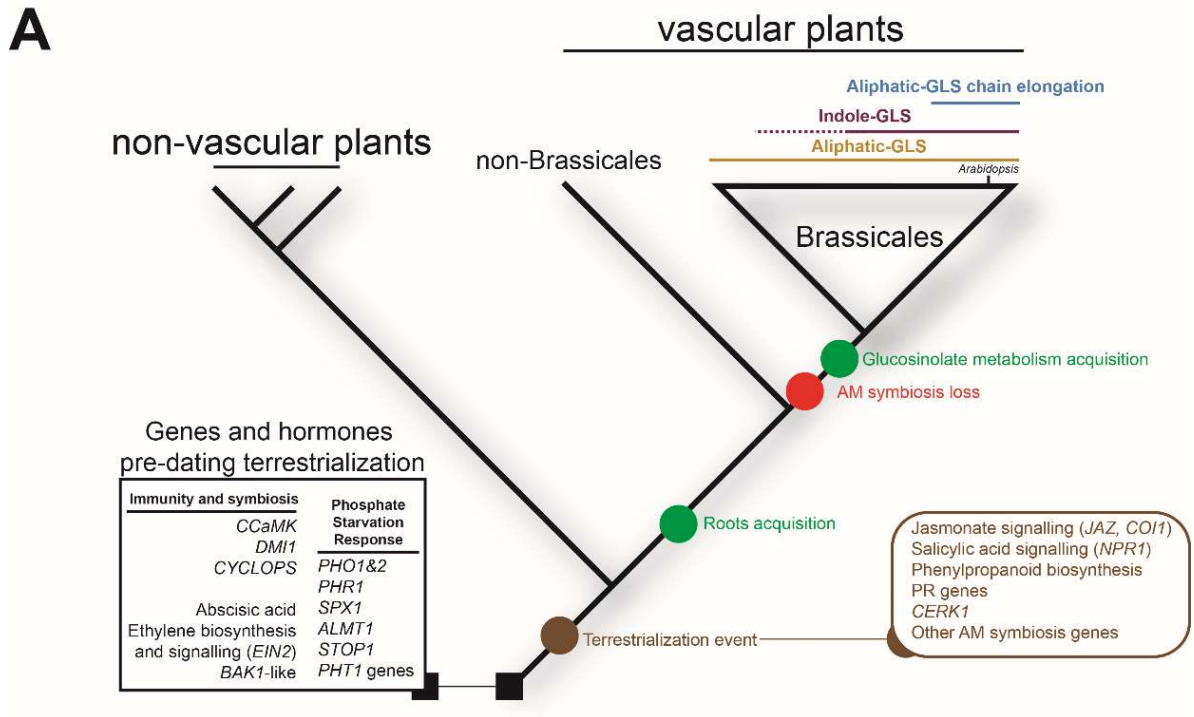

Figure 1: Plant interactions with fungal endophytes relies on ancient genes and recent innovations
A. Land plant cladogram contextualizing symbiotic and immune traits. Abbreviations related to symbiosis: AM = Arbuscular Myccorrhizae, *CCaMK* = Calcium and Calmodulin-dependent protein kinase, *DMI1* = Does not Make Infections 1. Abbreviations related to immunity: *BAK1* = BRI1-associated kinase 1, *EIN2* = Ethylene Insensitive 2, *JAZ* = Jasmonate-Zim Domain, *COI1*= Coronatine Insensitive 1, PR = Pathogenesis-related, *NPR1*= Non-expressor of PR genes, *CERK1* = Chitin elicitor receptor kinase 1, *GLS* = Glucosinolates. Abbreviations of Phosphate Starvation Response genes: *PHO1&2* = PHOSPHATE 1 and 2, *PHR1* = Phosphate Starvation Response 1, *SPX1* = SYG1/Pho81/XPR1, *ALMT1* = Aluminium Activated Malate Transporter 1, *STOP1* = Sensitive to Proton Toxicity 1, *PHT1* = Phosphate Transporter 1.

AM symbiosis is a complex trait that requires hyphae accommodation

Another core characteristic of land plants predicted to have facilitated terrestrialization is the Arbuscular Mycorrhizal (AM) symbiosis, formed today between ~70% of plants and the specific group of Glomeromycotina fungi (Parniske, 2008; Brundrett & Tedersoo, 2018). In flowering plants, Glomeromycotina hyphae progress through the roots until structures termed "arbuscules" are formed specifically in the cortical cell layer (Luginbuehl & Oldroyd, 2017). Arbuscules are highly branched hyphal structures inside plant cells and are dedicated to nutrient fluxes (Luginbuehl & Oldroyd, 2017). Glomeromycotina hyphal networks deliver phosphate (Pi) to plants via arbuscules in exchange for photosynthates (Kiers *et al*, 2011; Luginbuehl *et al*, 2017; Rich *et al*, 2021). Even though the increase in photosynthetic rates associated with AM symbiosis offset the carbon sink cost (Kaschuk *et al*, 2009), the symbiosis is thought to be costly for host plants because the nutritional and stress tolerance benefits are context dependent (Bennett & Groten, 2022). Why ~30% of plants lost mutualism with Glomeromycotina is

intensely debated. It could be caused by evolution of new nutrition modes as in carnivorous plants (Brundrett & Tedersoo, 2018), root systems more efficient at Pi foraging as in *Lupinus sp.* (Oba *et al*, 2001; Ma *et al*, 2018) or immune innovations such as GLS in Brassicales (Anthony *et al*, 2020). Importantly, Glomeromycotina are obligate biotrophs that require association with plants (Parniske, 2008). Furthermore, analysis of the genome of *Rhizophagus irregularis* notably revealed a loss of the Fatty Acid Synthase 1 and absence of predicted cell wall degrading enzymes (Tisserant *et al*, 2013), suggesting strong dependency towards host for symbiosis establishment and nutrition. By contrast, other root endophytic fungi are equipped with repertoires of cell wall degrading enzymes (Mesny *et al*, 2021). AM symbiosis relies on a network of genes and molecules largely originating concomitantly with terrestrialization (Fig. 1) (Delaux *et al*, 2015; Bravo *et al*, 2016; Nishiyama *et al*, 2018). Subsequently, the AM symbiosis program was strongly conserved in all host plants with few innovations (Bravo *et al*, 2016), which contrasts with the diversification of immune systems. However, the capacity to accommodate hyphae must be a prerequisite for, or at least co-incident with, acquiring such a specialized, multi-step symbiosis over evolutionary time. Whether a single and ancient hyphae accommodation mechanism is the basis of AM symbiosis and other types of plant-fungi interactions is unknown. If a single general mechanism underlies hyphae accommodation, it is likely to be under immunity control, at least partially, because loss of AM symbiosis does not impair accommodation of other fungi (Hiruma *et al*, 2016; Qin *et al*, 2020).

Chitin-based molecules for symbiosis vs defense decisions

In the course of land plant evolution, AM symbiosis and immunity co-existed and therefore likely co-functioned. A number of findings point to immunity and symbiosis signaling intersections that are relevant also in non-AM hosts, including Arabidopsis. AM symbiosis was thought to be largely enabled by the secretion of lipochitooligosaccharides (LCOs, chitin chains decorated with a lipid moeity) by Glomeromycotina, as LCOs are sufficient to induce symbiosis-signaling (Sun *et al*, 2015). However, LCOs were found to be secreted by phylogenetically unrelated fungi with saprophytic, mutualistic and pathogenic lifestyles (Rush *et al*, 2020). This suggests that most fungi can activate symbiosis signaling via secretion of LCOs. Importantly, co-treatment of Arabidopsis leaves with flg22 and LCOs or short chained chitins quantitatively reduced immune outputs compared to flg22 alone (Liang *et al*, 2013). In addition, short and long chained chitins were found to induce *CERK1*-dependent defense associated and AM symbiosis genes simultaneously in *M. trunctatula* (Feng *et al*, 2019). Together, these data argue for chitin-based molecules occupying dual symbiosis and immunity

elicitor functions in AM hosts. In parallel, LCOs and short chained chitin dampen immune signaling in Arabidopsis, which perhaps play a role in shaping hyphal accommodation.

The evolution of root systems and PSR role in root-microbe interactions

The advent of roots revolutionized plant life. Now anchored with new organs, vascular plants specialized a part of their biology into exploration of the soil-matrix for nutrient foraging and interactions with microbes. How roots facilitate nutrition and microbiota assembly simultaneously is under intense study.

Root immunity is compartmentalized and specialized compared to leaf immunity

Akin to the process of terrestrialization, the invention of roots heavily relied on co-option of already established gene regulatory networks. For instance, the development of root hairs (tip growing cells) depends on genes also underlying the development of corresponding cells called "rhizoids" in non-vascular plants (Menand *et al*, 2007; Proust *et al*, 2016). Fossilized vascular plants harbor arbuscule-like structures in shoots whilst in existing vascular plants AM symbiosis takes place exclusively in roots (Remy *et al*, 1994; Luginbuehl & Oldroyd, 2017). It is likely that the root hairs and AM symbiosis traits relied on comprehensive co-option of their respective gene regulatory networks into roots. By contrast, in the case of Arabidopsis, clear qualitative and quantitative differences occur between leaf and root immunity. For instance, commonly used leaf defense response markers such as *PR1* and *PDF1.2* were shown to be less or not expressed in roots, respectively (Attard *et al*, 2010). Furthermore, to my knowledge, no strong NLR triggered root immunity as in leaf ETI is known — except in the restricted case of *Glycine max*-rhizobacterial symbiont incompatibility, although this occurs without observed cell-death (Zhang *et al*, 2021). In analysis of root responses, it is important to consider the organ level serial delimitation of roots into meristematic, elongation, and differentiation zones (Somssich *et al*, 2016). In Arabidopsis, the expression of MAMP responsive genes was compartmentalized into the differentiation zone for chitin or the elongation and meristematic zones for flg22 (Millet *et al*, 2010; Zhou *et al*, 2020). Notably, endophytic Sebacinales fungi preferentially colonize the differentiation zone (Lahrmann *et al*, 2013), suggesting that spatially restricted immune responses to MAMPs such as chitin influence accommodation sites.

A recent and ingenious study used laser ablation to show that localized damage is required for adjacent root cells to mount a strong immune response in terms of PRR expression and associated prevention of non-pathogenic bacterial colonization (Zhou *et al*, 2020). By contrast, it is well established that damage is not required to mount effective immune responses after MAMP perception across leaf tissues (Zipfel & Oldroyd, 2017). Therefore, it remains unclear

whether root immunity differs fundamentally from leaf immunity in amplitude and quality or if local damage was the missing input masking root/leaf similarities in past studies. Nevertheless, a specialized root immunity with relatively higher activation thresholds is coherent with the constant exposure of roots to soil-borne microbes, from which a microbiota is assembled. Accordingly, the above-mentioned root/leaf differences suggest a partial co-option of immune networks in roots and/or so far undetermined features specifically modulating root immunity.

The PSR influences immunity at the transcriptional level

Roots are the main nutrient acquisition site in vascular plants (Rellán-Álvarez *et al*, 2016) and some microbiota members can improve nutrient uptake (Hiruma *et al*, 2016; Harbort *et al*, 2020; Van Der Heijden *et al*, 2016). Phosphate (Pi) is an essential macronutrient repeatedly linked to plant root interactions with microbes (Das *et al*, 2022; Castrillo *et al*, 2017; Hiruma *et al*, 2016). Plants undergoing Pi limitation activate the PSR, comprising transcription factors and post-translational regulators, which orchestrate increased expression rates of Pi transporters, mainly in the plasma-membrane anchored *PHT1* family (Rouached *et al*, 2010). The PSR system pre-dates terrestrialization (Rubio *et al*, 2001) (Fig. 1) and it is well established that low Pi promotes plant engagement in AM symbiosis (Balzergue *et al*, 2011). Recently, it was demonstrated that the PSR transcription factor *PHR2* allows early signaling, root colonization and mycorrhizal Pi uptake in rice (Das *et al*, 2022). Thus, a direct relationship exists between the PSR and the AM symbiosis program, which, given the strong conservation of AM symbiosis features, is plausibly extendable to other AM host species. Pi-stressed plants therefore actively support mycorrhizal colonization for increased access to Pi (Das *et al*, 2022).

The phylogenetically restricted loss of AM symbiosis prompts the question whether non-AM hosts evolved compensatory mechanisms to alleviate Pi stress. Remarkably, a specific strain of *Colletotrichum tofieldae* was reported to enhance Arabidopsis Pi transporter expression and to transfer Pi upon root colonization—but strictly in Pi-limited conditions with an intact PSR (Hiruma *et al*, 2016). Thereby, the PSR is functionally engaged in a Pi-based partnership with a filamentous fungus, possibly substituting for Glomeromycotina in nature. Arabidopsis PSR-immunity interplay was most notably exposed by Castrillo and colleagues (Castrillo *et al*, 2017) using the *phr1phl1* double mutant that is unable to deploy the PSR (Bustos *et al*, 2010). In Pi-limited conditions and compared to Col-0, the *phr1phl1* mutant showed enhanced transcriptional activation of immune genes in roots and improved resistance to leaf pathogens (Castrillo *et al*, 2017). Therefore, PSR activation generally downregulates immunity locally in roots and systemically in shoots. Whether PSR transcription factors directly bind to immunity

genes promoters to modulate their expression is insufficiently explored. In the presence of bacteria, expression of the camalexin synthesis gene *PAD3* was higher in the *phr1phl1* double mutant compared to Col-0, but the opposite was true for other Trp-metabolism genes, such as *MYB34, GSTF10* and *CYP79B2* (Castrillo *et al*, 2017). However, only *MYB34* was reported as a *PHR1* target (Barragán-Rosillo *et al*, 2021). These findings suggest that, upon immunity stimulation, Pi-stressed plants may modulate and not simply reduce metabolic immune outputs. In support of this hypothesis, a comparative study of 41 fungal endophytes isolated from Arabidopsis roots in natural conditions found that 13/41 fungi, including classically pathogenic genera such as *Fusarium* and *Alternaria*, switched from being detrimental to neutral or from neutral to beneficial, when co-cultured on low Pi compared to high Pi media (Fig. 2B) (Mesny *et al*, 2021). Therefore, either improved plant outcomes of interacting with fungi occur via the PSR-immunity relationship or Pi is a limiting factor for fungal detrimental traits. During Pi limitation without an immune input, several primary metabolites, phenylpropanoids and aliphatic-GLS showed increased accumulation in shoots and roots in a *PHR1* dependent manner (Pant *et al*, 2015). Therefore, roots are likely to coordinate nutrition and microbiota assembly via the PSR influence over immunity and symbiosis. Whether concurrent PSR and immune inputs fine tune metabolic outputs is thus far unclear.

Thesis aims

The work presented in this dissertation aims to study immune processes underlying root-fungal endophyte interactions using Arabidopsis as a model plant. In the first chapter, I describe my investigation into immune pathways contributing to fungal accommodation in roots. In this experimental system, I employed the model fungi Sebacinales and already established immune-deficient Arabidopsis mutants to quantify fungal biomass in roots and associated effects on plant shoot fresh weight. In the second chapter, I set out to interrogate the influence of PSR on aliphatic- and indolic-GLS production as model metabolite outputs. I selected a root colonizing endophyte isolated from Arabidopsis natural populations that had been linked to Pi status *in vitro* to investigate the impact of PSR and associated GLS patterns on fungal accommodation. Using microscopy, whole transcriptome analysis and GLS quantification, I provide a detailed view of how Pi and immunity interact to modulate GLS profiles. Based on the GLS quantification, I propose that the PSR impacts shoot to root GLS translocation as well as rates of synthesis and breakdown differentially depending on the type of GLS considered.

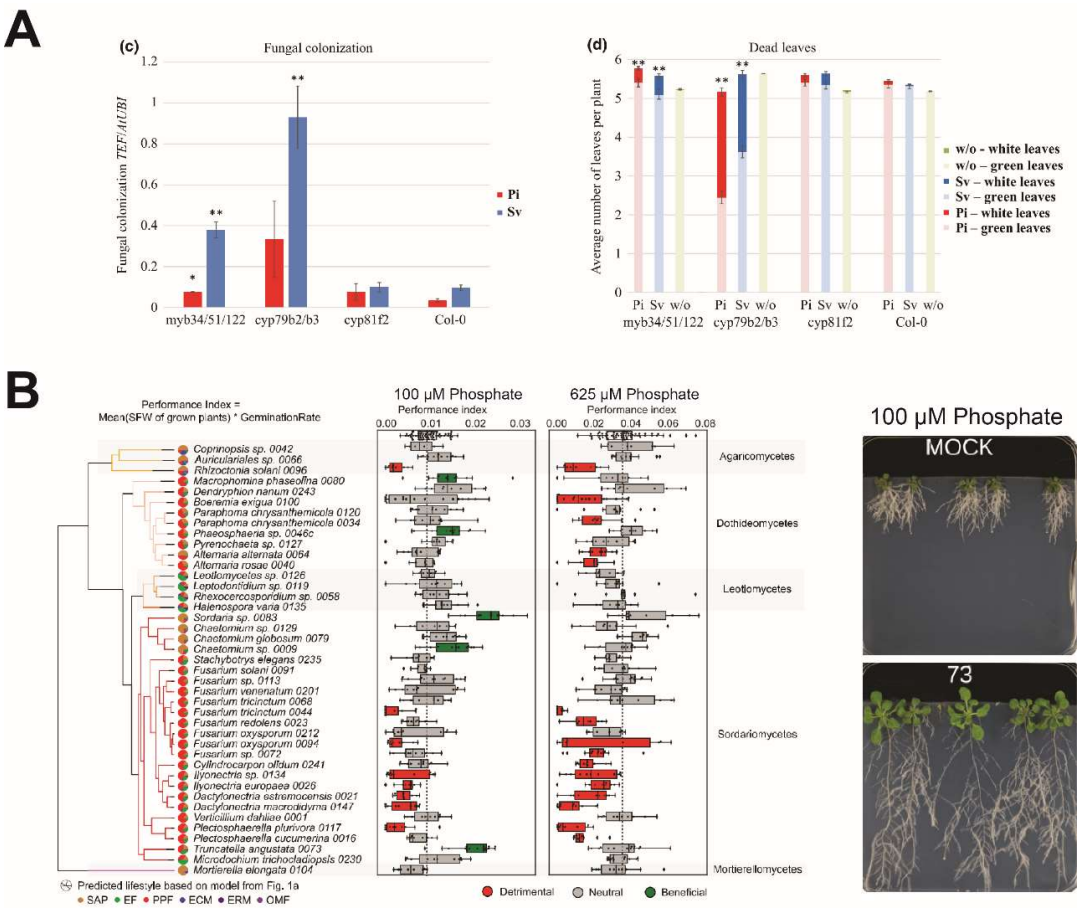

Figure 2: Key studies and materials for the presented thesis
A. Sebacinales species are detrimental to the Trp-derived metabolites depleted *cyp79b2/b3* mutant. Pi = *Piriformospora indica* (now *Serendipita indica*) and Sv = *Serendipita vermifera*. w/o = without (mock controls) (Lahrmann et al. 2015). **B.** MPIPZ culture collection fungal endophytes display varying effects on Arabidopsis shoot fresh weight grown on 100 µM or 625 µM phosphate ½ MS 28 days post inoculation (Mesny et al. 2021) Pictures on the far right show typical Mock and *Truncatella angustata* (F73) inoculated plants at 100 µM phosphate. Pictures are courtesy of Fantin Mesny and unpublished.

Chapter 1: Investigating general immune mechanisms related to fungal accommodation in roots

Genetic disruption of plant immune genes could lead to changes fungal biomass in roots and associated effects on shoot fresh weight. To begin the search for immune pathways related to either or both of these outcomes, the *Arabidopsis thaliana* (Arabidopsis) *cyp79b2/b3* double mutant (Trp-derived metabolite free (Böttcher *et al*, 2009)) was selected as an immunocompromised reference. In previous studies, inoculation of diverse fungal endophytes caused *cyp79b2/b3* to reliably show both reduced shoot fresh weight and enhanced fungal load in roots compared to wild-type Col-0 (Nongbri *et al*, 2012; Lahrmann *et al*, 2015; Hiruma *et al*, 2016). The aim was to rapidly obtain conditions in which these outcomes are reproduced using *Serendipita vermifera* (Sv), a more aggressive endophyte than its relative *Serendipita indica* (Si) (Lahrmann *et al*, 2015). To reach a stage at which *cyp79b2/b3* behaves as previously found, exploration of different parameters was carried out (see Methods).

Sv causes similar shoot fresh weight penalties in Col-0, *cyp79b2/b3* and *deps* on 1/10 Plant Nutrition Media

A first screen for altered shoot fresh weight at 14 days post inoculation (dpi) on different Plant Nutrition Media (PNM) concentrations was conducted. Alongside Col-0 and *cyp79b2/b3*, the immune phytohormone *dde2 ein2 pad4-1 sid2-1 (deps)* quadruple mutant (Tsuda *et al*, 2009) and the danger associated molecular pattern (DAMP) receptor *pepr1/2* double mutant (Ross *et al*, 2014) were included. This array of mutants allowed me to disable DAMP signaling, phytohormones and chemical defenses to perhaps detect differences in Sv accommodation. Regardless of genotype, shoot fresh weights were not impacted by Sv inoculation on ½ PNM or full-strength PNM (Fig. 3A). By contrast, on 1/10 PNM, Col-0, *cyp79b2/b3* and *deps*, but not *pepr1/2*, showed a shoot fresh weight penalty when inoculated with Sv compared to their respective mock controls (Fig. 3A). Furthermore, regardless of media concentration, no Sv-induced yellowing of the leaves was observed as in Lahrmann *et al,* 2015 (Lahrmann *et al*, 2015) (not shown). Therefore, 1/10 PNM arose as a co-culture media on which Sv effects on Arabidopsis genotypes can be detected.

However, it was surprising that the shoot fresh weight penalty on 1/10 PNM was of the same magnitude in *cyp79b2/b3,* Col-0 and *deps* (Fig. 3A), suggesting that the conditions of this first assay do not recapitulate the published detrimental outcomes in *cyp79b2/b3*. Furthermore, the time point and/or inoculation parameters and/or Sv inoculum could be responsible for the fact

that the *cyp79b2/b3* did not show greater shoot fresh weight penalty than Col-0 upon inoculation. To address this, fresh Sv and Si colonies were obtained from the Zuccaro lab (University Köln) and the time point of analysis was shifted to 5 dpi. Si has the advantage of producing chlamydospores, which are convenient for precise dosage in inocula. Investigating an earlier time point could compromise the detection of fungal effects on shoot fresh weights. However, it had the virtues of keeping root tissues free of likely secondary growth whilst potentially uncovering early contribution of immune signaling to intraradical accommodation.

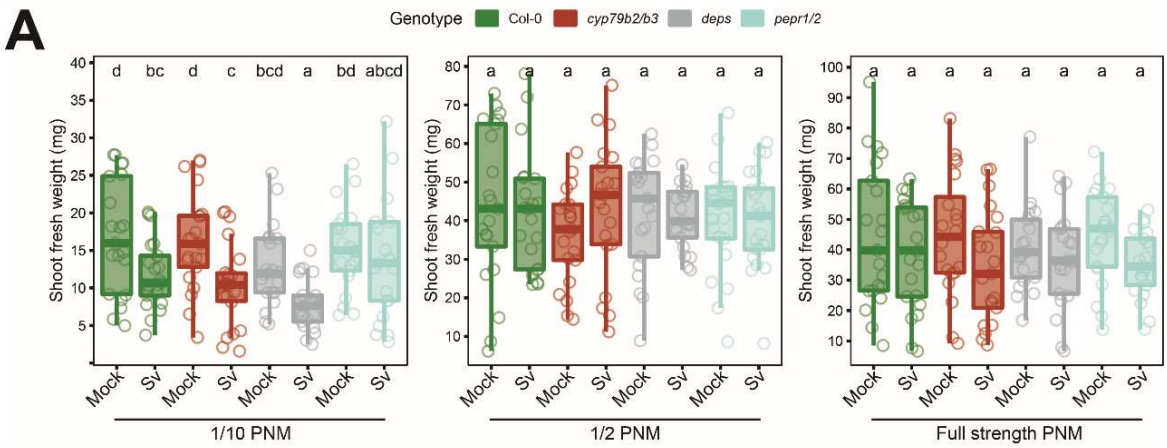

Figure 3: *Serendipita vermifera* causes shoot fresh weight penalties on 1/10 Plant Nutrition Medium
A. First preliminary assay, shoot fresh weights of individual Arabidopsis plants grown on different PNM concentrations for 14 dpi of Sv or mock by root dipping. Three distinct agar plates with seven seedlings each were used per condition. Letters represent statistical significance groupings according to pairwise Mood tests (1/10 PNM) and Kruskal-Wallis tests with post-hoc Dunn tests (0.5 and full strength PNM) with p-value thresholds of 0.05.

Arabidopsis might rely on cell-surface signaling to control Si colonization

In another large-scale experiment, no significant effects of Sv nor Si were detected on shoot fresh weights (Fig. 4A and B). Similarly, only a marginal root growth stimulation for Sv on *cyp79b2/b3* compared to mock control was observed (Fig. 4A and C). Analysis of whole root fungal load by qPCR after root surface cleaning revealed that Sv, but not Si, colonized roots to a larger extent in *cyp79b2/b3* than in Col-0 (Fig. 4D and E). Interestingly, both *deps* and *bak1bkk1* (common MAMP co-receptor double mutant) showed enhanced Si accommodation (Fig. 4E). However, the values obtained for Sv were almost one order of magnitude lower than for Si (Fig. 4D and E). These data pointed to a clear problem with the Sv mycelium inoculation compared to Si that had to initiate growth from spores.

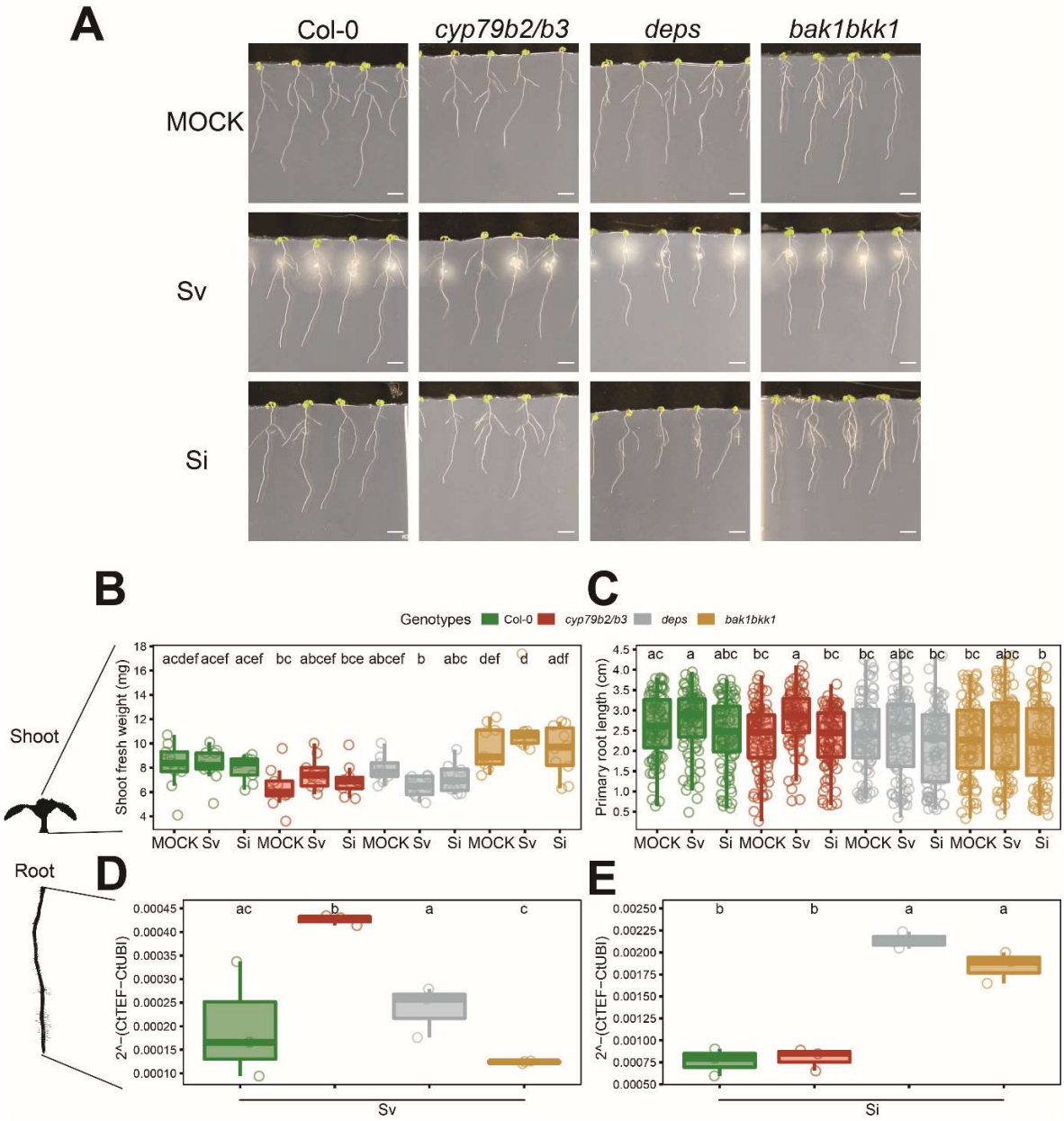

Figure 4: Cell surface signaling might intervene in root-Si interactions
A. Pictures of Arabidopsis seedlings on 1/10 PNM 5 dpi with either mock, Si or Sv. Scale bars = 0.5 cm. **B.** Pooled shoot fresh weights from one plate and **C.** Individual primary root growth (= root length 5 dpi – root length 0 dpi) of Arabidopsis seedlings. **D.** Sv and **E.** Si root fungal load at 5 dpi. Individual data points represent the fungal load from three pooled plates of whole roots as determined by qRT-PCR after RNA isolation. Letters represent statistical significance groupings according to pairwise Mood tests for **C, D, E** and ANOVA with post-hoc Tukey's HSD test for **F** with p-value thresholds of 0.05. Assay using droplet inoculation with nine distinct agar plates containing 7 seedlings each per condition.

No assays showed results comparable to published studies with Si or Sv: altered fungal accommodation and reduced shoot fresh weight and/or root growth in *cyp79b2/b3*. Additionally, the overarching goal was to discover pathways affecting root colonization other than Trp-derived metabolites. Because the enhanced Si load in *bak1bkk1* at 5 dpi was promising in these conditions, I selected Si, *bak1bkk1* and *cerk1* (chitin receptor mutant) to investigate the

role of cell-surface signaling in fungal accommodation. The *deps* quadruple mutant was left out on the grounds that too many pathways might be impacted in this background. However, the fact that *cyp79b2/b3* did not show enhanced Si load compared to Col-0 under the tested conditions prompted me to increase Si inoculum dose from 1 000 to 10 000 spores per plant and a selection of the top 2 cm root segment below the hypocotyl for fungal load analysis (Fig. 5B).

Additionally, a later time point of 10 dpi was included. Experiments with three independent repeats were initiated using these parameters. During the completion of the independent repetitions, no altered shoot phenotype was detected at 6 dpi (not shown) nor at 10 dpi (Fig. 5A). Therefore, shoot fresh weights were not recorded. Additionally, primary root growth was recorded but not affected by neither genotype nor inoculation (not shown). Within a given genotype, Si biomass in roots increased from 6 to 10 dpi, indicating successful detection of Si intraradical growth progression (Fig. 5B). Furthermore, the 6 dpi Si biomass measured by qPCR approximately doubled compared to 5 dpi using 1 000 spores/plant (Fig. 4E) which was coherent with the Si dose increase and the root fragment selection. However, within either 6 or 10 dpi, no differences were detected between genotypes, including *cyp79b2/b3* (Fig. 5B). This suggested a potential problem with the *cyp79b2/b3* seed batch employed. Accordingly, three repetitions of an experiment focusing on Si load in roots were conducted using in parallel Col-0 and *cyp79b2/b3* seeds from the Parker lab (own lab, MPIPZ) and the Hacquard lab (MPIPZ). No significant differences in fungal load were detected between the seed batches at 6 dpi (Fig. 5C). The above presented experiments suggest an unknown issue pertaining to co-culture conditions (*e.g.* light quality), media preparation, or Sebacinales fungi in my conditions. Overall, despite successful detection of increased Si biomass in roots depending on dose and time point (Fig. 4E to relate to Fig. 5B) and RT-qPCR results consistency between assays (Fig. 5B and C), the *cyp79b2/b3* phenotype could not be reproduced. Therefore, the feasibility of investigating the contribution of diverse immune pathways to a hypothetical general hyphae accommodation mechanism in Arabidopsis roots using Sebacinales was reconsidered.

In conclusion, both the initial research question and Sebacinales fungi were discarded as a framework. Consequently, one or two fungal strains were to be selected and developed as models according to the purposes of a new project.

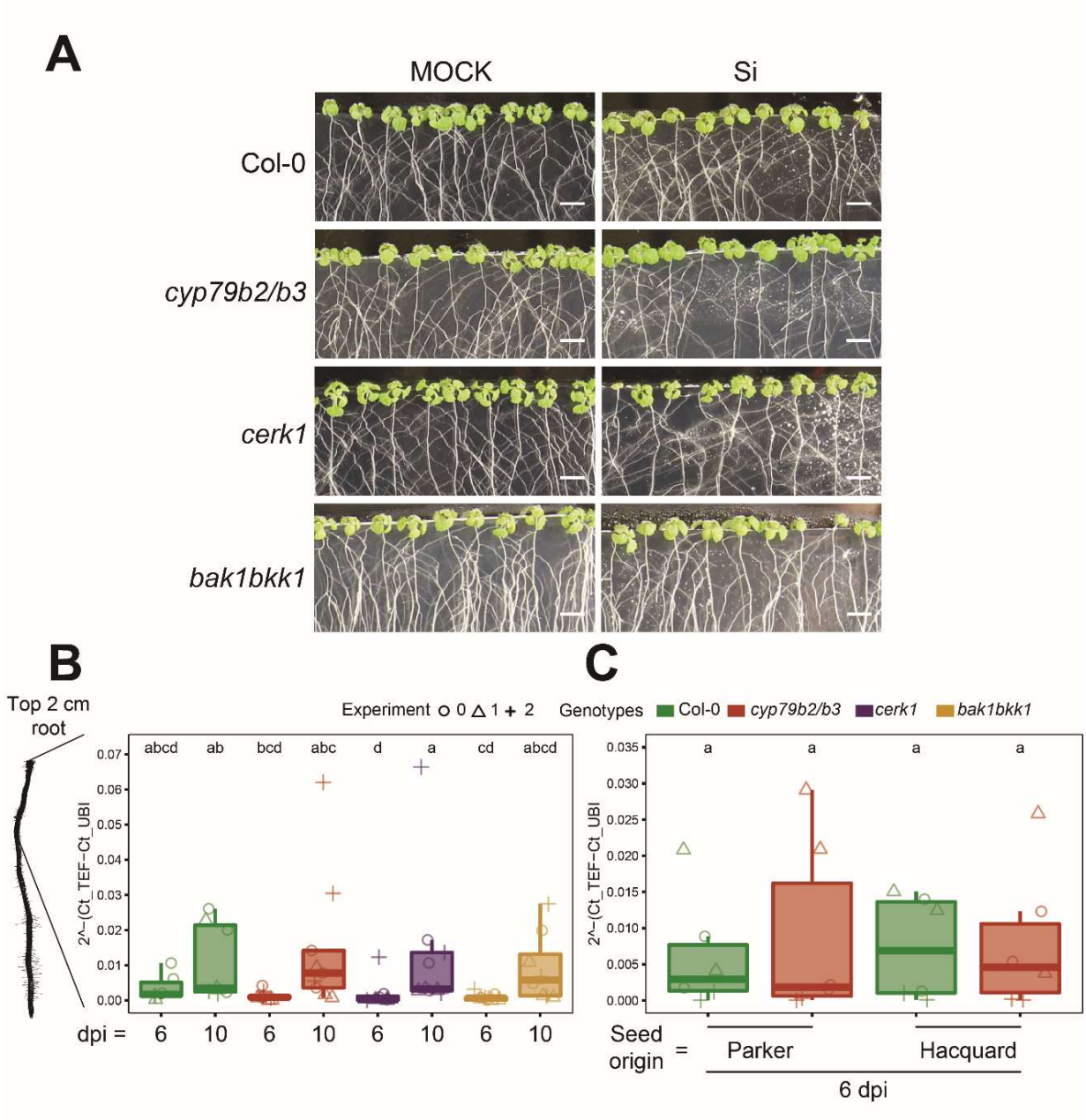

Figure 5: The previously published *cyp79b2/b3* phenotype caused by Si infection is not reproduced
A. Pictures of the top 2 cm of Arabidopsis plants 10 dpi of Si or mock. Scale bars = 0.5 cm. **B.** and **C.** Si biomass in roots as determined by RT-qPCR. Letters represent statistical significance groupings according to pairwise Mood test for **B** and Kruskal-Wallis with post-hoc Dunn test for **C** with p-value thresholds of 0.05.

Chapter 2: Characterization of glucosinolate production dynamics in response to native fungal endophytes

In recent years, growing interest has been directed at the link between immunity and the Phosphate Starvation Response (PSR) and at the consequences of this link on plant-microbe homeostasis (Hiruma *et al*, 2016; Castrillo *et al*, 2017; Frerigmann *et al*, 2021). Namely, it was shown that activation of the PSR globally dampen immunity at the transcriptional level, leading to enhanced pathogen susceptibility in phosphate (Pi) stressed Arabidopsis plants (Castrillo *et al*, 2017). Additionally, a recent pre-print attempted to provide a greater degree of detail by linking the negative PSR regulator *NLA* to greater accumulation of the Tryptophan (Trp)-derived compound camalexin and to various transcriptional alterations in specific phytohormone related genes (Val-Torregrosa *et al*, 2021). Together, these studies suggest that the PSR indirectly or directly affect the transcriptional and metabolite levels of immunity, and perhaps that the PSR does not negatively regulate all aspects of immunity. Therefore, I set out to investigate whether the PSR specifically affects two distinct immune pathways by picking indole- and aliphatic-glucosinolate accumulation (GLS) as metabolic readouts. Root-fungi interactions are an adequate frame for asking this question due to the established relationships between filamentous fungi and Pi status (Hiruma *et al*, 2016; Frerigmann *et al*, 2021; Mesny *et al*, 2021) or Trp-derived metabolites (Nongbri *et al*, 2012; Wolinska *et al*, 2021; Lahrmann *et al*, 2015; Hiruma *et al*, 2016; Frerigmann *et al*, 2021). I selected two native endophyte strains from the MPIPZ culture collection: F73 (*Truncatella angustata*) and F34 (*Paraphoma chrysanthemicola*) because of their different effects on Arabidopsis shoot fresh weight grown on contrasting Pi concentrations in ½ MS (Fig. 2B) (Mesny *et al*, 2021). At 100 µM Pi compared to 625 µM Pi, F73 is beneficial whilst F34 switches from slightly detrimental to neutral (Fig. 2B). This suggests that, with certain endophytes, Pi limitation may drive improved outcomes for plant growth, either via the PSR-immunity relationship, or alternatively via a direct effect of bioavailable Pi on the specific fungi. Moreover, both F34 and F73 have average relative abundances in Western Europe compared to other fungal endophytes (Mesny *et al*, 2021). The focus on short-term assays using root inoculation was kept to explore early signaling effect of the PSR on GLS pathways.

Developing F73 and F34 as model endophytes

Ideally, a model fungal endophyte offers the possibility of a precise and homogenous inoculum (spores over mycelium suspension), tractability with molecular methods (*e.g.* qPCR) and reliable colonization of plant tissues. First, two repetitions of a preliminary assay were

conducted to determine the behavior of F34 and F73 using root inoculation, whilst keeping the same ½ MS Pi concentrations and inoculum preparation as in the work of Mesny and colleagues (Mesny *et al*, 2021). Harvest times were determined during the first assay, when potential fungal effects on plant growth would be detected by eye. At 100 µM Pi, shoot fresh weight was identically decreased by the presence of either fungi compared to mock regardless of whether the harvest was carried out at 10 or 14 dpi. By contrast, at 625 µM Pi, the shoot fresh weights showed no significant differences when compared to mock, regardless of treatment and time point (Fig. 6A and B), suggesting an effect of Pi on the interactions formed between the plant and the employed fungi using root inoculation.

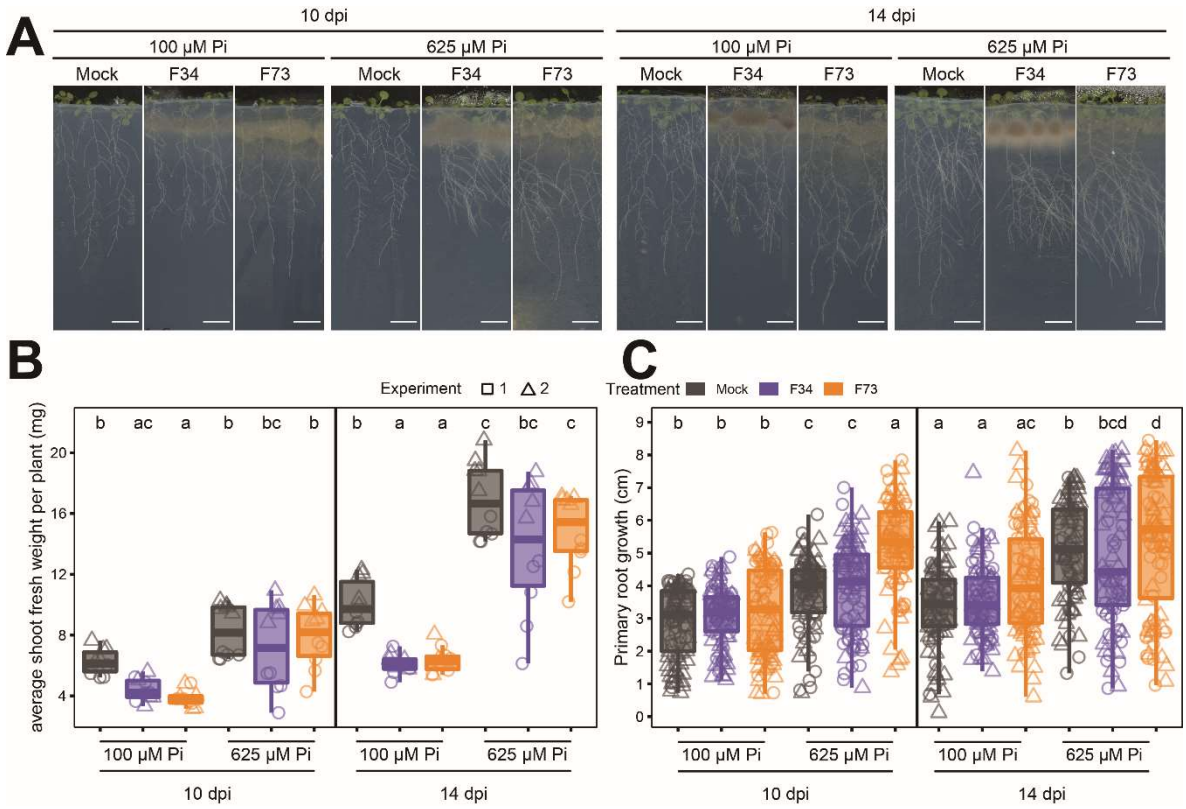

Figure 6: Culture collection endophytes F34 (*Paraphoma chrysanthemicola*) and F73 (*Truncatella angustata*) decrease plant shoot fresh weight when inoculated on roots.
A. Pictures of Arabidopsis grown on ½ MS plates containing the indicated Pi concentrations inoculated either with mock (10 mM $MgCl_2$) or with a fungus. **B.** Average fresh weights of approximately 10 pooled shoots per plate. **C.** Primary root growth (= primary root length harvest day – root length 0 dpi) per plant. Letters in **B.** and **C.** represent statistically significant groupings based on pairwise Mood tests within a given time point. P-value threshold = 0.05.

However, it should be noted that shoot fresh weights differences at 625 µM Pi between repetitions was observed (Fig. 6B). F73 inoculated plants showed a statistically significant primary root growth promotion at 625 µM Pi at both time points compared to mock (Fig. 6C).

Given the high inocula doses and the proliferation of F73 on the agar media, the larger root growth could indicate a competition for media nutrients, prompting the plants to forage more efficiently. Overall, despite the high inocula doses, the plants showed only minor shoot growth penalties. This suggests that, in contrast to previous long-term studies, F34 and F73 impart mild detrimental effects to plant health when inoculated on roots during short-term agar plate assays. These effects may be caused by intraradical colonization by F34 and F73 (biotrophy and/or "growth vs. defense trade off") or harm due to the inocula containing dead hyphae and/or cell disruption products.

To test the latter idea and evaluate if my employed system simply suffered from inefficient inoculation, my next step was an attempt to induce sporulation to try to improve inocula. I grew F34 and F73 on diverse fungal media with or without black-light irradiation, but detected no spore production (not shown). Therefore, I established three aims: i) Develop a protocol for production of "clean" inocula (free or with reduced hyphae disruption products), ii) perform shorter-term assays (7 dpi harvest) and iii) determination of hyphae localization in roots using confocal microscopy. Briefly, to produce fungal biomass for "clean" inocula, mycelia were obtained from cultures in liquid media. Then, fungi were thoroughly blended using a laboratory mixer, allowed to regenerate, washed and inoculated on roots (see methods). This resulted in a homogenous inoculum for F73 whereas the F34 mycelium suspension still contained lumps of various sizes (Fig. 7A), which could impair inoculation of consistent amounts of F34 per root. This inocula preparation method was nonetheless applied to both F34 and F73 in three independent repetitions of a short-term assay. Importantly, the fungal dose was lowered from 50 mg/ml to 2 mg/ml to determine whether a lower dose would result in similar outcomes as in Fig. 6.

Interestingly, compared to mock, both fungi imparted significant shoot fresh weight penalties at 7 dpi regardless of Pi concentration (Fig. 7C). Remarkably, the only significant difference in primary root growth was a reduction attributed to F34 at 625 µM Pi (Fig. 7D). These results suggests that the inoculum preparation method can alter interaction outcomes on shoot fresh weight, as no differences were observed at 625 µM Pi in the previous assays (Fig. 6B). Alternatively, if the shoot fresh weight changes are due to biotrophy, it could be that the previous high inoculum dose prevented root colonization at 625 µM Pi (Fig. 6B).

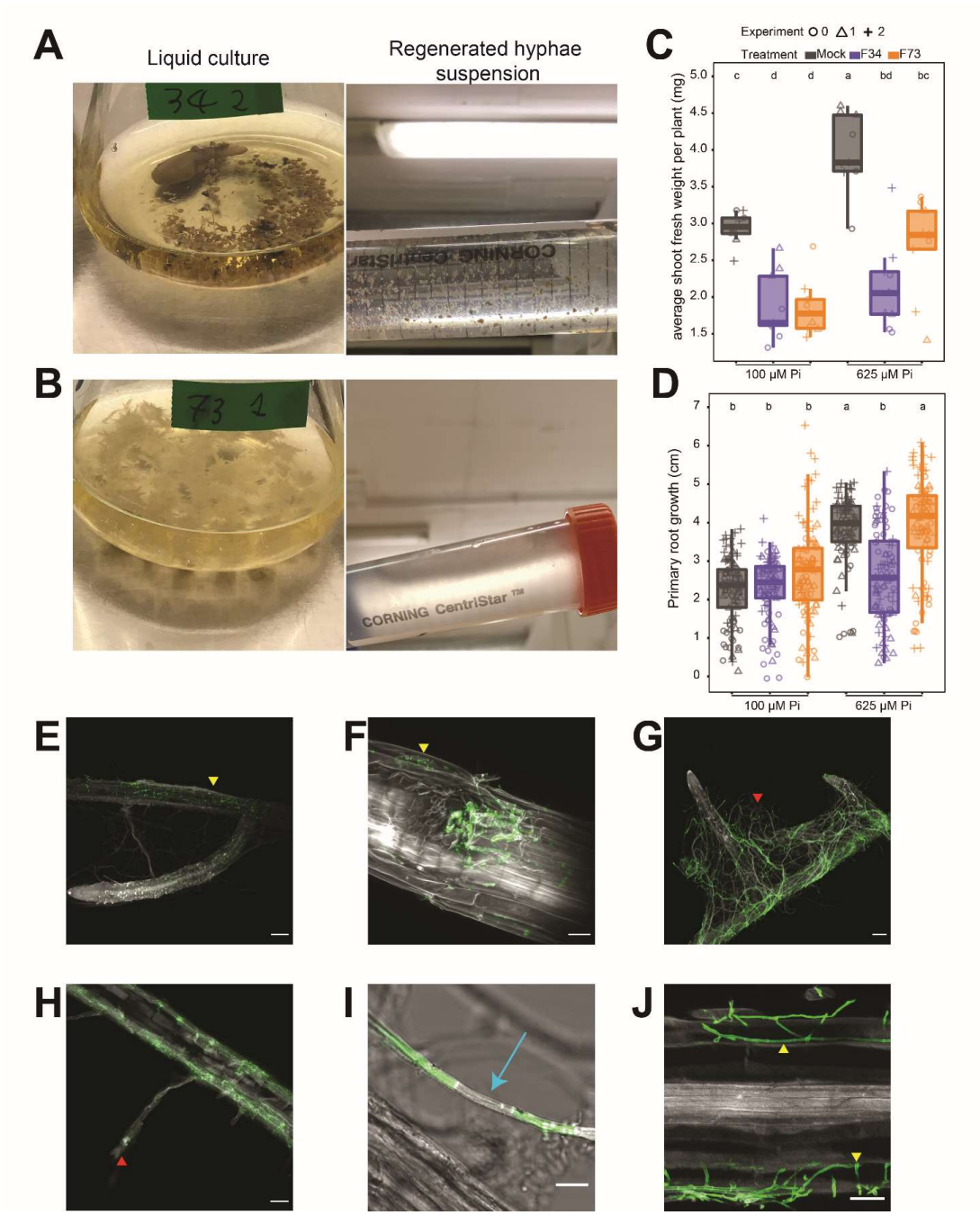

Figure 7: F73 and F34 inflict shoot fresh weight penalties by colonizing roots intracellularly
A. F34 liquid culture morphology (left) and regenerated hyphae suspension homogeneity (right). **B.** F73 liquid culture morphology (left) and regenerated hyphae suspension homogeneity (right). **C.** Average shoot fresh weight of Arabidopsis plants 7 dpi of either mock, F34 or F73 on 100 µM or 625 µM Pi. Data points represent the weight of pooled shoots from one plate divided by number of shoots weighed. **D.** Primary root growth of plants, data points represent the primary root growth of individual roots. Letters represent statistically significant groupings based on an ANOVA with post-hoc Tukey's HSD for **C.** and Mood test for **D.** with P-value thresholds of 0.05. **E.-J.** Confocal microscopy analysis of F34 or F73 colonized roots using Wheat Germ Agglutinin-CF488 and CalcoFluorWhite. **E.** F73 hyphae presence on the inoculated root part, scale bar = 100 µm. **F.** Maximum intensity projection of a Z-stack on a F34 inoculated root, scale bar = 20 µm. **G.** F73 inoculated root following "gentle" extraradical hyphae removal attempt, scale bar = 100 µm. **H.** F73 inoculated root part following "thorough" extraradical hyphae removal attempt, scale bar = 100 µm. **I.** Extraradical hyphae of F73 without KOH treatment, scale bar = 10 µm. **J.** F73 inoculated root with KOH treatment, scale bar = 20 µm. Yellow arrowheads designate intracellular colonization events while red arrowheads point to undesirable events following attempts manual removal of extraradical hyphae. Cyan arrow points to a WGA unstained F73 cell neighboured by two WGA stained cells.

A few samples from these experiments were subjected to confocal microscopy analysis to determine hyphae localization in roots. Both F34 and F73 were found to colonize the differentiation zone on which they are inoculated (Fig. 7E) and could, under my experimental settings, achieve intracellular infection of epidermal cells (Fig. 7F). Eventually, exclusive quantification of intraradical fungal biomass via qPCR would be part of a model endophyte system. Whether extraradical hyphae could be removed manually during harvest was assessed by treating a few roots with gentle or thorough manual scrubbing (n=4 each, see methods). Neither methods were satisfactory, as too much extraradical hyphae remained (Fig. 7G) or sizable sample damage was inflicted (Fig. 7H). Therefore, quantifications of intraradical colonization via qPCR would rely on prior root surface sterilization (see methods). It was also apparent that the Wheat Germ Agglutinin (WGA) chitin staining was unhomogenous (Fig. 7I) suggesting both fungi mask their chitin using epitopes. Accordingly, a KOH incubation step was introduced in subsequent staining procedures, which improved tissue clearing and WGA binding to chitin (Fig. 7J). Overall, confocal microscopy observations suggest that F34 and F73 impart shoot fresh weight penalties to Arabidopsis at 7 dpi via intracellular colonization of root tissues. F73 was selected for further studies because of its amenability to homogenous hyphae suspension (Fig. 7B). Following F73 genomic DNA extraction and serial dilutions, an array of qPCR primers were assessed for efficiency (Supp. Fig. 1). The primer pair with the efficiency closest to 100% was selected for subsequent experiments (Primer pair 4, Supp. Fig. 1).

Next, to assess the plant GLS responses to F73, we measured indole- and aliphatic-GLS amounts in roots or shoots at 2 and 7 dpi on a Pi gradient. GLS amounts variations according to inoculation or Pi were clear at 7 dpi although some differences in shoots were detectable at 2 dpi. Notably, the sulfated long chained aliphatic-GLS 8-methylsulfinyloctyl (8MSO) was depleted by the presence of F73 compared to mock in both shoots and roots at 7 dpi (Fig. 8A and B). The F73-imparted 8MSO depletion might have been amplified at 100 µM P in both organs (Fig. 8A and B). However, at 2 dpi, 8MSO was present in stable low quantities across conditions, with mock-inoculated plants on 100 µM Pi showing the lowest amounts (Fig. 8A and B). By contrast, the indole-GLS 4-hydroxy-3-indolylmethyl (4MOI3M) showed systematic increased amounts in presence of F73 compared to mock. This was the case across the tested conditions, except in roots at 2 dpi where 4MOI3M was mostly undetected regardless of Pi (Fig. 8C and D). This assay suggested that the combination of F73 and Pi treatments modulate the amounts of at least 8MSO and 4MOI3M in a distinct, tissue-specific way, which may provide robust end-point measurements in this system. Variations in amounts could be caused by increased or reduced rates of synthesis and/or breakdown and/or exudation. Additionally,

GLS can be translocated between organs (Chen et al. 2001). Whether and to what extent these regulatory processes are involved here is unclear. Nonetheless, F73 combined with a Pi gradient appeared as appropriate to investigate potential impacts of the PSR on the aliphatic- and indole-GLS pathways. However, a final system improvement attempt was made by introducing Sucrose in germination media to boost seedlings size and 625 µM Pi was replaced by 1250 µM Pi as a Pi replete condition.

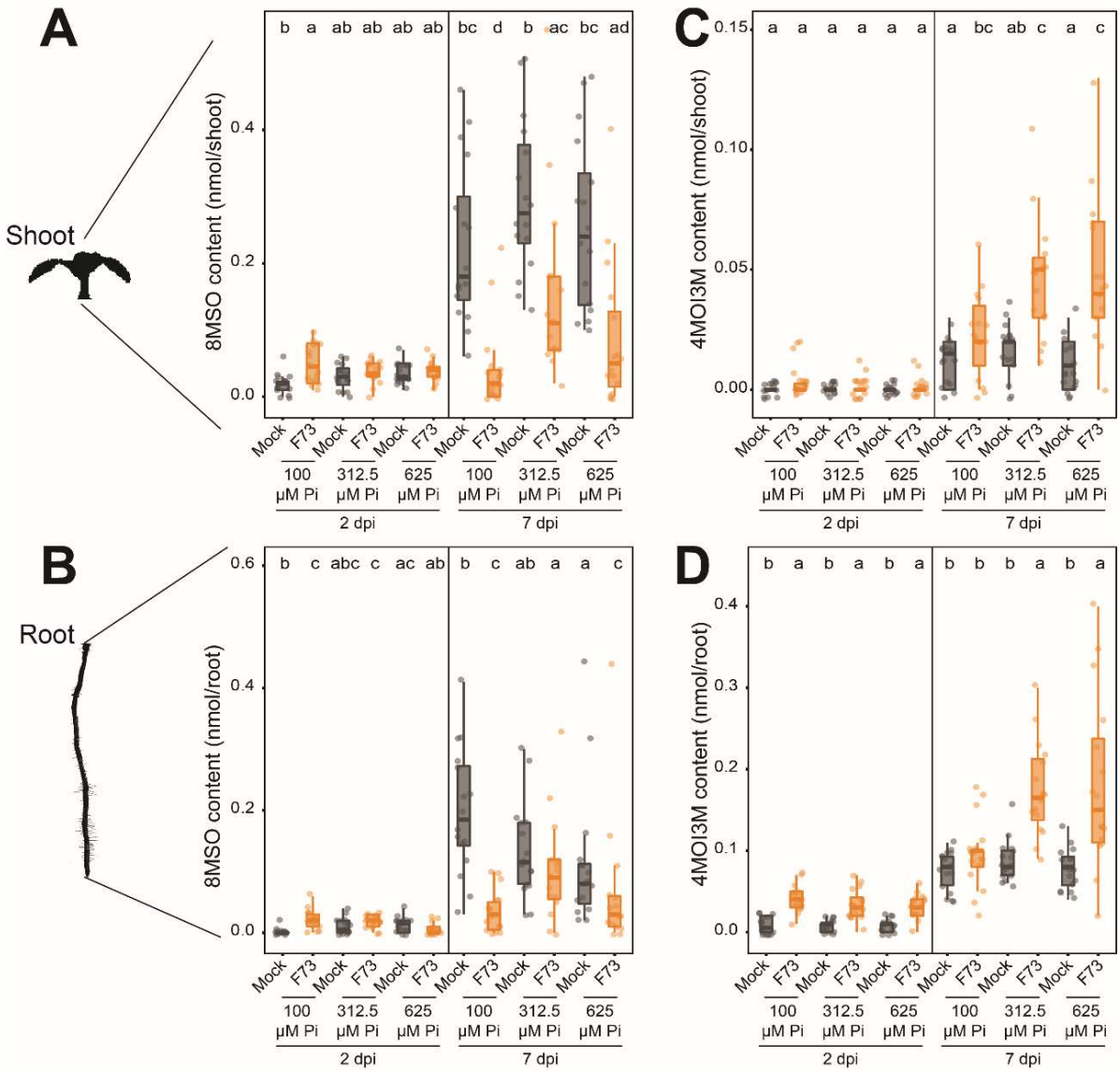

Figure 8: F73 induces 8-methylsulfinyloctyl (8MSO) glucosinolate depletion and 4-methoxy-3-indolylmethyl (4MOI3M) glucosinolate accumulation at 7 dpi
A. 8MSO in shoots **B.** 8MSO in roots. **C.** 4MOI3M in shoots **D.** 4MOI3M in roots. Letters represent statistical groupings with p-value thresholds of 0.05 using Mood tests for **B.**, **C.**, **D.** and **A.** at 7 dpi and ANOVA with post-hoc Tukey's HSD for **A.** at 2 dpi.

100 µM Pi causes a mild Phosphate Starvation Response compared to 1250 µM Pi

Morphological hallmarks of Pi starvation include shorter primary root, higher number of lateral roots and an increase in number and length of root hairs (Lynch, 2011). These hallmarks are

abolished if agar plate grown roots are directly exposed to light (Gao *et al*, 2021). I tested whether Pi and/or F73 modified primary root growth and lateral root numbers at 2 and 7 dpi. Compared to 1250 µM Pi, 100 µM Pi elicited a slight but significant increase in primary root growth at both 2 and 7 dpi (Fig. 9A), no differences were observed for lateral root occurrence (Fig. 9B). Consistent with previous assays, F73 induced a significant increase of primary root growth at 7 dpi in the Pi replete conditions (here 1250 µM Pi, Fig. 9A). However, no changes in lateral root numbers were imparted to F73 compared to mock (Fig. 9B). Root hair numbers and lengths were clearly higher in 100 µM Pi grown plants compared to 1250 µM Pi prior to inoculation (Fig. 9C, D and E). These data suggests that, as a Pi limiting condition, 100 µM Pi is sufficient to induce a Pi starvation phenotype that does not cause dramatic differences in root system morphology compared to 1250 µM Pi.

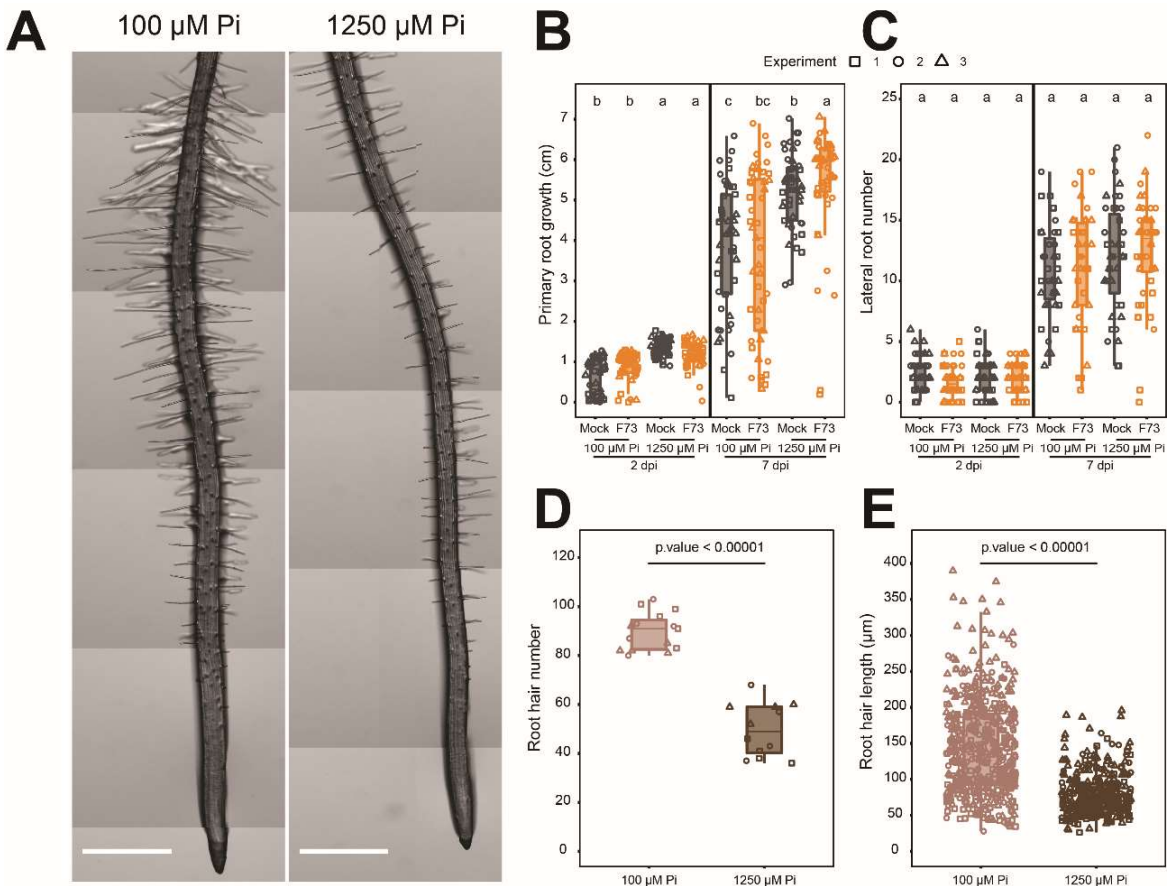

Figure 9: Chosen experimental conditions allow a mild but detectable Pi limitation phenotype.
A. Stitched stereomicroscope pictures of root tips prior to inoculation, scale bars = 300 µm. **B.** Primary root growth and **C.** lateral root numbers. Letters indicate statistical groupings with p-value thresholds of 0.05 using Mood tests for both time points in **A.** and 2 dpi in **B.** while for 7 dpi in **B.** an ANOVA with post-hoc Tukey's HSD was conducted at 7 dpi. **D.** Root hair number with student test and **E.** root hair length with Mood test.

F73 is an efficient endophyte of the Arabidopsis differentiation zone

Having established appropriate Pi-limited and replete conditions, the F73 intracellular colonization ("entry") was investigated in relation to Pi status and root zones. First, potential developmental differences between 100 µM Pi and 1250 µM Pi were ruled out because the same degree of initiation in secondary growth was observed below the hypocotyl (Fig. 10B and C).

To test for root zone-dependent permissiveness to F73 entry, two inoculation locations were tested on two distinct sets of plants. On one set, inoculation was performed 0.5 cm below the hypocotyl and F73 entry was assessed in this area (Fig. 10A). The other set of plants was inoculated 1 cm below the primary root tip and F73 entry was assessed in the primary root tip as well as 100 to 500 µm above the primary root tip (Fig. 10A). A "colonization score" based on hyphae adherence to root (adherence = 1, no hyphae = 0) and intracellular penetration (inside = 1, outside = 0) was established on the root zones investigated. Per repetition of the experiment, the colonization score was calculated by adding root adherences and cell penetrations and dividing the sum by the number of plants tested. F73 could attach to and enter root cells as soon as 1 dpi (Fig. 10D and F) and proliferated extensively inside epidermal and cortical cells of primary and lateral roots over time (Fig. 10E). When F73 was inoculated on the differentiation zone, in most cases, the colonization score reached the maximum value of 2 regardless of Pi as soon as 2 dpi (Fig. 10F). By contrast, both the zone above the primary root tip and the primary root tip itself were less permissive to F73 entry (Fig. 10G and J, respectively), although occasional infections occurred (Fig. 10H and K, respectively). The colonization score did not frequently reach the possible maximum above the primary root tip (Fig. 10I) and never in the meristem itself (Fig. 10L). Overall, it can be concluded that F73 enters Arabidopsis differentiation root parts rapidly after localized inoculation.

F73 triggers a spatial expansion of *CYP79B2* expression domain in roots

To probe the dynamics between F73 and the onset of Trp-metabolism, I examined two independent lines of Arabidopsis plants expressing a transcriptional reporter for Trp-derived defense metabolites. This consisted of a plasma membrane-localized fluorophore driven by the *CYP79B2* promoter (*pCYP79B2::SYP122-mScarlet)*.

Regardless of Pi, inoculation and time point, reporter-specific fluorescent signals were detected in the differentiation zones and lateral root emergence sites (Fig. 11A and B). Intriguingly, CYP79B2 expression was restricted to the inner root cylinder in mock conditions and at 0 and 1 dpi of F73 inoculation (Fig. 11C-G), suggesting a vascular or peri-vascular expression

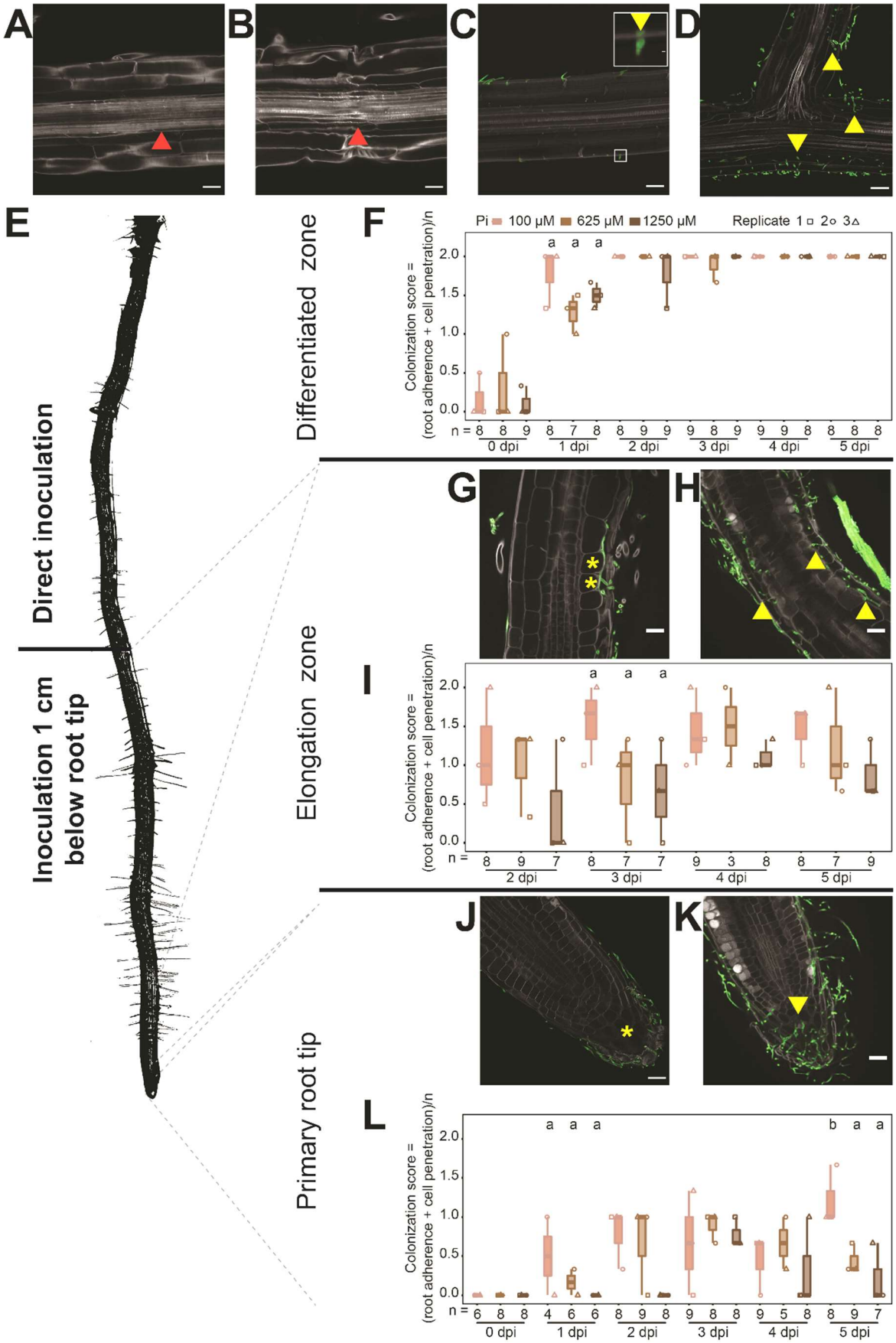
A
B
C
D
E
Direct inoculation
Inoculation 1 cm below root tip
Differentiated zone
Elongation zone
Primary root tip
F
Pi 100 µM 625 µM 1250 µM
Replicate 1 2 3
Colonization score = (root adherence + cell penetration)/n
n = 8 8 9 8 7 8 8 9 9 9 8 9 9 9 8 8 8 8
0 dpi 1 dpi 2 dpi 3 dpi 4 dpi 5 dpi
G
H
I
n = 8 9 7 8 7 7 9 3 8 8 7 9
2 dpi 3 dpi 4 dpi 5 dpi
J
K
L
n = 6 8 8 4 6 6 8 9 8 9 8 8 9 5 8 8 9 7
0 dpi 1 dpi 2 dpi 3 dpi 4 dpi 5 dpi

Figure 10: F73 efficiently infects and proliferates inside root cells below the hypocotyl regardless of Pi status. **A.** 100 µM Pi and **B.** 1250 µM Pi differentiation zones showing identical onset of secondary growth in terms of pericycle cell divisions (red arrowheads), n = 15 across 3 independent repeats each, scale bars = 20 µm. **C.** Maximum intensity projection of a root at 1 dpi, scale bar = 20 µm. Inset magnifies region framed in white, inset scale bar = 1 µm. Yellow arrowhead point to an hyphae fragment adhering to and initiating entry in an epidermal cell. **D.** Lateral root emergence site at 4 dpi, scale bar = 20 µm. Yellow arrowheads point to extensive F73 colonization. **E.** Root picture transformed into a black and white guide for the analysis of root zones permissiveness to F73 entry. **F.** Colonization score of the differentiation zone. Letters indicate statistical groupings of an ANOVA with post-hoc Tukey's HSD test with a p-value threshold of 0.05. **G.** F73 hyphae adhering to elongating root cells at 3 dpi, yellow asterisks mark intracellular infection-free plant cells, scale bar = 20 µm. **H.** F73 in elongating root cells at 4 dpi, yellow arrowheads point to intracellular infection events, scale bar = 20 µm. **I.** Colonization score of the elongation zone. Letters indicate statistical groupings of an ANOVA with post-hoc Tukey's HSD test with a p-value threshold of 0.05. **J.** Typical primary root tip at 3 dpi with infection restricted to the root cap, infection free region marked with a yellow asterisk, scale bar = 20 µm. **K.** Instance of primary root tip at 4 dpi, yellow arrowhead marks an intracellular infection, scale bar = 20 µm. **L.** Colonization score of the primary root tip. Letters indicate statistical groupings of a Kruskall-Wallis with post-hoc Dunn test (1 dpi) and a Mood test (5 dpi) with p-value thresholds of 0.05.

domain independent of Pi or time point. By contrast, at 2 dpi in presence of F73, the fluorescent signal appeared to widen and include outer tissues such as the cortex and/or the epidermis. For each differentiated root zone picture, the fluorescence signal intensity was measured across the root width and processed for plotting and statistical analysis (see methods). A F73-induced widening of the fluorescent signal was confirmed at 2 dpi regardless of Pi (Fig. 11I), indicating that *CYP79B2* expression domain expands to include at least the cortical cell layer.

F73 induces both PSR genes expression and Pi dependent immune dynamics and the *cyp79b2/b3* mutant shows perturbed glucosinolate metabolism and immunity

To follow up on the above-established dynamics of root colonization and *CYP79B2* expression patterns, we performed a whole-transcriptome analysis and investigated which PSR and GLS metabolism genetic networks underlie responses to F73. Whole root samples of Col-0 and *cyp79b2/b3,* were sampled for transcriptome profiling at 100 µM Pi or 1250 µM Pi, two and seven days after inoculation of F73 or mock.

Plotting of the plant transcriptome samples distances by PCA showed a clear separation according to harvest time and inoculation, but not Pi (Fig. 12A). Genotype weakly clustered F73-inoculated plants, but not mock, and this was more apparent at 7 dpi (Fig. 12A). Moreover, 4 samples were labelled "Probable outliers" on the PCA because of their clear dissimilarity from their expected groups (Fig. 12A).

Overall, only 4 out of 64 plant samples (6.25%) were identified as probable outliers. Because the 95% confidence interval was not calculated, whether these 4 samples are true outliers was not assessed and therefore they were not excluded from the analysis.

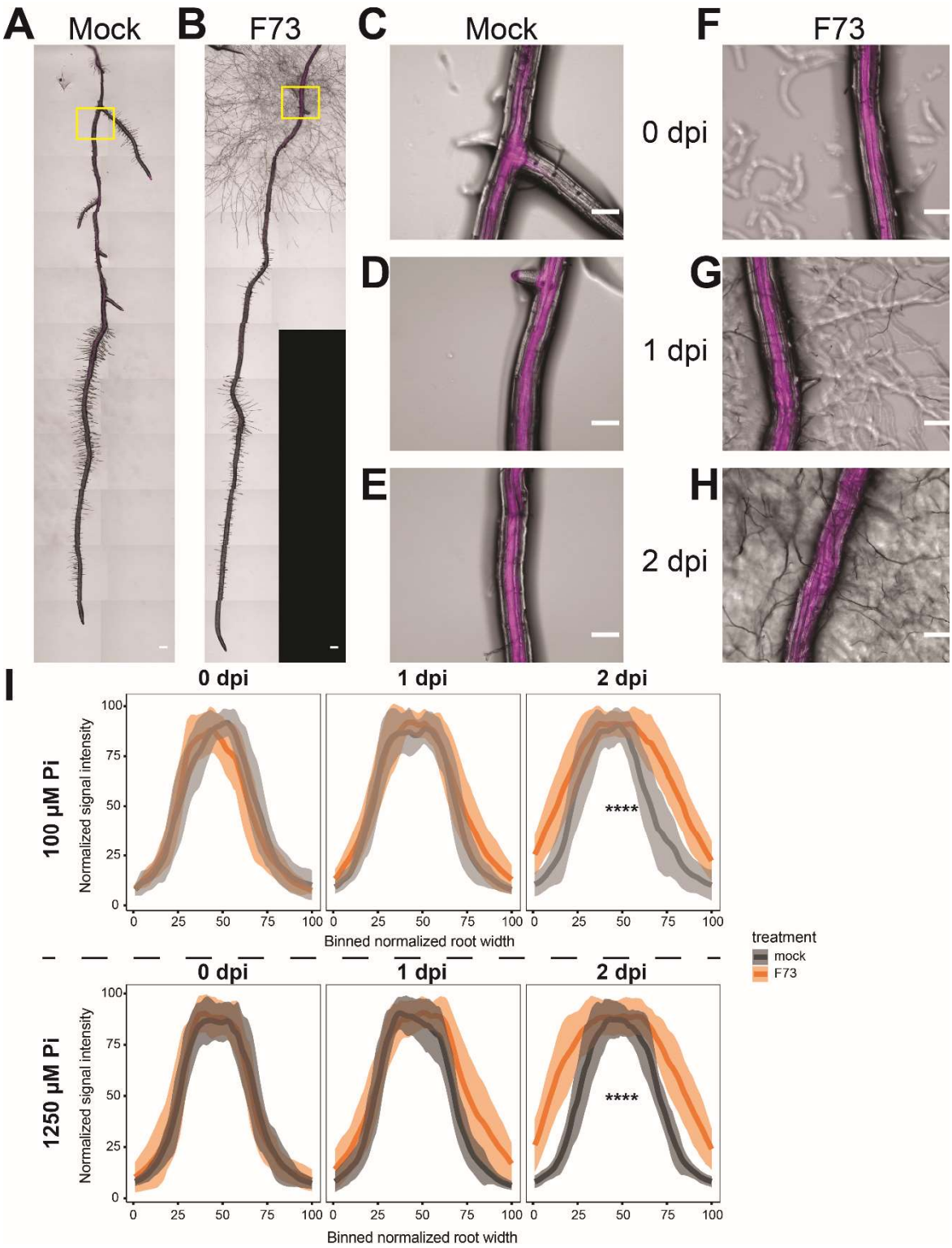

Figure 11: F73 induces an expansion of *CYP79B2* expression domain in *pCYP79B2:SYP122-mScarlett* #5 and #7 lines.

A. Stitched overview of a mock-treated root at 2 dpi. **B.** Stitched overview of a F73-treated root at 2 dpi. Scale bars = 100 µm. Yellow frame in **A.** and **B.** indicate the typically magnified zone. **C., D**. and **E.** Magnified mock-treated roots at the indicated time points. **F., G.** and **H.** Magnified F73-treated roots at the indicated time points. **I.** Quantification of fluorescent signal across binned normalized root widths. Thick lines indicate fluorescent signal average of F73- or mock-treated roots and areas surrounding the corresponding thick lines indicate standard deviation. Scale bars = 100 µm. Pictures shown are from line #5 at 100 µM Pi and are representative of the observed expression pattern regardless of line number or Pi concentration. Student tests in **I.** were performed on the area under the curve of F73- and mock-treated roots. Asterisks indicate p-values < 0.0001.

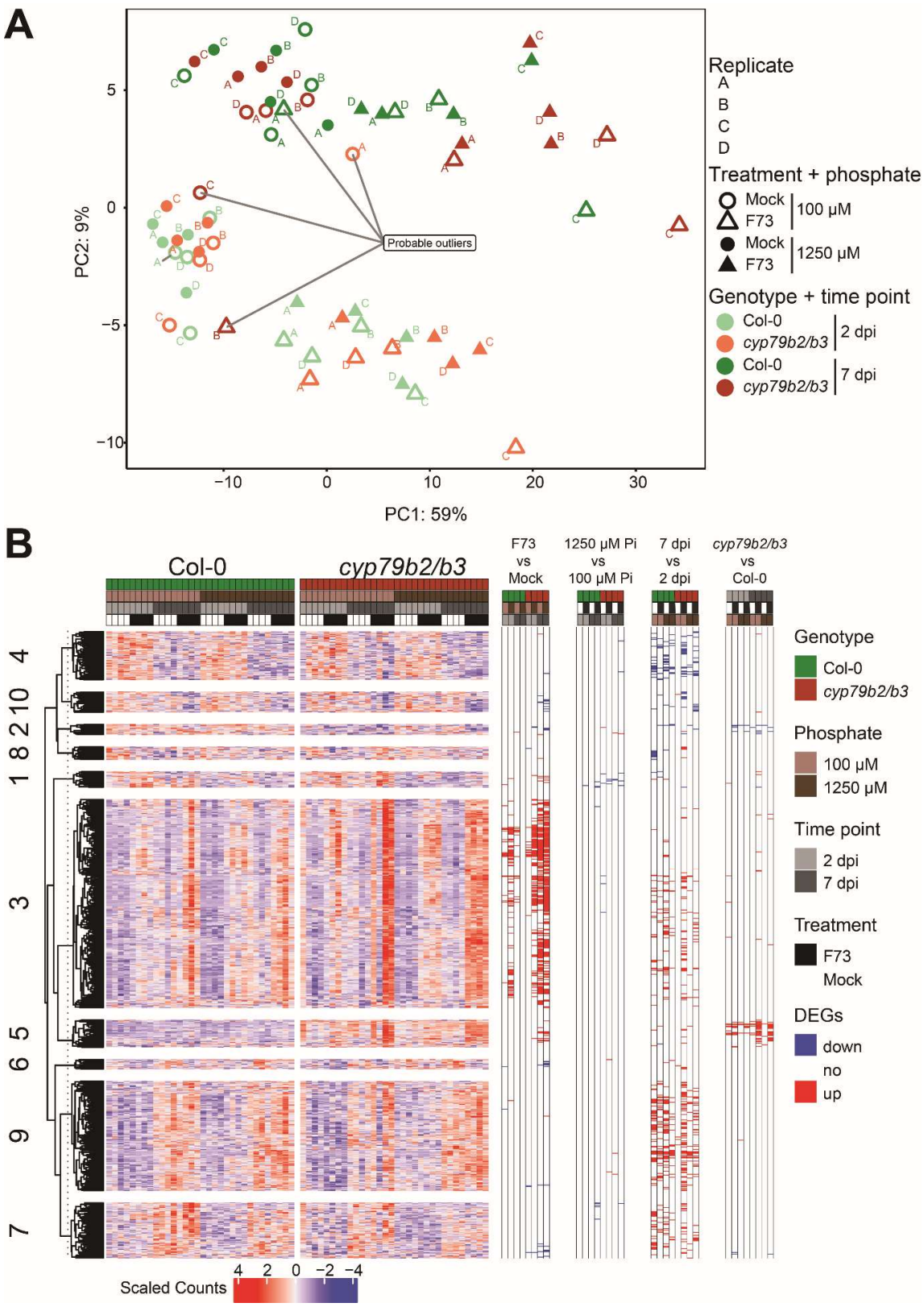

Figure 12: F73 and time point are responsible for most of the transcriptional changes in Arabidopsis Col-0 and *cyp79b2/b3*.
A. PCA plot of samples distances. **B.** Scaled counts (middle) of DEGs obtained by pairwise comparisons (right). Cluster obtained by *k*-means ($k = 10$) are shown as dendrograms (left).

Following *k*-means based clustering and counts scaling, a heatmap was constructed with plant differentially expressed genes (DEGs, total = 690 genes) scaled counts and conditions (Fig. 12B). Surprisingly, comparing 1250 µM Pi with 100 µM Pi within the combinations of other conditions resulted in few plant DEGs and therefore no clear Pi responsive cluster (Fig. 12B). However, this is coherent with the similar Col-0 root systems (Fig. 9) and F73 infection dynamics (Fig. 10) regardless of Pi concentration. Cluster 3 (c3) was the largest identified cluster with 272 genes responsive to F73 (Fig. 12B). Gene Ontology (GO) term analysis of c3 resulted in enrichment of responses to nitrogen compound, oxidative stress, hypoxia, Jasmonic Acid (JA) and processes related to indole-compounds and cell wall catabolism (Fig. 13A). C5 contained 37 genes and enriched in GO processes related to JA, sulfur and indole-containing compounds (Fig. 13B). Two clusters (c7 with 72 genes and c9 with 142 genes) were upregulated at 7 dpi regardless of Pi, inoculation or genotype (Fig. 12B). However, c7 was enriched in only two GO terms and cluster 9 enrichment was similar to c3 (not shown).

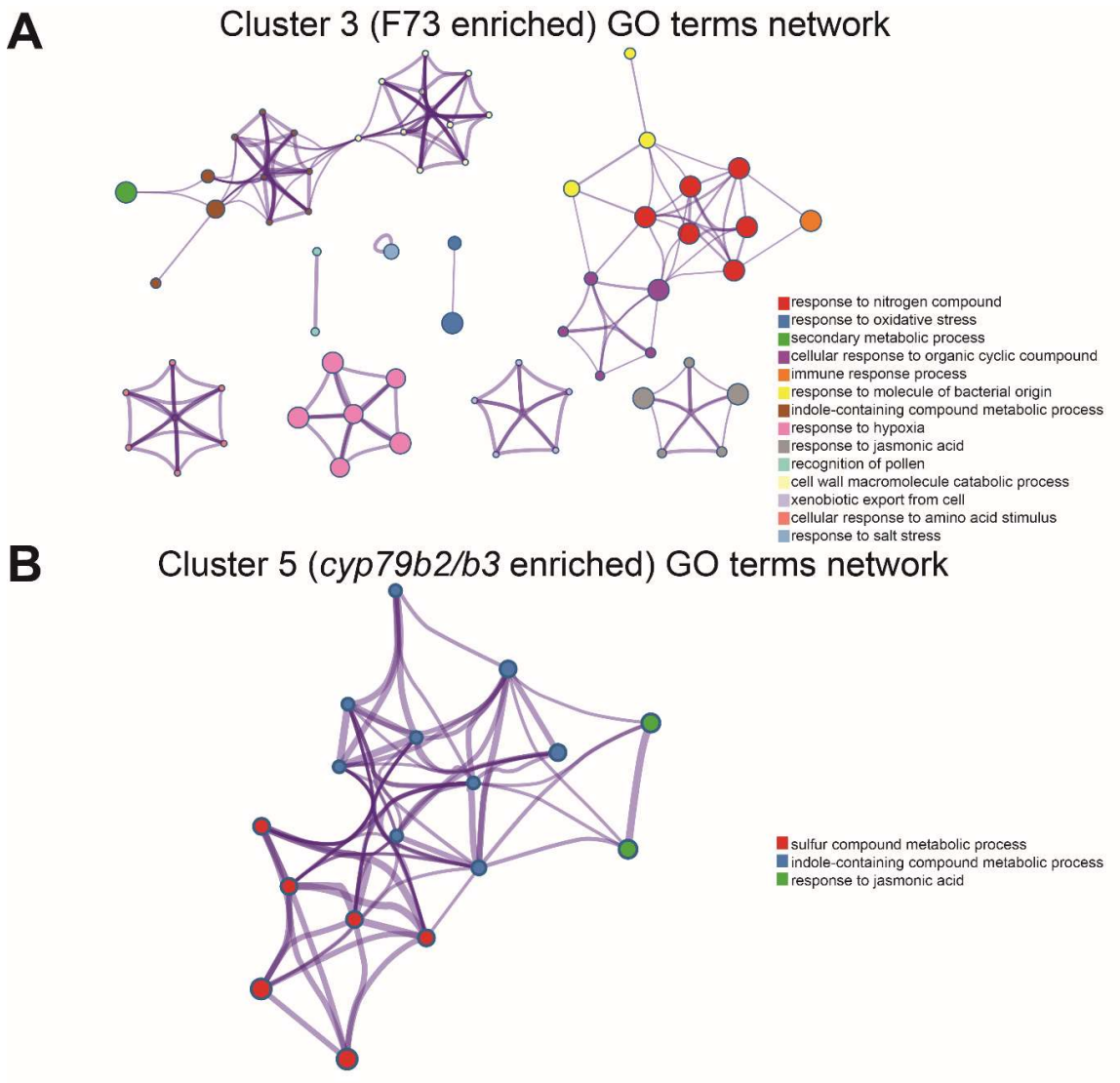

Figure 13: F73 and *cyp79b2/b3* responsive clusters are enriched for GO terms
A. GO terms enriched in Cluster 3. **B.** GO terms enriched in Cluster 5. Each node represent an enriched GO term colored by their cluster ID. Size of nodes represent the number of genes with the GO term and nodes share an edge when their similarity is > 0.3.

To better understand the PSR-GLS transcriptional dynamics, a heatmap targeted on the main PSR genes linked to immunity (Castrillo *et al*, 2017) and from an exhaustive GLS and camalexin genes inventory (Prof. Dr. Meike Burow, personal communication) was generated. Comparisons of 1250 µM Pi vs 100 µM Pi in Col-0 at 2 dpi revealed that *AT4* (positive PSR regulator) showed significantly higher expression at 100 µM Pi in presence of F73, but not mock (Fig. 14A). Other PSR genes (*SPX1* and *2, IPS1, PHT1.2* and *1.4* and *PHF1*) also became significantly differentially expressed in Col-0 at 7 dpi solely in presence of F73 (Fig. 14A). These pairwise comparisons indicate that, in our system, the Col-0 transcriptional levels of PSR genes were not strong enough to cross the fold-change and p-value cut-offs of DEGs analyses. However, F73 directly or indirectly activates the expression of PSR genes at 100 µM Pi. Unexpectedly, comparisons of Pi concentrations in the *cyp79b2/b3* mutant yielded PSR genes upregulated at 100 µM P regardless of treatment. In absence of F73, *AT4* and *SPX1* were significantly upregulated in *cyp79b2/b3* at 2 dpi, and *SPX2, IPS1, PHT1.2 and 1.4* were also induced at 7 dpi (Fig. 14A). Further within the frame of Pi concentrations comparisons, the *cyp79b2/b3* and Col-0 transcriptomes did not significantly differ in presence of F73. The observation that *cyp79b2/b3* shows activation of a part of the PSR in mock conditions could hint at an effect of Trp-derived metabolites on the PSR.

Next, the plant transcriptional changes due to the *cyp79b2/b3* mutation compared to Col-0 were analyzed. The present dataset provides us with an opportunity to discover potential compensatory mechanisms that might have been previously overlooked in *cyp79b2/b3* and therefore confounded the roles of Trp-derived metabolites. GLS related genes such as *CYP83B1*, *GSTF9,* myrosinases (*MBP1* and *2*) (Fig. 14A) and Trp related genes such as *TSB2*, *IGPS* and *TSA1* (not shown) were consistently induced across conditions in *cyp79b2/b3*. Sulfotransferases (indole-inclined *SOT16* and aliphatic-inclined *SOT17*) that catalyse sulfate group transfer to desulfo-GLS (Klein *et al*, 2006) were also constitutively induced except at 7 dpi in mock conditions (Fig. 14A). Additionally, JA-signaling genes such as *JAZ5*, *JAZ9*, *JAZ13* and *AOC2* were consistently upregulated in *cyp79b2b3*, whilst *VSP2* was downregulated (not shown). These data reveal that *cyp79b2b3* shows constitutively higher expression of genes involved in both Trp and GLS synthesis and constitutively altered JA-signaling compared to Col-0.

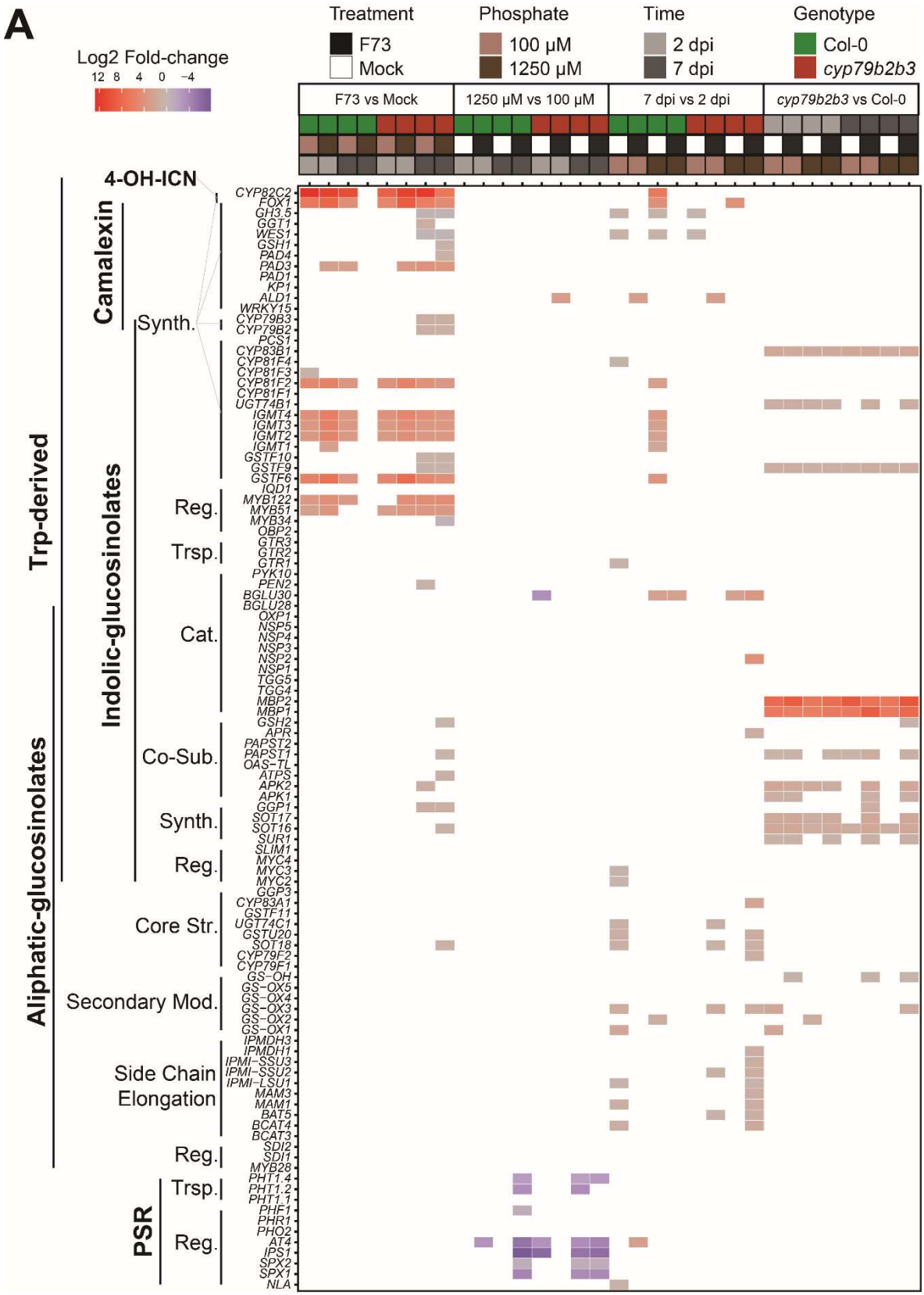

Figure 14: Phosphate Starvation Response (PSR), glucosinolate (GLS) and Tryptophan (Trp) metabolism genes expression profiles in pairwise comparisons

A. Comprehensive heatmap of PSR, GLS and Trp-metabolism genes expression changes. Role of genes is displayed as abbreviations: Reg. = Regulation, Trsp. = Transporter, Secondary Mod. = Secondary modification, Cor Str. = Core Structure, Synth. = Synthesis, Co-Sub. = Co-Substrate related, Cat. = Catabolism. White rectangles indicate p-adj > 0.05.

Perturbed JA signaling in *cyp79b2/b3* could be responsible for the induction of glucosinolates related genes (Harun *et al*, 2020). Alternatively, JA also influences developmental pathways in roots (Jang *et al*, 2020). Interestingly, *MRD1*, a gene downregulated in the soluble methionine over-accumulator *mto1-1* mutant (Singh *et al*, 2022), was systematically downregulated in *cyp79b2/b3* (not shown). The downregulation of *MRD1* suggests an increase in soluble methionine perhaps channelled into aliphatic-GLS biosynthesis. However, no aliphatic-GLS biosynthesis specific enzyme was detected as constitutively upregulated in *cyp79b2/b3* (Fig. 14A).

Lastly, F73-induced genes were examined by comparing F73 and mock conditions. Pi concentration was a governing factor in the number of F73-induced genes in a time point dependent manner (Fig. 12B). Namely, at 2 dpi, more genes were F73-induced at 1250 µM Pi than at 100 µM Pi in Col-0 (219 vs. 73, respectively) and in *cyp79b2/b3* (274 vs 51, respectively) (Fig. 15). The opposite was true at 7 dpi only in Col-0, with 1 and 48 genes F73-induced at 1250 µM Pi at 100 µM Pi, respectively (Fig. 15A). At 7dpi, the *cyp79b2/b3* maintained a larger transcriptional response, as F73 induced 411 and 333 genes at 1250 µM Pi and 100 µM Pi, respectively (Fig. 15A). Mainly, genes robustly induced by F73 include Trp metabolism genes (*e.g. MYB51/122, CYP82C2*, *IGMT4, FOX1, IGMT2-4* and *PAD3*) (Fig. 14A), *WRKY* transcription factors, cell-wall associated genes (*WAK3/5* and *EXT19*), class III peroxidases and TIR-domain containing genes (*TN3/7/9/11*) (not shown). Within Trp-metabolism genes, the *FOX1-CYP82C2* module stood out as robustly displaying higher expression (Fig.14A), suggesting a preferential synthesis of 4-OH-ICN compared to camalexin or indolic-GLS. Overall, F73 induces an immune response stronger in Pi replete roots compared

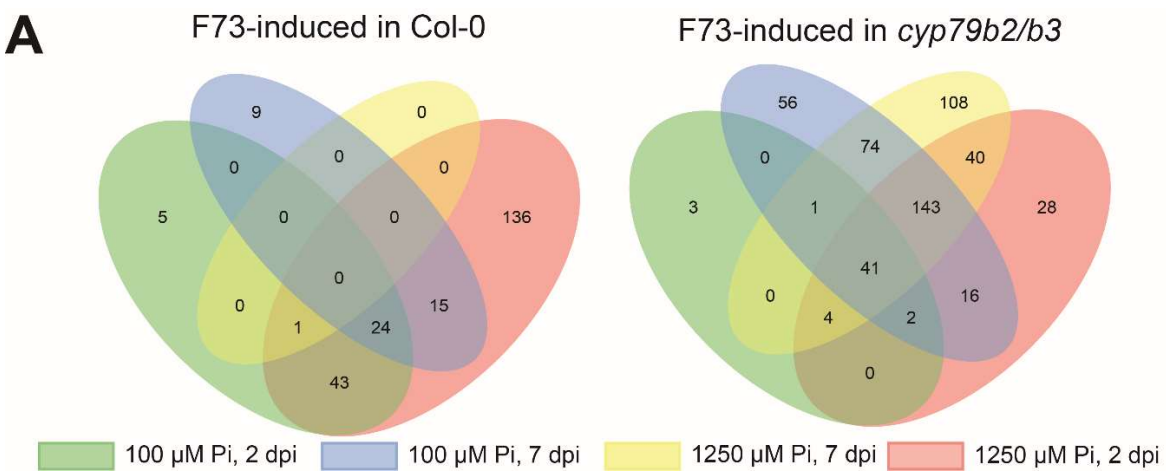

Figure 15: Pi status-dependent F73 responses dynamics in Col-0 but not *cyp79b2/b3*
A. Venn diagrams of genes upregulated in response to F73 in Col-0 and *cyp79b2/b3*.

to Pi limited roots at 2 dpi. Then, in Col-0 at 7dpi, an immune response was still observable at 100 µM Pi but not 1250 µM Pi. This suggests either a PSR-dependent deployment rate of root immunity or that, at 7 dpi, F73 suppresses immunity at 1250 µM Pi but not at 100 µM Pi. The immune responses persisting in the *cyp79b2/b3* mutant at 7 dpi suggests a drastically different interaction with F73 compared to Col-0, potentially imparted to an altered F73 behavior in absence of Trp-derived metabolites.

F73 modulate GLS profiles in a Pi and organ dependent manner

We next asked whether GLS profiles are altered by Pi and/or F73. To this end, we measured indole- and aliphatic-GLS in shoots and roots of Col-0 using Ultra High Pressure Liquid Chromatography coupled to Mass Spectrometry (see methods). PCA analysis of GLS profiles revealed a clear separation according to organ and time point, but not Pi or F73 treatment (Fig. 16A).

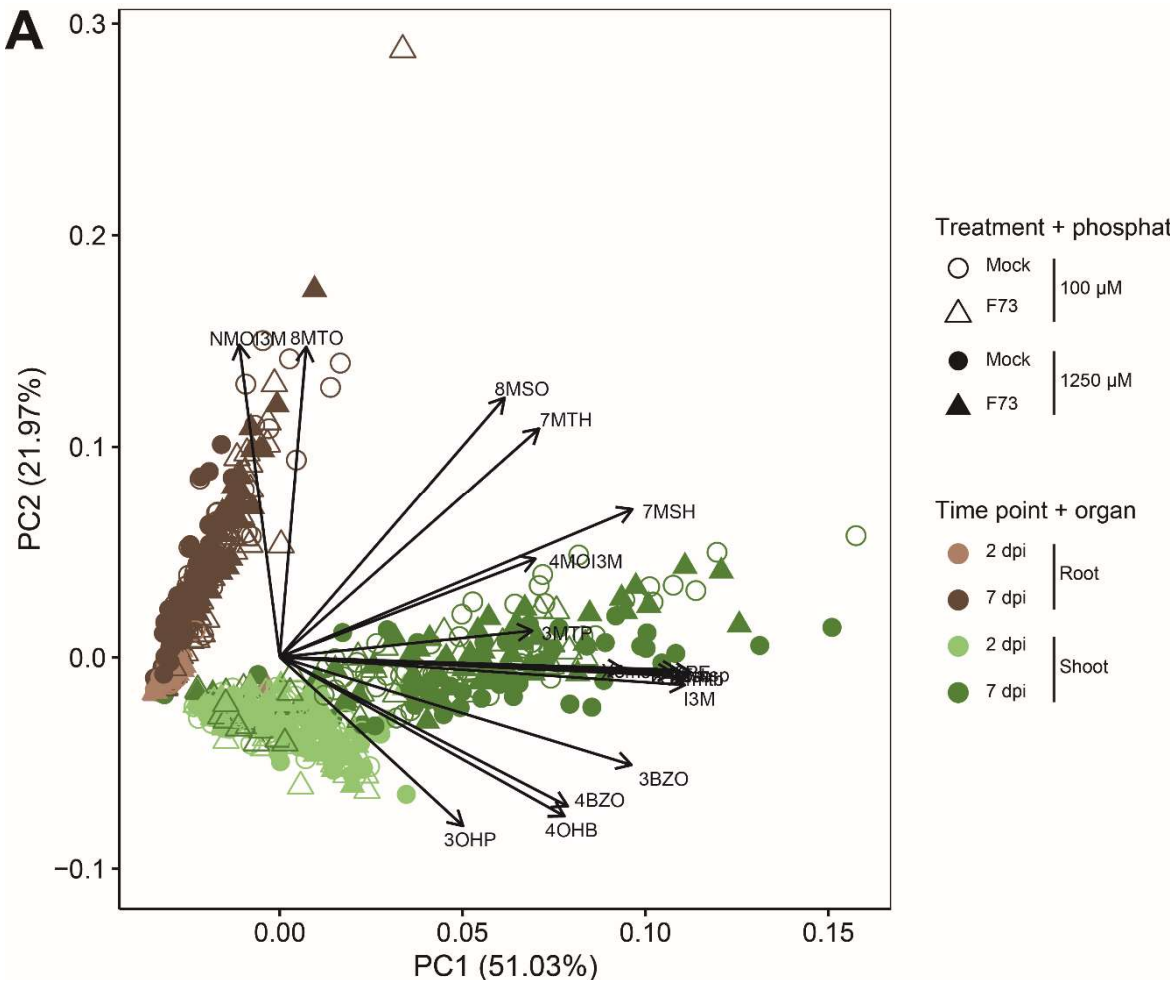

Figure 15: Timepoint and organ cluster Col-0 glucosinolates (GLS) profiles
A. PCA plot of GLSs profiles.

Strikingly, a PERMANOVA analysis revealed that 35% of the GLS profiles variance was unexplained (R2 column, "Residual") (Table 1). Experiment replicate accounted for less than 0.2% of variance (Table 1), whereas organ and time point accounted for 28% and ~21.4% of variance, respectively (Table 1). Pi, treatment, and the Pi-treatment interaction were responsible for approximately 0.4%, 0.25% and 0.1% of variance, respectively (Table 1). Effects of the same magnitude held true including when shoots and roots, and their respective 7 dpi sub-datasets, were analyzed separately (not shown). Overall, the PERMANOVA suggests that Pi and F73 have only minor impacts on overall GLS profiles in our experimental setup.

	Df	SumOfSqs	R2	F	Pr(>F)
organ	1	12864.676	0.2800838	600.02017	0.001
timepoint	1	9820.9497	0.2138172	458.05801	0.001
phosphate	1	189.61131	0.0041281	8.8436436	0.001
treatment	1	111.95549	0.0024374	5.2217056	0.005
replicate	1	78.744619	0.0017144	3.6727205	0.032
organ:timepoint	1	5778.2614	0.1258016	269.50336	0.001
organ:phosphate	1	187.651	0.0040855	8.7522131	0.001
timepoint:phosphate	1	101.04959	0.0022	4.7130444	0.007
organ:treatment	1	118.06096	0.0025704	5.5064705	0.009
timepoint:treatment	1	172.81866	0.0037625	8.0604193	0.001
phosphate:treatment	1	62.657955	0.0013642	2.9224239	0.059
organ:timepoint:phosphate	1	95.093635	0.0020703	4.4352535	0.014
organ:timepoint:treatment	1	174.73574	0.0038043	8.1498334	0.001
organ:phosphate:treatment	1	27.463779	0.0005979	1.2809356	0.279
timepoint:phosphate:treatment	1	57.935831	0.0012614	2.7021797	0.084
organ:timepoint:phosphate:treatment	1	30.999951	0.0006749	1.4458658	0.228
Residual	749	16058.864	0.3496262	NA	NA
Total	765	45931.53	1	NA	NA

Table 1: A PERMANOVA on GLS profiles reveals subtle influence of Pi, F73 and Pi-F73 interaction in altering GLS profiles.

To map which GLS metabolites were affected in what way by Pi and treatment, F73 effect sizes (Cohen's d) were plotted on a heatmap, allowing tandem comparison of Pi concentrations nested within corresponding organs and time points. F73 effect sizes were mostly small or negligible at 2 dpi regardless of organs (Fig. 17A). Strikingly, the indolic 4-hydroxy-3-indolylmethyl (4MOI3M) showed consistent medium to large F73 effect sizes regardless of Pi and organ (Fig. 17A), indicating that F73 robustly induce 4MOI3M accumulation. For indolic-, all long chained and few short chained aliphatic-GLS at 7 dpi, F73 effect sizes were noticeably reversed in roots at 1250 µM Pi compared to shoots at 100 µM Pi (Fig. 17A), suggesting root and shoot GLS profiles respond differently to Pi and F73.

Finally, amounts of GLS selected as representative of diverse groups (short chained, long chained oxidized/reduced aliphatic and indolic) were visualized, focusing on the 7 dpi time point. Interestingly, the amounts of the short chained aliphatic-GLS 3BZO and 4MTB showed similar F73-induced Pi dependent shoot depletion but Pi independent root increase (Fig. 17B).

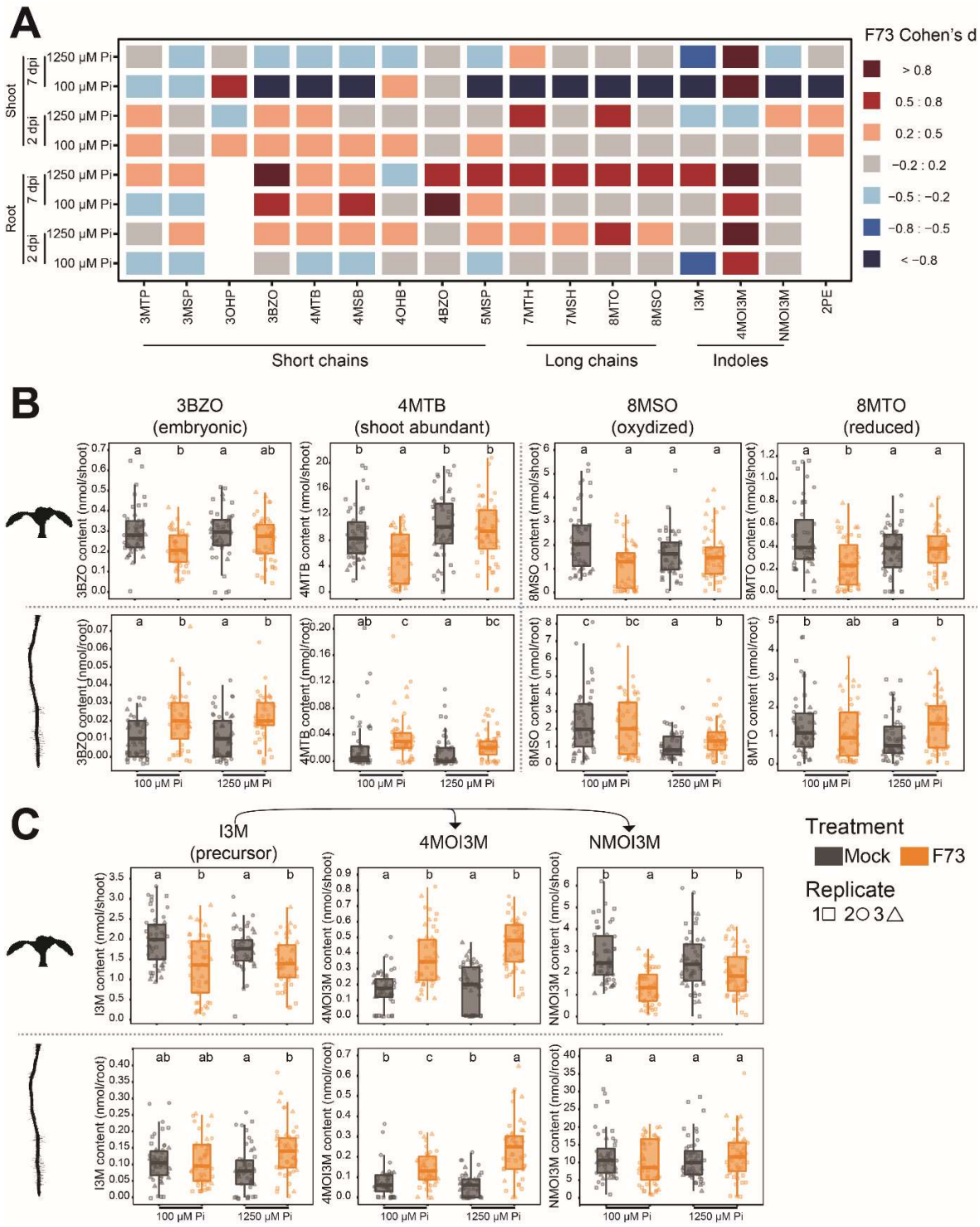

Figure 17: Pi impacts F73-induced GLS profiles in an organ dependent manner
A. F73 effect sizes (Cohen's d = (F73mean – Mockmean) /pooled standard deviation). **B.** Representative aliphatic-GLS and **C.** indolic-GLS raw amounts per organ at 7 dpi. Letters represent statistical groupings based on pairwise comparison according to Mood tests except root NMOI3M (Kruskal Wallis) and shoot 4MTB (ANOVA) with p-value thresholds of 0.05.

Because 3BZO is not *de novo* synthesized in seedlings of Arabidopsis Col-0 (Kliebenstein *et al*, 2007) and 4MTB main site of synthesis is shoots (Meier *et al*, 2019), the concomitant shoot decrease and root increase suggest either shoot to root translocation and/or a decline of breakdown rates. Notably, 8MSO and 8MTO followed the same pattern in shoots (Fig. 17B). Further, it was remarkable that the amounts of these long chained aliphatic-GLS were higher at 100 µM Pi compared to 1250 µM Pi in roots without F73 (Fig. 17B), suggesting a constitutive effect of the PSR on the synthesis of long chained aliphatic-GLS in roots. Conversely, F73 inoculation imparted a statistically significant increase in root 8MSO/8MTO amounts at 1250 µM Pi but not 100 µM Pi (Fig. 17B). The indolic I3M was also depleted in shoots upon F73 inoculation regardless of Pi, similar to one of its derivatives NMOI3M (Fig. 17C). In roots, a significant I3M increase was detected only at 1250 µM Pi, whilst NMOI3M amounts were stable and 4MOI3M increased in both roots and shoots regardless of Pi (Fig. 17C). It is tempting to speculate that, upon F73 inoculation, I3M is preferentially channelled into 4MOI3M synthesis in shoots and roots. Accordingly, the parallel stability of I3M and NMOI3M amounts in roots would also reflect an increase in their respective synthesis rates. Overall, the distinct effects of Pi and F73 on the diverse GLS types hint at an influence of the PSR on GLS translocation, synthesis and breakdown rates.

4MOI3M amounts stood out as robustly increasing upon F73, therefore I assessed whether commercially available 4MOI3M-K salt would impair F73 growth in liquid Minimal Medium supplemented with Artificial Root Exudates (ARE). No differences in F73 growth were observed along a concentration gradient over 4 days, suggesting an inert version 4MOI3M can neither inhibit nor be utilized by F73 *in vitro* (Fig. 18A).

Trp-derived compounds interfere with F73 growth rate and virulence at the transcriptional level

To deepen our understanding of the above-described F73-immunity dynamics and to discover fungal responses to Trp-derived metabolites, we re-analyzed our transcriptomic data and performed a dual mapping of the reads to Arabidopsis or F73 genomes. In terms of numbers of fungal reads, no major differences could be imparted to either Pi, genotype or time point (Fig. 19A). Plotting of F73 transcriptome profiles revealed clear clustering according to genotype and time point, but not Pi (Fig. 19B). Therefore, we carried out a DEG

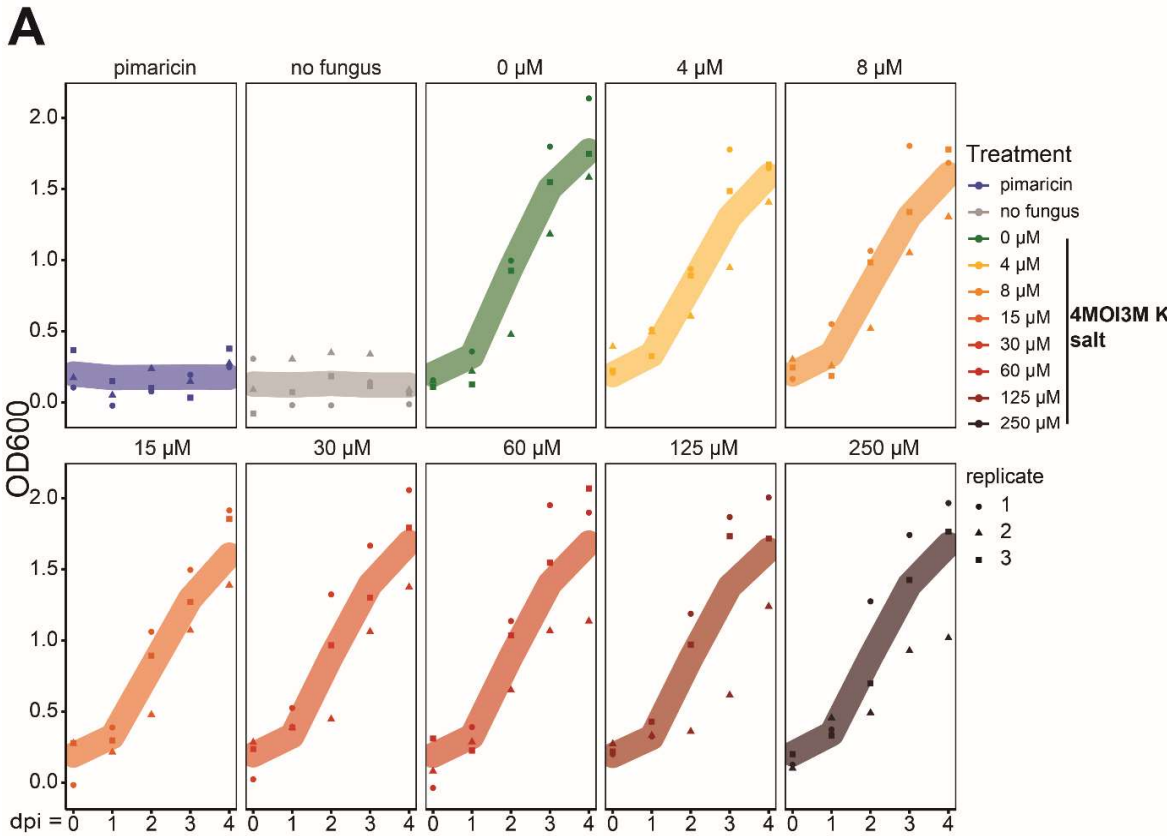

Figure 18: 4MOI3M-K salt does not inhibit F73 growth in liquid Minimal medium supplemented with Artificial Root Exudates

A. Time course monitoring F73 growth by OD600 measurment at the different indicated 4MOI3M-K salt concentrations or 0.1 mg/ml pimaricin (antifungal agent). Line represent the average of the displayed 3 points.

analysis of F73 inoculated on *cyp79b2/b3* versus Col-0. A core set of 37 and 10 genes were robustly up or down regulated in *cyp79b2/b3*, respectively (Fig. 20A). Gene sequences from this core set were submitted to manual annotation curation following the Joint Genome Institute (JGI) Mycocosm protein annotation pipeline (Grigoriev *et al*, 2014). Protein annotation of the core set was successful (except for 1 gene) and revealed that up regulated genes in *cyp79b2/b3* are mostly related to, for example, the TCA cycle and amino acid metabolism (Fig. 20B).

Conversely, 4 out of the 10 genes downregulated were annotated as "NmrA-like family" (Fig. 20B), which are implicated in filamentous fungi nutrition and pathogenicity (Peng *et al*, 2022; Li *et al*, 2021). These observations suggest that, F73 is more metabolically active in *cyp79b2/b3* compared to Col-0. Genes up regulated also contained 8 predicted effector proteins, potentially translocated via the canonical or non-canonical secretion pathways (Fig. 20B). Overall, DEGs analysis on F73 transcriptome gathered evidence that Trp-metabolism robustly affects energy utilization and the expression of predicted effectors in the fungus.

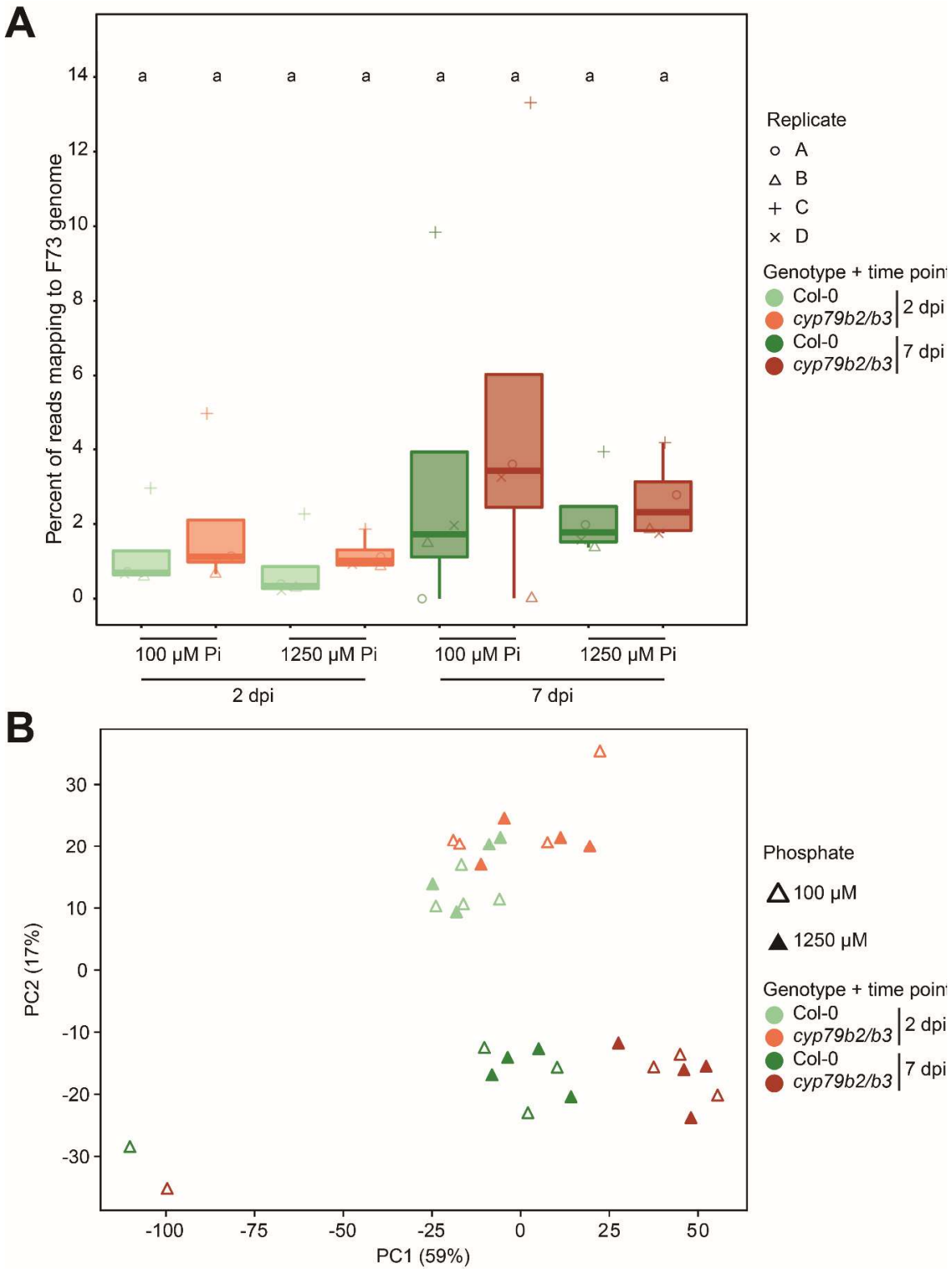

Figure 19: Reads mapping to F73 genome
A. Percent of reads (total per sample = 20 000 000 reads) in F73-inoculated samples mapping to F73 genome. Letters represent statistical groupings according to a Kruskall-Wallis test with p-value threshold of 0.05. **B.** PCA plot of samples distances.

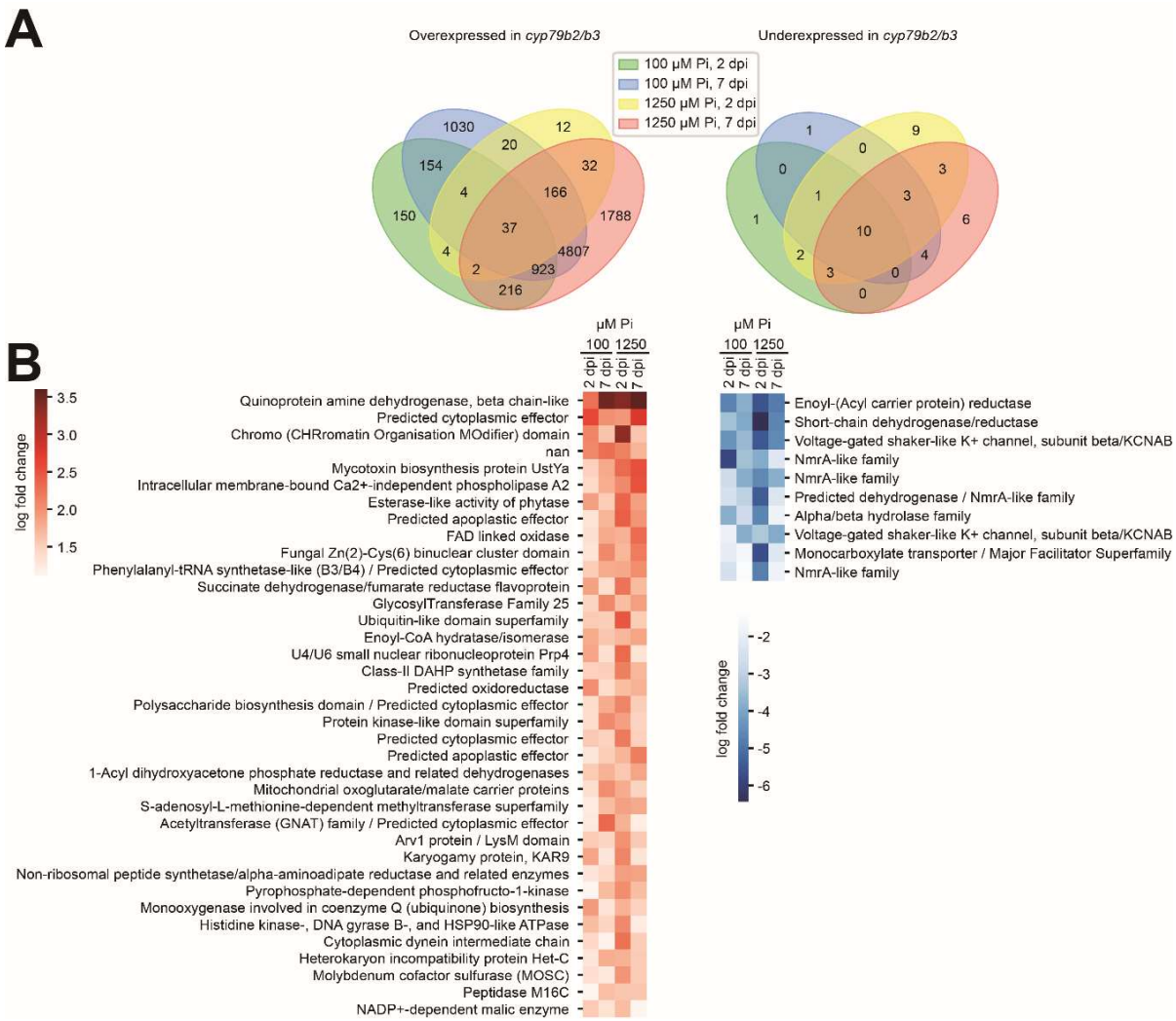

Figure 20: Genetic depletion of Trp-derived metabolites robustly deregulate virulence and energy metabolism in F73.
A. Venn diagrams showing the number of F73 genes more highly or less expressed in the *cyp79b2b3* mutant compared to Col-0. **B.** Heatmap of F73 proteins highly or less expressed across all conditions in the *cyp79b2b3* mutant.

Genetic depletion of Trp-derived metabolites or aliphatic-GLS does not perturb the Arabidopsis-F73 homeostasis in short term agar plate assays

The *cyp79b2/b3* and the aliphatic-GLS depleted *myb28/29* double mutants were tested for altered interaction with F73 compared to Col-0. Compared to their respective mock controls, F73 inoculated mutants were not distinct from Col-0 in terms of shoot fresh weight (Fig. 21A) and intraradical F73 biomass (Fig. 21B). Thus, in our setup, within the timeframe examined and irrespective of P status, the interaction with F73 appears to not be destabilized by the lack of either Trp-derived metabolites or aliphatic-GLS. To confirm this observation, a long-term (4 weeks post inoculation of seeds) Gnotobiotic soil-matrix experiment was conducted ("flow-

pot", see methods and (Kremer et al, 2021)). Whereas F73 was expected to be overall neutral, I introduced a flow-pot "pathogen control" (F134, Neonectria radicicola) detrimental to Col-0 (Durán et al, 2018) and enriched in *cyp79b2/b3* roots (Wolinska et al, 2021). In an isolated experiment repetition, F73 inflicted genotype-dependent penalties in terms of shoot fresh weight (Fig. 22A and B) and normalized chlorophyll content (Fig. 22A and C). Surprisingly, and despite the absence of bacterial contamination in all pots (not shown), F134 was not detrimental to Col-0 but completely killed *cyp79b2/b3* (Fig. 22A, B and C). However, these results could not be replicated as in subsequent attempts both fungi killed all plants regardless of genotype (Fig. 22A). A more thorough assessment of the role of Trp-derived metabolites or aliphatic-GLS in Arabidopsis-F73 interactions should be pursued in future work.

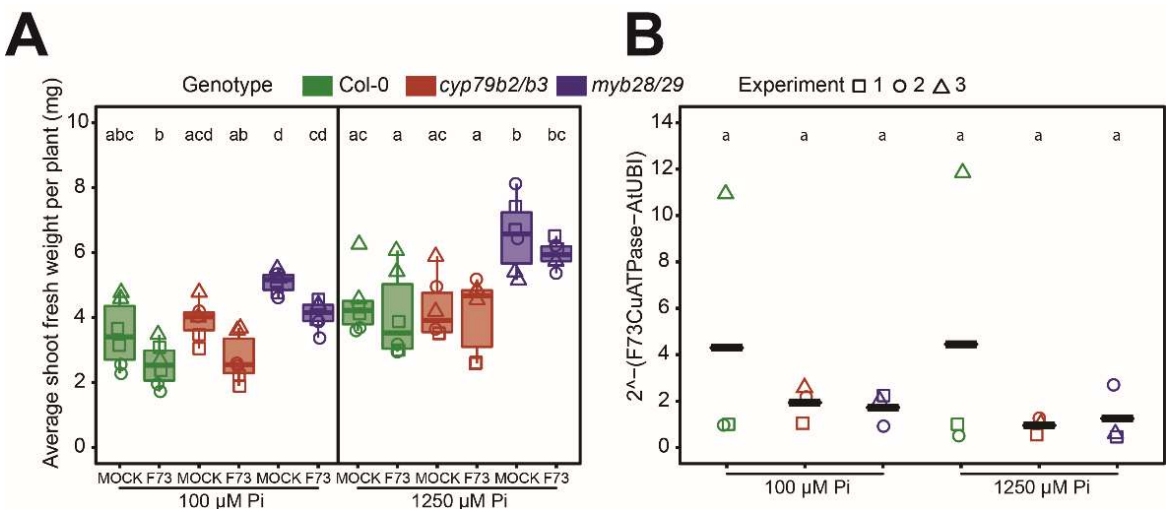

Figure 21: No contributions of Trp-derived metabolites or aliphatic-glucosinolates to interactions with F73 in short term assays on agar plates.
A. 7 dpi shoot fresh weights and **B.** intraradical F73 biomass. Letters indicate statistical groupings using p-value thresholds of 0.05 in **A.** using ANOVA with post-hoc Tukey's HSD tests and in **B.** Kruskal-Wallis with post-hoc Dunn tests.

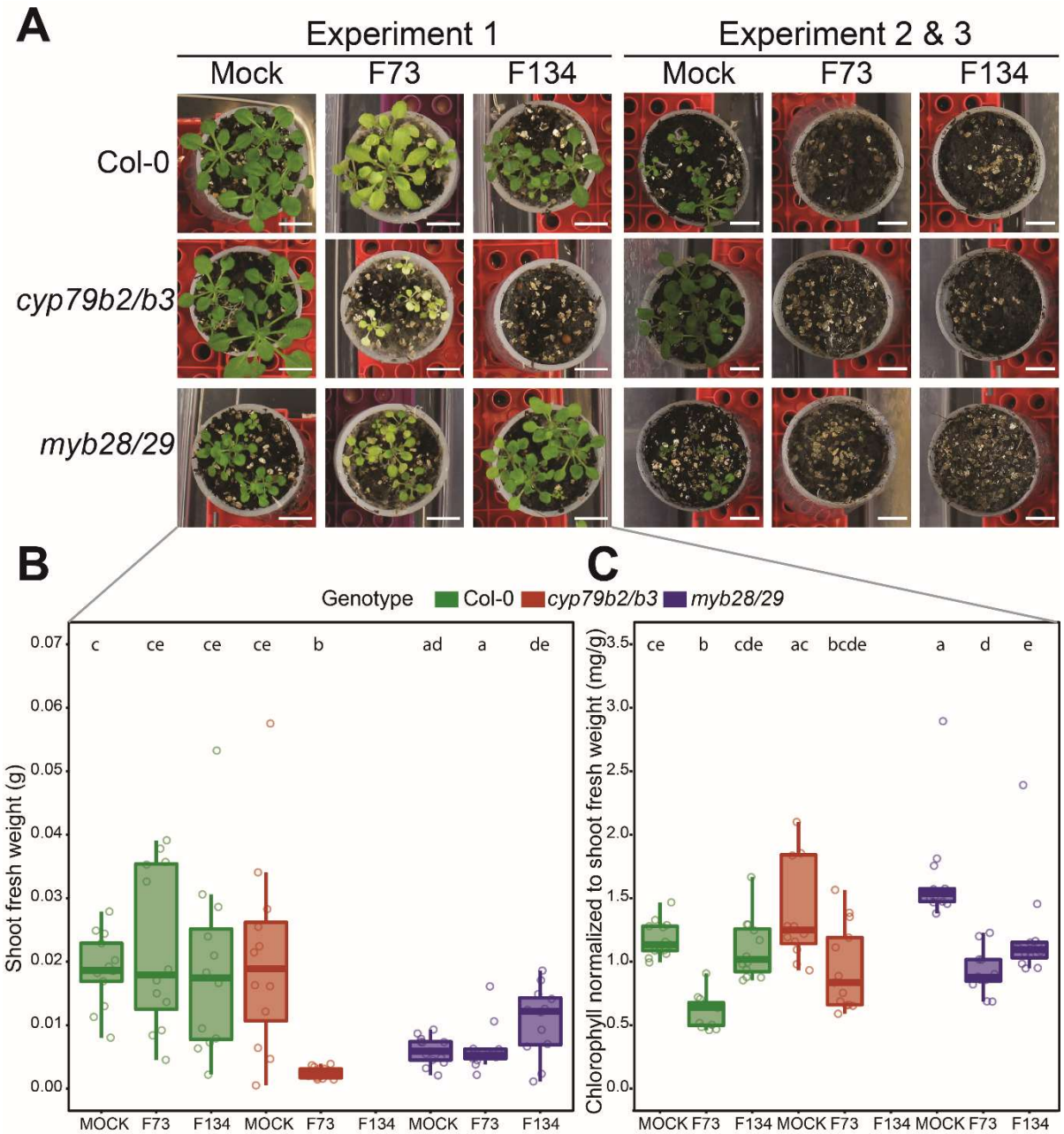

Figure 22: F73 and F134 kill plants regardless of genotype in bipartite interaction in the flow-pot system
A. Pictures of flow-pots above ground parts 4 weeks post inoculation. **B.** shoot fresh weights and **C.** normalized chlorophyll content from experiment 1 in **A.** Letters indicate statistical groupings from Mood tests in **B.** and **C.** using p-value thresholds of 0.05.

Discussion

Lack of harmful effects of Sebacinales on the *cyp79b2/b3* mutant and technical limitations of the present study

Many plant-fungi interactions involve fungal hyphae entering plant cells and establishing biotrophy. In the first chapter of this thesis, I planned to test whether Arabidopsis root immune pathways are responsible for regulating such interactions. However, I could not replicate the published *cyp79b2/b3* phenotype, and therefore abandoned this research question and Sebacinales as model fungi.

The results in chapter 1 were unexpected because mutations in *cyp79b2/b3* caused a robust phenotype, including with Sebacinales in previous studies (Nongbri *et al*, 2012; Lahrmann *et al*, 2015). The *cyp79b2/b3* genotype was validated by PCR (not shown), suggesting one or more technical issues. Moreover, up to 60 plants were employed per condition (*i.e.* timepoint * treatment * genotype) per experiment repetition, which should improve detection of phenotypes. Besides day/night cycles, media and temperature parameters, it is possible that light source type or quality were critical factors impairing replication of published results with Sebacinales. However, all experiments were conducted in the same type of growth chamber in which *Colletotrichum tofieldae* became detrimental in *cyp79b2/b3* roots (Hiruma *et al*, 2016; Frerigmann *et al*, 2021), suggesting that the non-replication of published results is caused by an unknown issue.

Nevertheless, due to their broad host-range, Sebacinales represent a promising model to study the mechanisms of intracellular hyphae accommodation and root colonization. The ability of Sebacinales to infect numerous plants ultimately allows comparative studies using distinct plants to refute or support lineage-specific immune mechanisms regulating colonization by filamentous fungi.

Although agar plates present the advantages of nutrient modulation, easy access to roots for harvest, location-specific inoculation/treatments and whole root systems imaging, they differ substantially from natural or field-like conditions. ((Kremer *et al*, 2021; Ma *et al*, 2019) and references therein). First, root systems growth is two-dimensional on the surface of agar plates

and exposed to light as opposed to three-dimensional in opaque soil-like matrixes. Second, agar can interfere with precision imaging such as confocal microscopy because it is not a completely transparent solidifying agent. Third, easy access to nutrients (and perhaps to O_2) can cause high microbe proliferation on agar, especially filamentous fungi (Fig. 6A). An innovative study designed a "transparent soil" built from a combination of alginate beads and liquid media (Ma *et al*, 2019). The transparent soil allows confocal microscopy, modification of nutrient concentrations, sources and homogeneity while providing a three-dimensional matrix recapitulating soil-like root architecture and mechanical properties (Ma *et al*, 2019). Unfortunately, in a few preliminary attempts, Arabidopsis did not germinate well nor was readily transferred and subsequently grown in transparent soil (not shown). After optimization of germination, Arabidopsis could be co-cultured on transparent soil with microbes, which would provide a greater structural and physiological relevance to root colonization or live imaging.

Root immune competence guides fungi colonization

The interplay between development and immunity is probably a key factor in structuring and harnessing the root microbiota. I observed that the differentiation zone (DZ) was clearly more permissive to F73 intracellular colonization compared to the root apical meristem (RAM) or the elongation zone (EZ) (Fig. 9). Similarly, *S. indica* preferentially colonizes the DZ (Lahrmann *et al*, 2013). One could expect that a relative paucity of colonization in the RAM and EZ would be underpinned by strong immune responses to fungi. Instead, *CYP79B2* expression is absent from the RAM and EZ (Fig. 10) as are responses to chitin (Millet *et al*, 2010). Fungal colonization of plant tissues and cells relies heavily on i) secretion of effector proteins for plant defense suppression and ii) carbohydrate-active enzymes (CAZymes), including plant cell wall degrading enzymes (Mesny *et al*, 2021; Lo Presti *et al*, 2015; Redkar *et al*, 2022a, 2022b). Specific CAZymes families predicted to target cellulose, xylan and pectin arose as genomic signatures of endophytism in Arabidopsis fungal root endophytes, including F73 (Mesny *et al*, 2021). Considering that Arabidopsis cell wall composition varies depending on the root zone considered (Wilson *et al*, 2015; Somssich *et al*, 2016), it is likely that CAZymes from fungal endophytes operate more efficiently in the DZ. By contrast with responses to fungi, root immune responses to bacteria are mostly restricted to the EZ and RAM (Zhou *et al*, 2020; Emonet *et al*, 2021; Millet *et al*, 2010). Interestingly, within the larger context of microbiota reconstitution experiments with fungi and bacteria, fungal communities alone are detrimental to plants but presence of bacteria rescue plant growth mostly via antagonism towards fungi

(Durán *et al*, 2018). Although the spatial localization of microbes in these reconstitution experiments was not examined, it is tempting to speculate that root development and immunity are tightly coordinated to optimize microbiota assembly and plant health. Relatively young cells in the RAM and EZ would ward off fungal infections i) with cell wall features resistant to fungal CAZymes and ii) by appropriately recruiting bacterial communities. Once these cells aged and differentiated, their cell wall and immune potential would be reshaped in concert to allow fungal accommodation.

Phosphate availability changes immune dynamics

In plant-fungi interactions, the relationship between the ancient Phosphate Starvation Response (PSR) network (Rubio *et al*, 2001; Rico-Reséndiz *et al*, 2020) and relatively recent immune repertoires is unclear. I therefore aimed to test whether the PSR fine-tunes immune outputs at the metabolite level by choosing aliphatic-and indole-glucosinolates (GLS) as "defense" readouts and a strain of *Truncatella angustata* (F73) as an endophyte functionally linked to phosphate (Pi) (Fig. 2B) (Mesny *et al*, 2021). I did not observe an influence of Pi on all aspects of the Arabidopsis-F73 interaction. Pi concentration did not alter F73 colonization dynamics (Fig. 10), spatio-temporal dynamics of the *CYP79B2* promoter (Fig. 11), GLS-related gene expression (Fig. 14) nor overall GLS profiles (Fig. 16). However, Pi impacted the number of immunity-related F73-responsive genes in Col-0 roots in a temporally dependent manner (Fig. 15A and Fig. 23). This is a significant find because PSR literature has so far focused on single time point measurements (Castrillo *et al*, 2017; Pant *et al*, 2015; Barragán-Rosillo *et al*, 2021). Moreover, the present study is unique in the sense that it examined early time points after fungal inoculation in relatively young seedlings (14 days old maximum). The dynamics of early signaling events can have a strong effect on the outcomes of plant-pathogen interactions (Bhandari *et al*, 2019). Thus, our study potentially captures important events that might drive root-fungal endophyte interactions.

F73 and Pi availability in concert alter glucosinolate profiles

At the metabolite level, low Pi reliably caused a constitutively higher accumulation of long chained aliphatic-GLS in both roots and shoots (Fig. 17B and Fig. 23). A previous study using a hydroponic culture system observed that 30 µM Pi induced the accumulation of all aliphatic-GLS examined: the long-chained 8-Methylsulfinyl-n-octyl (8MSO) and 7-Methylsulfinyl-n-pentyl as well as the short-chained 5-Methylsulfinyl-n-pentyl (5MSP), 4-Methylpentyl, and 4-Methylthio-n-butyl (4MTB) using 16 days old seedlings (Pant *et al*, 2015). In our agar plate-

based system, the increased constitutive aliphatic-GLS accumulation at 100 µM Pi was not predicted by the transcriptomic data, as no significant induction of aliphatic-GLS biosynthesis genes was observed in the same tissues (Fig.14A), in line with previous studies (Sønderby *et al*, 2010). In shoots, F73 induced a depletion of the majority of indolic-GLS, short-chained and long-chained aliphatic-GLS only at low Pi, suggesting a fungal effect on GLS translocation from shoot to root at low Pi (Fig. 23). The GLS shoot to root translocation could presumably be reflected in changes in expression of *GLUCOSINOLATE TRANSPORTER* (*GTR*) genes. Our root transcriptomic data shows F73 does not trigger *GTR* expression changes (Fig. 14A), which contrasts with herbivory inducing simultaneously local *GTR* expression and GLS accumulation in *Brassica rapa* roots (Touw *et al*, 2020). Conversely, high Pi consistently caused higher accumulation of F73-induced aliphatic-GLS, the indolic-GLS I3M and 4MOI3M in roots (Fig. 17B and C) in line with Pi-replete conditions potentiating immunity (Castrillo *et al*, 2017; Val-Torregrosa *et al*, 2021). Yet, indolic-GLS biosynthesis genes expression levels were stable (Fig. 14A) suggesting a disconnection between transcript and metabolite as for aliphatic-GLS (Sønderby *et al*, 2010). Together, my analysis suggests that the PSR impacts GLS translocation from shoot to root and rates of synthesis and breakdown, depending on the type of GLS considered. A key step to test this hypothesis would be to employ PSR mutants (*e.g. phr1phl1* double) in experiments targeted at GLS accumulation measurements and homeostasis with F73.

100 µM Pi is an appropriate Pi concentration to probe PSR-immunity dynamics

I assessed how my experimental parameters and results compare to the PSR literature relevant to root-fungi interactions, glucosinolate productions and transcriptional reprogramming. In my experimental setup, only a mild PSR was observed in terms of root hair number and growth (Fig. 9D and E) due to the use of 100 µM Pi instead of generally lower Pi concentrations used by others: 50 µM Pi (Hiruma *et al*, 2016), 30 µM Pi (Pant *et al*, 2015), 10 µM Pi (Barragán-Rosillo *et al*, 2021) or 5 to 50 µM Pi (Castrillo *et al*, 2017). Compared to these lower Pi concentrations, I chose 100 µM Pi that allowed me to limit but not starve the Arabidopsis plants. I reasoned that a limiting condition would expose in a more reliable way to a PSR-immunity link as opposed to strong nutritional stress that could cause pleiotropic effects. Between the two Pi concentrations employed in this work, the overall root systems were found to be similar (Fig. 9B and C) and no initiation of secondary growth difference were observed (Fig. 10B and C), which reduced the possibility of developmental stage or age-dependent effects on immunity (Berens *et al*, 2019).

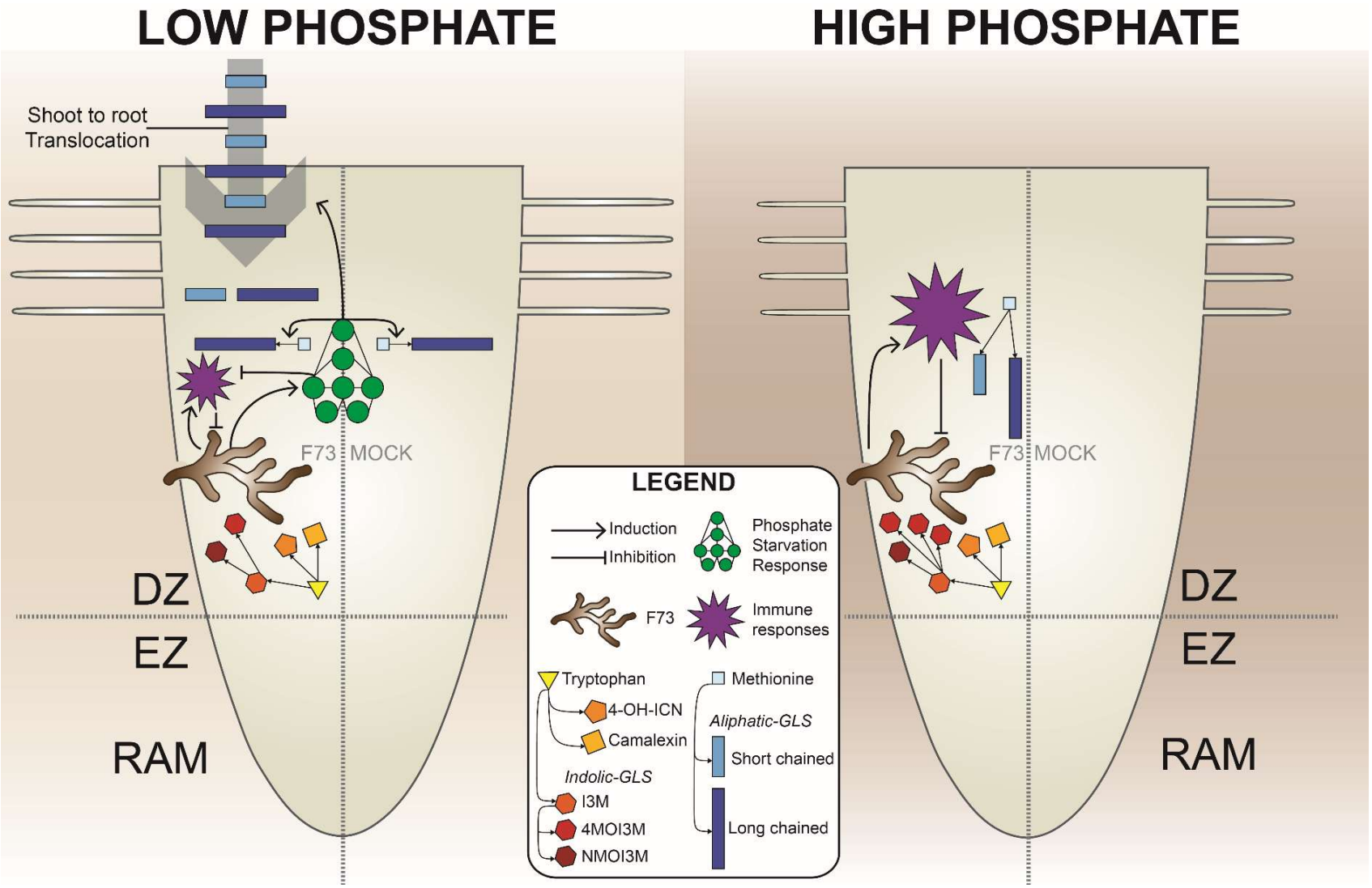

Figure 23: Working model summarizing the findings of the chapter 2 of this dissertation.
Abbreviations: DZ = Differentiation zone, EZ= Elongation zone, RAM = Root apical meristem. F73= *Truncatella angustata*, GLS= Glucosinolate, I3M = 3-indolylmethyl, 4MOI3M = 4-methoxy-3-indolylmethyl, NMOI3M = 1-methoxy-3-indolylmethyl, 4-OH-ICN = 4-hydroxyindole-3-carbonyl nitrile.

Nevertheless, it was surprising to see no or very few differentially expressed genes (DEGs) detected by DESeq2 (Love *et al*, 2014) between 1250 µM Pi and 100 µM Pi in the RNA-seq experiment (Fig. 12B and Fig. 14A). One possible explanation is that my plants were germinated and grown on the same Pi concentration in contrast to studies that relied on germinating plants on Pi replete media before transfer to Pi stress condition (Castrillo *et al*, 2017; Hiruma *et al*, 2016). All harvests specifically took place during the dark period for plants and perhaps the circadian clock influences PSR gene expression, as documented for immunity (Gao *et al*, 2022) or microbiota assembly (Newman *et al*, 2022).

Plant growth rescue and root colonization via PSR activation

It is interesting that F73 induced the expression of major PSR regulators and transporters at 100 µM Pi (Fig. 14A and Fig. 23) because that hints at a F73 function in the microbiota and/or general plant colonization strategies employed by microbes. Alternatively, F73 and Arabidopsis might compete for nutrients, including Pi. Arabidopsis grown at 100µM Pi benefited from F73 in terms of shoot fresh weight and root growth compared to mock 28 dpi of seeds (Fig. 2B) (Mesny *et al*, 2021), not 7 dpi of roots (this work). A cause for this discrepancy could be that microbe behavior can be influenced by polysaccharides in seed mucilage (Meschke & Schrempf, 2010; Hu *et al*, 2019). Otherwise, so far undetermined germinating seedling immune dynamics strongly impact long term interactions with microbes. It is possible that a F73-induced "over-activation" of the PSR at 100 µM Pi would be sufficient to improve plant growth compared to mock treatment. The root endophyte *Colletotrichum tofieldae* triggers Pi transporter gene expression in Arabidopsis (Hiruma *et al*, 2016). Whether F73 is able to translocate Pi to plants as found for *C. tofieldae* (Hiruma *et al*, 2016) is unclear. Such "over-activation"-dependent growth rescue was also seen for iron in the Arabidopsis *bts* mutant defective in repression of iron nutrition, as it performs better than Col-0 under iron-limited conditions (Hindt *et al*, 2017).

If the PSR proves to be responsible for modulating immune metabolic outputs in a variety of contexts, I would anticipate that PSR activation is a common microbial strategy for establishing colonization and benefits from the plant. A microbial-induced PSR might drive metabolic fluxes—rechanneling biosynthesis of immune chemicals towards non- or weakly-toxic compounds. Conversely, from the plant side, the PSR-induced metabolic profiles might modulate microbe functions or behavior for improved plant growth.

Trp-derived metabolites potentially act as general anti-fungal toxins

The precise roles of aliphatic- and indolic-GLSs, camalexin and 4-hydroxyindole-3-carbonyl nitril (4-OH-ICN) in plant microbe interactions remain undetermined. In line with a robust *cyp79b2/b3* deleterious phenotype when inoculated with diverse fungi (Nongbri *et al*, 2012; Lahrmann *et al*, 2015; Hiruma *et al*, 2016; Frerigmann *et al*, 2021), the most parsimonious evolutionary scenario would be that these plant molecules target common, rather than specific, microbial components. However, phylogenetically widespread and lineage-specific microbial components are not necessarily mutually exclusive targets for plant immune metabolites. Besides *in vitro* studies employing non-physiological concentrations of aliphatic-GLS and Trp-derived metabolites, an informative analysis implicated the 4MSB-derived sulforaphane in disarming virulence of the bacterial leaf pathogen *Pseudomonas syringae* (Wang *et al*, 2020). Sulforaphane selectively alters a critical and conserved cysteine in a virulence transcription factor from pathogenic *Pseudomonas*, thereby interfering with an entire pathogenesis pathway (Wang *et al*, 2020). Additionally, sulforaphane inhibits the ability of another virulence transcription factor to bind to DNA in *Xanthomonas* (Wang *et al*, 2022). Thus, sulforaphane is an example of a GLS product targeting different proteins in distinct microbe lineages.

In our work, we achieved a DEG analysis of F73 growing on *cyp79b2/b3* vs Col-0 at 2 and 7 dpi of roots. Absence of all Trp-derived metabolites robustly repressed NmrA-like family genes and upregulated predicted effectors and genes related to amino acid metabolism or TCA cycle in F73 (Fig. 20B), suggesting an enhanced F73 growth rate and virulence in *cyp79b2/b3*. In diverse fungi, NmrA-like genes are implicated in modulating N and C source utilization and in positively regulating stress tolerance ((Peng *et al*, 2022; Li *et al*, 2021) and references therein). With regards to pathogenesis, NmrA-like genes are positive and negative regulators of virulence in plant (Peng *et al*, 2022) and insect (Li *et al*, 2021) pathogens, respectively. Given that F73 induced the expression of camalexin, 4-OH-ICN and indolic-GLS biosynthesis genes (Fig. 14A) and triggered the accumulation of almost all GLS in Col-0 roots (Fig 17), I assume that it is a combined action of Trp-derived metabolites responsible for transcriptomic changes in F73. From my analysis, I speculate that Trp-derived metabolites interfere with fungal components related to growth, such as cell wall synthesis enzymes or plasma membrane-anchored transporters (*e.g.* for N or C sources). Fungi develop and acquire nutrients at an increased rate in absence of the Trp-derived metabolites stress and this indirectly causes downregulation of NmrA-like genes and upregulation of effectors and TCA cycle genes.

Importantly, given the above-mentioned disconnection between aliphatic-GLS biosynthesis genes transcript levels and GLS amounts (Sønderby *et al*, 2010), I cannot exclude that some or all F73 DEGs are attributable to an aliphatic-GLS profile specific to *cyp79b2/b3*. I did not find that the robust F73-induced accumulation of indolic-GLS 4MOI3M (Fig. 17C) results in obvious toxicity of this compound on F73 *in vitro* (Fig. 18). The most likely explanation is therefore that, in my system, 4MOI3M serves as a signaling molecule, as shown for β-1,3-glucan callose formation (Clay *et al*, 2009) that could act as a structural barrier against F73. Callose-staining assays in wild type and *cyp79b2/b3* that is devoid of 4MOI3M, would need to be performed to test this hypothesis.

Outlook and main future steps

The data and results presented in chapter 2 are a framework for deeper investigations into the presumed PSR-GLS link and the consequences on Arabidopsis-root fungal endophyte homeostasis. Modeling the GLS quantification data would lead to a better understanding of how experimental parameters shape the accumulation of each GLS. However, the data are not normally distributed for the majority of GLS (not shown), impairing the use of standard linear models. Following careful analysis of distribution types and/or data transformation methods per GLS compounds, tailored "generalized" linear models can be applied to calculate estimated marginal means (EMMs). Discrepancy, or absence thereof, between observed means (raw data) and EMMs (modeled data) indicate whether unknown parameters influenced the accumulation of each GLS. In analyzing differences between EMMs (*e.g.* within F73-treated roots at 7 dpi, 8MSO amounts at 100 µM Pi vs at 1250 µM Pi), the data can be further modeled taking into account the observed accumulation of other GLS. EMMs therefore provide iterative and powerful tools to thoroughly assess the factors influencing GLS accumulation.

An experiment quantifying GLS in PSR mutants could also include *cyp79b2/b3* to test whether absence of Trp-derived metabolites alter aliphatic-GLS profiles. Then, the package "mixOmics" (Rohart *et al*, 2017) should be used on the RNA-seq and GLS quantification datasets to complement the DEG analysis performed using DESeq2 (Love *et al*, 2014). In mixOmics, the GLS-related genes expression levels would be assigned as "predictor variables" and the GLS amounts as "response variables". This would provide a new angle on the overall correlation between the datasets and address whether subsets of variables explain major sources of variations.

The time frame of my experiments did not include an alteration of Arabidopsis-F73 homeostasis. To follow-up on the increased signs of virulence and growth rate in F73 inoculated on *cyp79b2/b3* compared to Col-0 at the transcriptomic level, shoot fresh weight and root growth analysis should be monitored over a longer time period (*e.g.* 14 or 21 dpi). It is reasonable to predict that F73 will eventually be pathogenic in *cyp79b2/b3,* but it will be interesting to see whether this is Pi status dependent or not. If *cyp79b2/b3* performs better at 1250 µM Pi compared to 100 µM Pi, then Pi supply could perhaps be interpreted as partially rescuing lack of Trp-derived metabolites through its influence on other immune pathways. These longer-term experiments should also include the *cyp79b2/b3 myb28/b29* quadruple mutant (devoid of camalexin, 4-OH-ICN and all GLS) and PSR mutants. The use of PSR mutants might however destabilize immunity in general, not only GLS-related pathways. Additionally, PSR mutants likely will show less Pi acquisition at 100 µM Pi which could lead to developmental or age related effects.

Materials and methods

Materials and methods are divided into a "Materials" section (plant lines, microbes, chemicals, media, primers) and an "Experimental procedures" section detailing protocols employed.

Materials

Plant Materials

The *Arabidopsis thaliana* genotypes used in the work are in the Col-0 background and listed in Table 2

Table 2 – *Arabidopsis thaliana* Col-0 lines used in this work

Genotype	Reference
WT Col-0	Dangl lab, University of North Carolina, NC, USA
cyp79b2/b3	Böttcher *et al.*,2009, Plant Cell
dde2 ein2 pad4-1 sid2-1 (deps)	Tsuda *et al., 2009* PLoS Genet
bak1-5 bkk1	Schwessinger *et al.*, 2011, PLoS Genet
cerk1-2	Miya *et al.*, 2007 PNAS
pepr1/2	Ross *et al.* 2014 Embo J
myb2829	Sønderby *et al.,* 2010
pCYP79B2 ::SYP122-mScarlett	Tonni Grube Andersen, unpublished

Fungal Materials

The fungal strains used in the work are listed in Table 3

Table 3 - Fungal strains used in this work

Genotype	Reference
Serendipita vermifera	Warcup 1988 New Phytol
Serendipita indica	Verma *et al.* 1998 Mycologia
Neonectria radicicola (F134)	Durán, Thiergart *et al.*, 2018 Cell
Truncatella angustata (F73)	Durán, Thiergart *et al.*, 2018 Cell
Paraphoma chrysanthemicola (F34)	Durán, Thiergart *et al.*, 2018 Cell

Chemicals
All chemicals used in this work met laboratory purity and were obtained from diverse suppliers, including Merck (Darmstadt, GER), Roth (Karlsruhe, GER), Duchefa Biochemie (Haarlem, NL), Sigma-Aldrich (Hamburg, GER), ThermoFisher (MA, USA), VWR (Langenfeld, GER) and ExtraSynthese (Genay, FR).

Enzymes
DNA Polymerases

Different DNA Polymerases were used according to cloning purpose and complexity. An overview is given in table 4.

Table 4 - DNA Polymerases used in this work

Name	Purpose	Supplier
Phire II	standard PCR	ThermoFisher

Other enzymes

Other enzymes used include the RevertAid H Minus First Strand cDNA Synthesis kit (ThermoFisher)

Oligonucleotides
Oligonucleotides and primers are shown in Supplemental table 1. For regular oligo design primer3 (http://bioinfo.ut.ee/primer3/) was used. Oligonucleotides were ordered at Sigma-Aldrich (Hamburg, GER). Lyophilised primers were suspended in ddH2O to 100 µM stock concentration and diluted 1:10 to reach a working concentration of 10 µM.

Media
All media were prepared in beakers placed on top of a magnetic stirrer device for convenient pH adjustment (when required) and then sterilised in blue capped bottles by autoclaving at 121 °C for 20 min (1/2 MS and PGA) or 15 min (1/10 PNM). For all media the pH was raised with 1M KOH or decreased with 20% Acetic Acid when required.

Plant media
For the first chapter of the thesis, plants were germinated on ½ MS (Duchefa Biochemie, 2.2 g/L) + 0.5 % Sucrose, pH 5.7 with 1% plant agar (Duchefa Biochemie). After 6 days, they were transferred to PNM media solidified using agar (Fig. 3) or Gelrite (Fig. 4 and 5).

1/10 PNM from Stock solutions (stock solutions on the left, volume to add for 1L on the right):

KNO_3 500 mM	1 ml
KH_2PO_4 5g /100ml	1 ml
K_2HPO_4 2.5g/100ml	1 ml
$MgSO_4xH_2O$ 2M	1 ml
$Ca(NO_3)_2$ 200mM	1 ml
Fe-EDTA	2.5 ml
NaCl 2.5g/100ml	1 ml
Gelrite	12 g
H_2O	990 ml

Adjust pH to 5.6 with 20% acetic acid.

After autoclaving add 10 ml 1M MES.

Fe-EDTA

Add 2.5g $FeSO_4x7H_2O$ in 400ml

Add 3,72g $Na_2EDTA.2H_20$ (equal to 3.36g Na2EDTA)

Boil in microwave

Stir 30 min during cooling

Bring to final volume of 450 ml

Keep in 4°C in darkness

1 M MES: Dissolve 20 g MES in 75 ml of distilled water, stirring and adjusting pH to 6.0 with 5 M NaOH until MES is completely dissolved. Make up the volume to 100 ml, micro-filter sterilization and store at 4°C.

For the second chapter, and for the initial exploratory work on the relationship between Phosphate concentration and F73 (Fig.6,7 and 8), plants were germinated (+0.25% Suc) and then grown on reconstituted ½ MS from stock solutions.

For each liter for medium to be prepared, the following were added to approximately 500 ml of mQ water:

$MgSO_4$ 30 mM	25 mL
KH_2PO_4 25 mM	25 or 4 mL
NH_4NO_3 1 M	10 mL
KNO_3 0,94 M	10 mL
$CaCl_3$ 0,15 M	10 mL
$CoCl_2$ 0,53 mM	0,1 mL
$CuCl_2$ 0,5 mM	0,1 mL
H_3BO_3 50 mM	1 mL
KI 2,5 mM	1 mL
$MnCl_2$ 50 mM	1 mL
$NaMoO_4$ 0,52 mM	1 mL
$ZnCl_2$ 15 mM	1 mL
Fe-EDTA 20 mM	2,5 mL
KCl 70g/L	559 µL for 100 µM Pi media
MES salt	0.5 g
Sucrose (optional)	2.5 g
Plant agar (Duchefa)	9 g
H_2O	to 1000 mL

Adjust pH to 5,7 with KOH

When the exploratory part was over (Fig. 8. Onwards), the choice was made to use an MS powder deprived of Pi (2.08 g/L, Caisson labs, USA) and a 25 mM stock solution of KH_2PO_4

of which 50 ml were added when 1250 µM P media was prepared. Additionally, a single, long lasting supply of Phytoagar (9g/L, Duchefa) was incorporated because we reasoned that a single batch of gelling agent would homogenize residual P input variations. Sucrose addition, pH adjustment and MES use are the same as above, KCl input was raised to 1.225 ml in the 100 µM solution because a media at 1250 µM P receive twice more KH_2PO_4 compared to 625 µM media. Consequently, 625 µM K concentration was also adjusted using a total of 612.5 µL KCl solution.

Fungal media

In the first chapter for Fig. 2 and 3, Sebacinales were each grown on distinct media at 28°C in the dark. *Serendipita indica* was grown for 4 weeks on a combination of salts and microelements forming Complete Media (CM), which allowed chlamydospore generation and harvest:

20x salt solution:

$NaNO_3$	120 g
KCl	10.4 g
$MgSO_4$ * 7 H_2O	10.4 g
KH_2PO_4	30.4 g
H_2O	to 1000 mL

Autoclave and store at RT

Microelements:

$MnCl_2$ * 4 H_2O	6 g
H_3BO_3	1.5 g
$ZnSO_4$ * 7 H_2O	2.65 g
Kl	750 mg
Na_2MO_4 * 2 H_2O	2.4 mg
$CuSO_4$ * 5 H_2O	130 mg
H_2O	to 1000 mL

Autoclave and store at RT

CM medium (1 L):

20 x salt solution	50 mL
Peptone	2 g
yeast extract	1 g
casamine acids	1 g

microelements	1 mL
H_2O	to 950 mL

For plates add 15 g agar to medium.

Autoclave. Add 50 mL 40% Sterile Glucose after autoclaving. Store plates at 4°C.

Serendipita vermifera was grown on a MYP media for 2 weeks before mycelium harvest:

MYP Medium (1L):

Malt-extract	7.0 g
Peptone	1.0 g
Yeast-extract	0.5 g
H_2O	to 1000 mL

15 g agar for plates. Autoclave and store at 4°C.

Then, for Fig. 5 Si was grown for 1 week on VJS media (Osman *et al.* 2020):

VJS Medium (1L):

"V8 juice"	150 mL
$CaCO_3$	2 g
Sucrose	40 g
Plant agar (Duchefa)	12 g
H_2O	850 mL

Pour shortly (max. overnight) following autoclave and store for a maximum of 8 weeks at 4°C. After this storage period, media color turns to a lighter orange and Sebacinales growth is slower.

For the second chapter, fungi from the MPIPZ culture collection were all grown at 22°C in the dark on 26.5 g/L PGB or 39 g/L PGA (Potato Glucose Broth or Agar, Roth, Germany) for liquid cultures or plates, respectively. Growth duration was 2 weeks before mycelium harvest for all fungi irrespective of growth rates.

Minimal medium supplemented with Artificial Root Exudates (ARE)

M9 salt solution:

Na_2HPO_4	75.1118 g
KH_2PO_4	29.9398 g
NaCl	4.9966 g
NH_4Cl	5.0013 g

H_2O to 1000 mL

Adjust pH to 7.2 with NaOH autoclave and store in the dark

$MgSO_4$ 1000X:

$MgSO_4 * 7 H_2O$	24.647 g
H_2O	to 100 mL

Autoclave and store in the dark

$CaCl_2$ 3333X:

$CaCl_2 * 2 H_2O$	14.701 g
H_2O	to 100 mL

Autoclave and store in the dark

Microelements 100X:

$FeSO_4 * 7 H_2O$	$5*10^{-5}$ M
$MnSO_4 * H_2O$	$1*10^{-6}$ M
$CoCl_2$	$1*10^{-6}$ M
$ZnCl_2$	$1*10^{-5}$ M
$CuSO_4$	$1*10^{-6}$ M
H_3BO_3	$1*10^{-5}$ M
EDTA	$5*10^{-5}$ M
HCl	$1*10^{-3}$ M
$NaMoO_4$	$1*10^{-6}$ M
$NiCl_2 * 6 H_2O$	$2*10^{-7}$ M

Vitamins 100x (1L):

Thiamine-HCl	10.12 mg/ml
Nicotinic Acid	12.31 mg/ml
Folic Acid	1.99 mg/ml
Pyridoxine hydrochloride	20.56 mg/ml
4-aminobenzoic acid	4.11 mg/ml
Calcium D pantothenate	4.77 mg/ml
Biotin	1 mg/ml
H_2O	to 1000 ml

Adjust pH to 6.8 with KOH

ARE 5X (1L):

Glucose	4.1 g
Fructose	4.1 g
Saccharose	2.1 g
Citric acid	1.6 g
Lactic acid	1.6 g
Succinic acid	2.3 g
Alanine	2 g
Serine	2.4 g
Glutamic acid	2 g

Mix 1X:

M9	5 ml
$MgSO_4$	50 µl
$CaCl_2$	15 µl
Microelements	500 µl
Vitamins	500 µl
ARE	10 ml
H_2O	to 50 ml

Buffers and Solutions

A summary of buffers and their components used in this thesis is presented in table 7.

Table 7 - Buffers and Components

Application	Buffer	Components
Plant DNA extraction genotyping	DNA extraction buffer	200 mM Tris pH 7.5, 250 mM NaCl, 25 mM EDTA pH 7.5, 0.5 % SDS

Fast plant DNA extraction	Sucrose DNA extraction buffer	50 mM Tris pH 7.5, 300 mM NaCl, 300 mM sucrose
gDNA solvent solution	TE Buffer	10 mM Tris-HCl, pH 8.0, 1 mM EDTA
DNA electrophoresis	10x TAE running buffer	0.4 M Tris, 0.2 M acetic acid, 10 mM EDTA, pH 8.5
	6x DNA loading buffer	40 % (w/v) sucrose, 0.5 M EDTA, 0.2 %(w/v) bromophenol blue
Root surface sterilization	TE + detergent	TE buffer + 0.01% Tween 20
Plant and fungal gDNA extraction buffer	Cell lysis	100 mM Tris-HCl (pH 7,5), 50 mM EDTA (pH 8), 1.5 M NaCl, 2% CTAB
Microscopy	Phosphate Buffer Saline (PBS) pH 7.4	10X stock: 1.37 M NaCl, 27 mM KCl, 100 mM Na_2HPO_4, 18 mM KH_2PO_4

Experimental procedures

Plant methods

Seed production of *Arabidopsis thaliana* WT and mutant or reporter lines

Plants were grown using potting soil supplemented with 10 mg/L Confidor® WG 70 (Bayer, GER). Around 25 Arabidopsis seeds per pot were sown on moist soil prior to stratification in the dark for 48 h at 4 °C. Pots in trays were covered with a plastic lid fitted to tray dimensions and the trays were placed in growth chambers set to the following conditions: 10 h light, 14 h dark, 100-150 µmol m^{-2} s^{-1}, 22 °C, 65 % humidity for 7 days. After that germination period, most seedlings were uprooted to leave up to 5 plants per pot and the pots were transferred to 22 h light, 2 h dark, 100-150 µmol m^{-2} s^{-1}, 22 °C, 65 % humidity without tray lids. Watering of pots was performed by pouring water into the trays every 2 or 3 days until plants completed their life cycle. As soon as inflorescences matured, a wooden stick (approx. 45 cm long) was planted at the center of the pot to wrap the inflorescences around. Inflorescences were then grouped into a breathable bag of mixed compostion (plastic and paper) and harvested once the plants dry out completely.

***In vitro* coculture of plants and fungi**

Seed sterilization

To sterilize seeds of a given genotype, a small amount of seeds was poured into a silica column previously stored in 70% EtOH. The column was inserted into a 2 ml tube and 450 µl of 70% EtOH + 0.001% Tween 20 was added to the column. After 2 min of inverting, the column was spinned down 10 seconds using a tabletop centrifuge and the flow through was discarded. Then, 450 µL of 96% EtOH was added to the column before inverting 1 min and spinning down 10 seconds. After discarding the flow through, the column was spinned 1 min at 11 000 rcf to completely dry the column. The column is then opened under a flow hood and the seeds are left to dry from the ethanol 1 min before being poured in a pre-labeled sterile 1.5 ml tube. Finally, 1 ml of sterile miliQ water is added to the tube and the tube is vortexed thoroughly until all seeds are hydrated. The tube is either stored at 4°C for 2 days in the dark for flow-pot experiments or the seeds are directly handled as below for agar plate assays.

Seed germination for agar plate assays

Sterile seeds from above are placed on ½ MS + Suc (for Suc concentration please see above Media section in Materials) square plates using a P20 pipette set to aspirate/dispense 15 µL with sterile yellow tips. Several seeds are aspirated in one suction and then, with measured release of the pipetted volume, one by one arranged next to each other in straight lines (4 or 5 lines of 30-40 seeds each per plate). This allows convenient comparison of seedlings size and vigor when plants are to be selected for subsequent transfer onto coculture plates with fungi or mock treatment. Plates are then sealed using surgical tape (3M, USA) and stored in the dark at 4°C 48 h to stratify seeds.

Seed germination for agar plate assays

After stratification, plates containing seeds were transferred to a cabinet dispensing 80-120 µmol m^{-2} s^{-1} light depending on the location and number of plates on the cabinet shelves. Seedlings were grown for 6 days after germination.

Transfer and inoculation

Under a flow-hood, growth-matched seedlings (within a genotype and ½ MS P concentration combination) were transferred to non-Suc plates, either 1/10 PNM or corresponding ½ MS depending on the thesis chapter, using sterile tweezers. Importantly, the top 2 cm of the non-Suc plates agar was removed using a sterile spatula to prevent fungal growth from the agar unto on above ground plant parts. Seedlings were arranged next to each other with the hypocotyl being placed at the limit were the agar was cut out. For imaging purposes, 5 to 10 seedlings per plates but other assays typically ranged from 14 to 20 (precisely 16 for the GLS analysis

experiments). The plates were sealed using surgical tape and then transferred to the growth cabinet for 24 h.

Shuffling and light conditions

Generally, no more than two assays were overlapping at the same time in the cabinet and plates were shuffled randomly every 2 days to distribute light as homogenously as possible. The light intensity ranges from 80 to 120 µmol m^{-2} s^{-1}. Custom cases fitting to square plates were hand made from white (outside) and black (inside) 300 g/m^2 papers taped together.

Fungal inocula preparation

For the first chapter of the thesis, Sebacinales inocula were prepared as follows: On the day of inoculation, regardless of growth media, *S.indica* spores were harvested by pouring 5 ml of Tween water (MiliQ water + 20 µl of Tween 20 /l) on the plates and scrapping the mycelial mat surface using a sterile scalpel. The resulting spore suspension was pipetted out from the plates and on to a sterile miracloth filter placed on a sterile flask. This harvest step was repeated using another 5 ml Tween water and the flow through (spore suspension) was poured into a sterile 50 ml falcon for a 7 min centrifugation at 3 500 g at RT. A washing step consisting of discarding the supernatant and resuspension in 10 mL Tween water before an identical centrifugation was repeated twice. Finally, the spores are resuspended in 10 ml sterile water and counted on a Neubauer improved chamber before adjustment of the spore concentration to 400 000 spores/mL.

For *S.vermifera*, 7 days before inoculation, 10 ml of sterile water was poured onto a colony to then scrap mycelium using a sterile scalpel. The mycelium suspension is then filtered from big mycelium fragments and agar fragments and washed identically to above for *S. indica* spores, except that sterile water was used for all steps. After washing and resuspension in 1 ml of sterile water, the mycelium suspension was inoculated into 50 ml of liquid MYP in a sterile flask and the culture was shaken at 28°C for 6 days at 200 rpm. Mycelial chunks are then poured onto a sterile miracloth filter placed on a sterile flask and washed abundantly using sterile water. The resulting mycelial mass is then harvested using sterile tweezers and placed in a sterile 125 ml Kinematica Microtron (Kinematica AG, Malters, Switzerland) MB55 blending unit containing 50 ml of liquid MYP. The suspension was then blended twice by ramping the blending speed from 0 to 6 slowly, and then stopping rapidly. The resulting culture was then poured into a fresh sterile flask and grown for 24 H at 28°C 200 rpm. On the day of inoculation, regenerated hyphae are poured on a sterile miracloth filter, washed thoroughly using sterile water, dried by pressing gently the filter and then weighed in a sterile flacon. Finally, the inoculum was prepared to a

concentration of 40 mg/ml. Root dipping for Fig. 1A and a drop of 20 µl per root for Fig. 1B-D.

Development of F73 (and attempts for F34 and F134) from the MPIPZ culture collection as model(s) suited to my system required iterative parameter optimization described chronologically in the result section. The final inoculum preparation, as employed in the majority of experiments including microscopy time course, genetics, metabolomics and transcriptomics is described here. From a 2 week old plate, a mycelial mat rectangle approximately 1 cm in length * 0.5 cm in width was cut out and then flipped agar side up on the lid of the petri dish. Using a sterile scalpel, the agar was gently scrapped off as close as possible to the fungal hyphae now pressed down on the lid. This hyphal matt is then gently transferred, using sterile tweezers, to a sterile 2 ml screw cap tube pre filled with 500 µl 10 mM $MgCl_2$, two 3.15 mm ø and four to eight 1.588 mm ø metal beads (Mühlmeier Technik, Bärnau, Germany). The hyphae are then ground for 5 min in a the paint shaker (Skandex SK450, Fast& Fluid, Sassenheim, The Netherlands) and 7 µl of the suspension is inoculated in 100 ml of PGB. The culture is then grown at 22°C 120 rpm for 5 days. On the day of inoculation, half of the culture is harvested onto a sterile miracloth filter placed on top of a sterile flask, washed thoroughly with sterile water and transferred to a sterile 125 mL Kinematica Microtron MB55 blending unit containing 60 ml of PGB. After blending two times 0 to 8 slowly, the 60 ml of regenerating hyphae are transferred to a sterile flask containing another 40 ml of fresh PGB and the flask is placed back in the shaker for 1 H at 22°C 80 rpm. After regeneration, the hyphae are harvested on sterile miracloth, washed thoroughly with sterile water, dried by pressing the filter and then weighed in a sterile 50 ml tube. Finally, the hyphae suspension was adjusted to a concentration of 2 mg/ml and approximately 10 ml was poured in a sterile 5 cm ø round petri dish. The petri dish concomitantly grants easy access to the inoculum for inoculation and is also easily stirable by hand to avoid excessive hyphae aggregation.

Root inoculation

In the first chapter of the thesis, inoculation of Sebacinales was performed on the top 1 cm of the roots, below the hypocotyl. For *S. indica,* spore concentration was 10 000 spores per plant. For *S.vermifera,* inoculum concentration was from 40mg/ml to and was performed by spreading 500 µl of regenerated hyphae suspension over the pre-aligned seedlings.

For F73, and after method establishment, inoculation was performed by depositing a 5 µl drop of 2 mg/ml regenerated hyphae suspension 5 mm below the hypocotyl of each plant (0.01 mg of hyphae per root).

The plates were then sealed with surgical tape and placed upright in the growth chamber. In the case of F73 assays starting from the colonization speed assessment experiment (Fig. 10), plates were placed in hand-made paper cases to minimize light shining on roots. The cases are made of two layers of 300 g/m² black (inner layer) and white (outer layer) paper sheets, cut, folded and taped to fit plates.

Flow-pot experiment

The flow-pot were constructed as mentioned in the original publication (Kremer *et al*, 2021) except for peat-vermiculite mix sterilization. The mix was sterilized according to the following program: 20 min autoclave, 1 day of rest, 20 min autoclave, 1 day of rest, 2 weeks at 70°C, then the peat was rehydrated with 1 liter sterile water and it was autoclaved 2 more times 45 minutes during the same day 1 day before inoculation. The fungi were inoculated at a 2 mg/ml.

Harvest of plant material

Regardless of fungal species used, harvest of shoots and roots was always performed in the same manner, except for the Glucosinolate profiling and the RNA-seq experiments (please see below). First, pictures of plates were taken using either a Cannon EOSD700 equipped with a EW-82 16-35 mm Image stabilizer objective and mounted on a stand or an Epson V600 Scanner (Epson, Suwa, Japan) with a ruler next to the plates. Next, shoots were separated from roots by cutting the hypocotyl-root junction with a sharp scalpel blade. If the shoots were to be weighed, shoots were freed from residual condensation by being gently squeezed between two layers of absorbent paper. Then, the shoots were finally transferred to the precision scale for weighing. In the case of the single flow-pot experiment presented in this work, each shoot was placed in a 2 ml tube containing 1 ml DMSO for latter chlorophyl extraction.

In the first chapter, extraradical Sebacinales hyphae were removed by submerging the roots in sterile water and gently scraping the roots surface using a gloved finger. Then, the roots were dried using absorbent paper and transferred to 2 ml tubes pre filled with two 3.15 mm ø and four to eight 1.588 mm ø metal beads (Mühlmeier Technik, Germany).

In the second chapter, a manual root-surface cleaning method was also attempted, with different intensities, on F73 and F34 colonized roots. Manual cleaning was performed on individual roots in sterile water placed in a 9 cm ø petri dish. The plants were held by the hypocotyl using tweezers and a gloved finger rubbed the surface of the root by applying gentle pressure to immerge the root and press it against the bottom of the dish while scrubbing 3 times. The operation was repeated either 1 time on the other side of the root system ("gentle scrubbing") or 3 times per side of the root system ("thorough scrubbing"). However, a chemical surface

sterilization was preferred in all presented F73 fungal biomass quantification via RT-qPCR experiments. After harvest from the petri dish, accessible and excessive extraradical hyphal aggregates were removed using tweezers. Then, the roots were transferred to 2 ml tubes containing 1 ml TE buffer + 0.01% Tween 20 and pulse vortexed at max speed 3 times. After discarding the supernatant, this washing step was repeated and the supernatant was discarded. Next, 1 ml of 80% EtOH was added to the tubes and the tubes were inverted for 30 seconds. After discarding the EtOH, 1 ml of 3% bleach was added to the tubes and they were inverted 30 seconds to complete the surface sterilization. After removal of bleach, the roots were washed 3 times with 1 ml sterile water, 12 inversions and supernatant discarding. Care was taken to remove all water before addition of metal beads to the tubes, as above. In the case of the RNA-seq experiment, for each replicate, plates of a given condition were retrieved from the growth chamber before harvesting roots as fast and as precisely as possible, in front of the growth chamber. Roots were immediately transferred from the plates into pre-labelled, metal beads containing tubes.

In both chapters, the tubes were flash frozen as fast as possible using liquid nitrogen. The roots were ground at 30 hertz/sec for 1 min with a TissueLyser II (Qiagen, Hilden, Germany) and stored at -80°C before subsequent processing.

Root passage

To establish reliable stocks of F73, I performed a root passage. After 2 weeks of coculture between F73 and Arabidopsis, the roots were surface sterilized and placed on a PGA plate. Endophytic F73 grew out of the roots and formed a colony, which was, after 2 weeks of growth, thinly sliced in cubes. These cubes were placed in 1 ml screw cap tubes containing 0.5 ml of sterile 30% glycerol and the tubes we flash frozen in liquid N2. For every 3rd repeat of an experiment, the F73 stock was resurrected using sterile yellow tips scratching the frozen glycerol on to a PGA plate.

Chlorophyll extraction

Chlorophyll from individual shoots was extracted by heating up the tubes containing 1ml DMSO at 65°C for 1 hour, with 3 thorough inversions during this incubation time. The samples were then cooled to 4°C for a few hours before transferring 200 µl of each sample into a well from a flat bottom 96 well plate. For each well, optical absorbance was read at 645, 652 and 663 nm in a Tecan plate reader (Tecan Trading AG, Switzerland). Chlorophyll content was calculated using the 2 following formulas:

$Chlorophyll_{total}$ (mg/L)= A_{652}*1000/34.5

$Chlorophyll_{total}$ (g/L)= 0.0202*A_{663} + 0.00802*A_{645}

The results from the formulas is predicted to be close, which was verified before preferring the second formula due to its greater accuracy.

gDNA extraction

All steps described here were performed under a fume-hood. First, 1 mL extraction buffer with freshly added β-mercaptoethanol (50 µl / 100 ml buffer) was added to each sample and the tubes were inverted 3 times before incubation 10 min at RT with 600 rpm shaking. Then, 1 ml 25:1 chloroform:isoamylalcohol (ClA) was added and the samples were incubated in the same conditions 5 min to subsequently be centrifuged 20 min at 10 000 g and RT. Afterwards, 800 µl of supernatant was transferred to a fresh 2 ml tube and 160 µl of pure EtOH was added slowly under 300 rpm shaking before 5 min of inversions. Following addition of 960 µl of ClA, the tubes were inverted 5 min before performing a centrifugation step identical to above. Then, 800 µl of the supernatant were transferred to a fresh 1.5 ml tube containing 800 µl of isopropanol and mixing was performed by pipetting. The gDNA was then precipitated by incubating the samples at -20°C overnight before centrifugation 20 min 5 000 g at RT. All the supernatant was then discarded and 900 µl of ice cold 75% EtOH was added to was the gDNA pellet. After a brief spin down, careful removal of all EtOH and 10 min drying under the hood flow, 50 µl of TE buffer (pH 8) and 1 µl of RNAse A (10 mg/mL pH 7.4) were added. Finally, these pellets were incubated at 300 rpm for 30-60 min at 37°C until all pellets are completely dissolved. DNA concentration was determined using a nanodrop and samples were stored at -20°C.

RNA extraction

For all experiments (except the RNA-seq), RNA was extracted using TRIzol (Ambion, Life technologies, Carlsbad, USA) manufacturer's instruction. For the RNA-seq experiment, the TRIzol protocol was also employed until isopropanol precipitation. Afterwards, the solutions of precipitating RNA were passed unto ReliaPrep columns (Promega, Walldorf, Germany). Therefore, the ReliaPrep protocol was employed from step 4.B onwards according to the manufacturer instructions.

In all cases, RNA concentration was determined using a Nanodrop and adjusted to 200 ng/µL when Reverse Transcription was to be performed.

Reverse Transcription

cDNA synthesis was performed using the cDNA synthesis RevertAid reverse transcriptase kit (Thermo Scientific, Waltham, USA) according to manufacturer's instructions.

RT-qPCR

RT-qPCR was performed using a BioRad CFX96 Touch™ Real-Time PCR Detection System. For details see table 13 and table 14. Primer sequences can be found in table 6. For data analysis Excel and R were used (see below).

Table 9 - RT-qPCR reaction mix

Component	Volume
SYBR® Green Supermix	5 µl
forward primer (10 µM)	0.5 µl
reverse primer (10 µM)	0.5 µl
template cDNA	1 µl
ddH_2O	to 10 µl

Table 10 - RT-qPCR thermo-cycling program

Stage	Temperature (°C)	Time	Cycles
Initiation	95	30 sec	1x
Denaturation	95	10 sec	40x
Annealing	55	15 sec	
Elongation	72	10 sec	
Melt Curve	60 - 95	5 sec per 0.5 °C	1x

In vitro assessment of 4MOI3M salt effect on F73 growth

From 2 weeks old F73 plates, mycelia were harvested (see above F73 liquid culture protocol) and weighed in a sterile 2 ml screw cap tube containing metal beads. After addition of 500 µl of sterile 10 mM $MgCl_2$ and grinding on the paint shaker, concentration was adjusted to 100 mg/ml. Next, 200 µl of sterile water were placed in the wells edging a 96 flat-bottom well plate. Finally, a 4MOI3M salt concentration ranging from 250 to 4 µM, a blank control and a pimaricin control were set up in ARE.

Glucosinolates profiling

GLS analysis by LC-MS/triple quadrupole

For glucosinolate profiling, shoots and roots were harvested individually in racked collection microtubes (Qiagen) each containing one 3.15 mm ø metal bead. When a strip of sample was completed, the microtubes were sealed using Microtube caps (Qiagen) and flash frozen in liquid

nitrogen. After homogenation to a fine powder in a bead mill (3 mm bearing balls, 2 × 30 s at 30 Hz) and addition of 300 µl 85% (v/v) methanol (HPLC grade) containing 10 µM *p*-hydroxybenzyl glucosinolate (pOHb; PhytoLab, cat. No. 89793) as internal standard, samples were vortexed thoroughly and then centrifuged (5 min, 4,700× *g* , 4°C). Samples were prepared as desulfo-glucosinolates as previously described (alternate protocol 2, Crocoll et al., 2016). LC-MS/MS analysis was carried out on an Advance UHPLC system (Bruker, Bremen, Germany) equipped with a Kinetex® XB-C18 column (100 × 2.1 mm, 1.7 µm, 100 Å, Phenomenex, USA) coupled to an EVOQ Elite TripleQuad mass spectrometer (Bruker, Bremen, Germany) equipped with an electrospray ionization source (ESI). The injection volume was 1 µL. Separation was achieved with a gradient of water/0.05% (v/v) formic acid (solvent A) – acetonitrile (solvent B) at a flow rate of 0.4 ml/min at 40°C (formic acid, Sigma-Aldrich, cat. no. F0507, reagent grade; acetonitrile, HPLC grade). The elution profile was: 0–0.5 min 2% B; 0.5–1.2 min 2-30% B; 1.2–2.0 min 30–100% B; 2.0–2.5 min 100% B; 2.5–2.6 min 100–2% B; 2.6–4.0 min 2% B. The mass spectrometer parameters were as follows: ionspray voltage was maintained at 3500 V, cone temperature was set to 300°C and heated probe temperature to 400°C, cone gas flow was set to 20 psi, probe gas flow to 40 psi, nebulizer gas 60 psi, and collision gas to 1.5 mTorr. Nitrogen was used as cone and nebulizer gas, and argon as collision gas. Multiple reaction monitoring (MRM) was used to monitor analyte parent ion > product ion (Crocoll et al., 2016). Both Q1 and Q3 quadrupoles were maintained at unit resolution. Glucosinolates were quantified relative pOHb using experimentally determined response factors with commercially available standards in a representative plant matrix.

Imaging

Sample fixation and staining

During the first part of the second chapter, F34 and F73 colonized roots were harvested and fixed in 70% EtOH overnight. The EtOH was washed off 3 times using 1X PBS. Then, the roots were incubated for 30 min in the dark under 100 rpm agitation in a 1X PBS solution containing both 0.1% Calcofluor White (CFW, general cell-wall stain, Thermo Fisher) and 20 µg/ml Wheat-Germ Agglutinin conjugated to Alexa Fluor 488 (WGA, chitin stain, Biotium, Fremont, USA). Next, the staining solution in the wells is retrieved and stored back in a 50 mL falcon at 4°C in the dark, and reused for several months. Then the plants are washed once with PBS and imaged in 50% glycerol between a cover slip and a slice of Lumox® breathable film (Sarstedt, Nümbrecht, Germany).

After the first trials, a 20% KOH incubation overnight step was added before thorough washing and staining.

Confocal laser scanning microscopy
Imaging of F73 hyphae inside roots was performed on a Zeiss LSM 780 (Zeiss, Oberkochen, Germany) (first exploratory part) or a Zeiss LSM 880 (second part). For confocal laser scanning microscopy using the Zeiss LSM 780 a 40x water objective (W Plan-Apochromat 40x/1.1DIC D=0.14-0.19 was used with an Argon Laser and diode intensity of 0.5%, WGA-CF488 excitation at 488nm, detection between 520-580 nm, and CFW excitation at 405 nm and detection detection between 460-500 nm.

Stereomicroscopy
Imaging of the *pCYP79B2::SYP122-mScarlett* reporter line was performed on a Zeiss Axiozoom v16 connected to an Aura® light engine lamp (Lumencor, Beaverton, USA) and a Zeiss CL 9000 LED for bright field. Excitation wavelength: 488 nm, Bright field light intensity: 30%

Image analysis
Image processing, annotation and analysis was mostly done on ImageJ (imagej.nih.gov).

For analysis of root lengths, plate pictures were calibrated according to the ruler present in the picture. Next, root lengths were analyzed using the Pluggin NeuronJ, which, as input, requires 8-bit black and white images transformation followed by manual contrast adjustment until roots appeared clearly white on a uniformly black background. Then, the tracing tool of NeuronJ was used on each primary root that could be unambiguously distinguished from other roots or the plate border. Importantly, the tracings were always performed from left to right on each plate, as to easily attribute the two measures (inoculation day and harvest day) to individual plants. Root lengths were retrieved in a .csv file from the “measure tracing” function.

Confocal and wide-field microscopy images in .czi format were loaded into ImageJ for scale bar display, splitting of channels and maximum intensity projections. For confocal microscopy images displayed in Fig. xx, they were first deconvoluted using the Huygens software deconvolution wizard prior to ImageJ processing.

The analysis of fluorescent signal intensity of wide-field images was carried out as follows. First, the width of the line tool was set to 1000, effectively creating a rectangle. Then, the line tool was used across a straight root segment and the profile of the red channel was plotted, and the data extracted in .csv format. After compiling all root data in a single table, for each root separately, the root width (measured) and the fluorescence intensity signal (varying between lines, individuals, treatments and days) were normalized according to their respective maxima and multiplied by 100 to get widths and intensities scaled to 100 for all roots. Because

normalised root widths were then ranging from 0 to 100 in continual intervals of varying lengths, normalised root widths were coerced (binned) into discrete categories ranging from 1 to 100 to eventually allow signal intensity averaging and statistics.

Only root hairs number and lengths of the first 2000 µM from the root tip were counted and measured, respectively, in Fig. X

Data analysis

All statistical and graphical analyses were performed on R v4.2.2 using RStudio Desktop 2022/07/2+576. Packages employed: dplyr, ggplot2, multCompView, scale, tibble, tidyr, magrittr, RVAideMemoire, ComplexHeatmap, sva, stringr, ggpubr, cowplot, RColorBrewer, grid, gridExtra, cramer, agricolae, rcompanion, edgeR, glue, DESeq2, EnhancedVolcano, ggrepel and scales.

For each data type, except for the RNA-seq, the statistical pipeline in Fig. 22 was deployed.

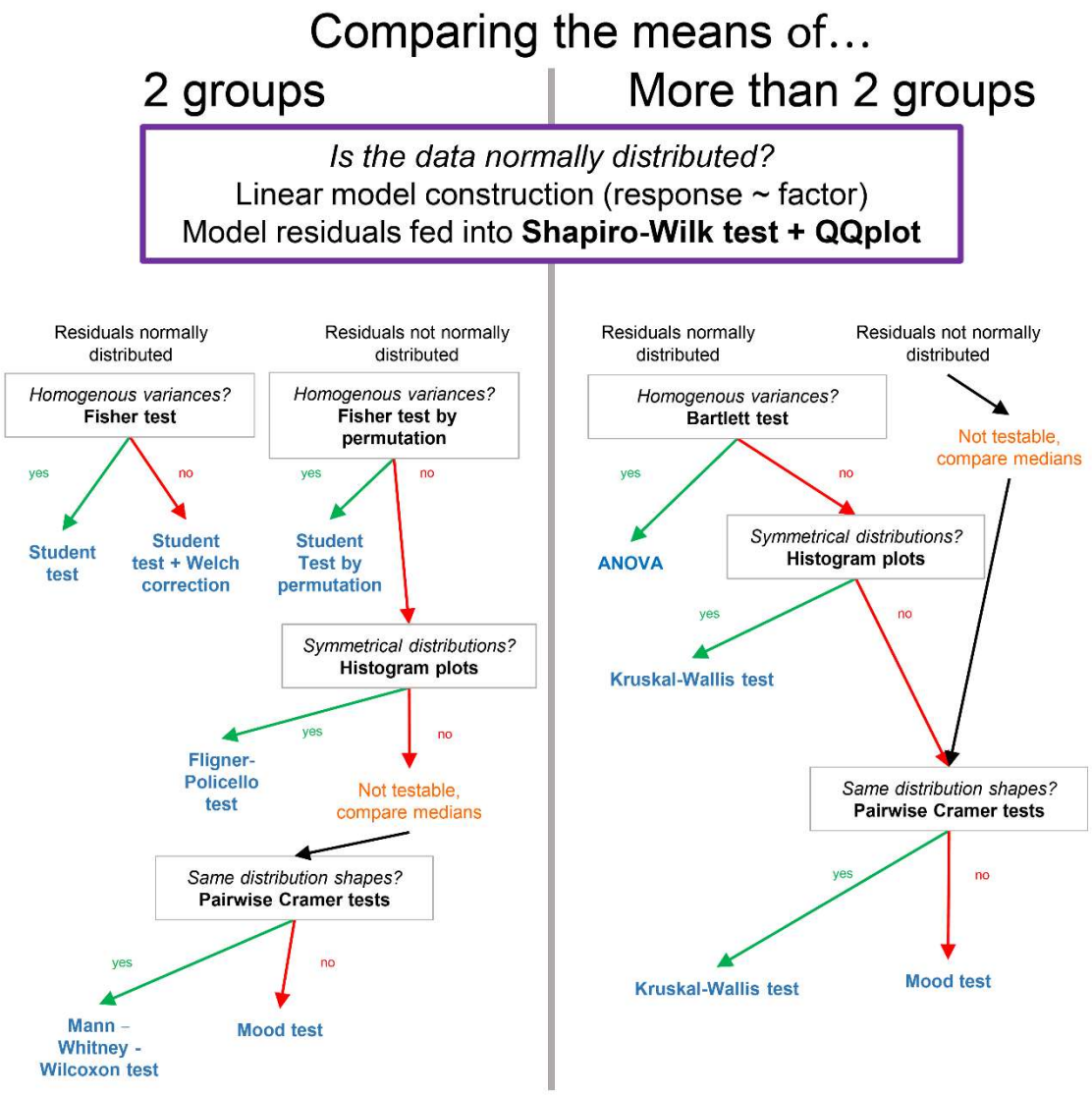

Figure 22: Statistical pipeline according to « *Aide-mémoire de statistique appliquée à la biologie – Construire son étude et analyser les résultats à l'aide du logiciel R, Maxime Hervé 2021* » (not available in english)

RNA-seq analysis

For the RNA-seq analysis, raw reads were trimmed with trimmomatic (Bolger *et al*, 2014), mapped to Arabidopsis genome (Araport11 - https://www.arabidopsis.org/) or *Truncatella angustata* F73 genome (Genbank bioproject PRJNA347197, assembly JAGPXC000000000, https://mycocosm.jgi.doe.gov/Truan1/Truan1.home.html, november 2022) genomes. Trimmed reads were mapped using Hisat2 (Kim *et al*, 2019) and counted using featureCounts (Liao *et al*, 2014). For the plant, read counts associated to each plant gene were then normalized to library size, corrected for batch effect (fully supervised) using the ComBat-seq function from the sva package (Leek *et al*, 2012) and then used to perform a differential gene expression analysis with DESeq2 (Love *et al*, 2014). After rlog transformation and median-centered transformation (scaled counts), *k*-means clustering was conducted based on Akaike information criterion and sum of squared error (k=10). Cluster results were visualized using the ComplexHeatmap package (Gu *et al*, 2016). GO enrichment analysis was conducted using Metascape (Zhou *et al*, 2019a).

For fungal reads, log2FoldChanges values were shrinked with the apeglm algorithm (Zhu *et al*, 2019). To gain functional insights in the F73 genes robustly deregulated in *cyp79b2b3* plants over different time points and phosphate concentrations, we manually curated gene descriptions from KOG, PFAM and InterPro, previously annotated by the JGI Annotation Pipeline (Mesny *et al*, 2021; Grigoriev *et al*, 2014)

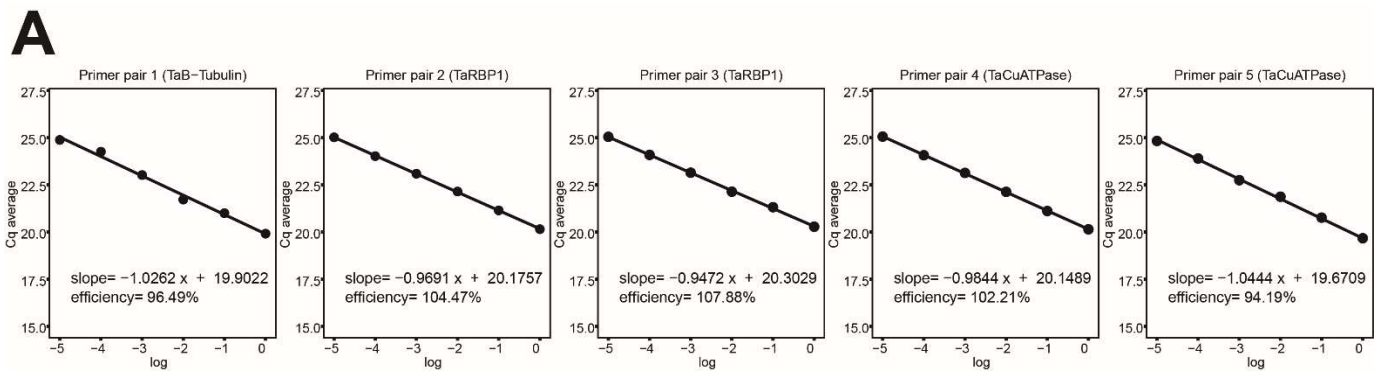

Supplemental figure 1: qPCR primers targeting various F73 genomic DNA regions.

Supplemental Table 1 – Oligonucleotides used in this study

Name	Description	Oligo Sequence (5' to 3')	Orientation	Purpose
nCU001	ACTIN2_Fw with nCU002	ATGGAAGCTGCTGGAATCCAC	Forward	qPCR on cDNA
nCU002	ACTIN2_Rv with nCU001	TTGCTCATACGGTCAGCGATA	Reverse	qPCR on cDNA
nCU045	SvTEF_Fw with nCU046	ATCCCAAGCAAGCCAATGTG	Forward	qPCR on cDNA
nCU046	SvTEF_Rev with nCU045	TGCCGTCAGTCTTCTCAACA	Reverse	qPCR on cDNA
nCU047	SiTEF_Fw with nCU048	GCAAGTTCTCCGAGCTCATC	Forward	qPCR on cDNA
nCU048	SiTEF_Rev with nCU047	CCAAGTGGTGGGTACTCGTT	Reverse	qPCR on cDNA
nCU051	gDNASvTEF_Fw with nCU052	CAGGCAAACCCTCAGTGAGC	Forward	qPCR on gDNA
nCU052	gDNASvTEF_Rev with nCU051	GCAAGTTTGCCGAGCTCATCG	Reverse	qPCR on gDNA
nCU053	gDNA AtUBI_Fw with nCU054	CCAAGCCGAAGAAGATCAAG	Forward	qPCR on gDNA
nCU054	gDNA AtUBI_Rev with nCU053	ACTCCTTCCTCAAACGCTGA	Reverse	qPCR on gDNA
nCU081	F34TEF1a_Fw with nCU082	CCGAAAGCAAGTCTCCAGTCAT	Forward	qPCR on gDNA
nCU082	F34TEF1a_Rev with nCU081	TACACAAGCACACCAGGCAA	Reverse	qPCR on cDNA
nCU083	F73TEF1a_Fw with nCU084	ACAAGTGTCCAGCCATATCCAG	Forward	qPCR on cDNA
nCU084	F73TEF1a_Rev with nCU083	ATATGCCTCCTGTCCTCTTCCT	Reverse	qPCR on cDNA
nCU085	F73B-Tubulin_Fw with nCU086	GTTCATCTTCAGACCGGCCA	Forward	qPCR on cDNA

nCU086	F73B-Tubulin_Rev with nCU085	CCGAAGTGCCGTTGTAGACT	Reverse	qPCR on cDNA
nCU087	F73B-Tubulin_Fw with nCU087	CATCTTCAGACCGGCCAGTG	Forward	qPCR on cDNA
nCU088	F73B-Tubulin_Rev with nCU088	GCCGTTGTAGACTCCATTGCT	Reverse	qPCR on gDNA
nCU089	F34B-Tubulin_Fw with nCU090	GAGATTGTTCACCTCCAGACCG	Forward	qPCR on gDNA
nCU090	F34B-Tubulin_Rev with nCU089	GTGCCATTGTAGACACCGGA	Reverse	qPCR on gDNA
nCU091	F34B-Tubulin_Fw with nCU092	CTACTTCAACGAGGCCTCCG	Forward	qPCR on gDNA
nCU092	F34B-Tubulin_Rev with nCU091	CCCAGTTGTTACCAGCACCA	Reverse	qPCR on gDNA
nCU093	F73B-Tubulin_Fw with nCU094	AGCAATGGAGTCTACAACGGC	Forward	qPCR on gDNA
nCU094	F73B-Tubulin_Rev with nCU093	CCGGAAGCCTCGTTGAAGT	Reverse	qPCR on gDNA
nCU095	F73B-Tubulin_Fw with nCU096	ATGGAGTCTACAACGGCACTTC	Forward	qPCR on gDNA
nCU096	F73B-Tubulin_Rev with nCU095	GCACGTACTTGTTGCCGGAA	Reverse	qPCR on gDNA
nCU097	F34B-Tubulin_Fw with nCU098	GAGATTGTTCACCTCCAGACCG	Forward	qPCR on gDNA
nCU098	F34B-Tubulin_Rev with nCU097	GTGCCATTGTAGACACCGGA	Reverse	qPCR on gDNA
nCU099	F73B-Tubulin_Fw with nCU100	ATTGTTCATCTTCAGACCGGC	Forward	whole gene amplificati on from gDNA or cDNA
nCU100	F73B-Tubulin_Rev with nCU099	TTACTCCTCCTCGGGCAGA	Reverse	whole gene amplificati

				on from gDNA or cDNA
nCU101	F34B-Tubulin_Fw with nCU102	ATTGTTCACCTCCAGACCGG	Forward	whole gene amplification from gDNA or cDNA
nCU102	F34B-Tubulin_Rev with nCU101	GCCTCCTCATCGTACTCCTC	Reverse	whole gene amplification from gDNA or cDNA
nCU103	Fw primer for fungal ITS1 with nCU104	TCCGTAGGTGAACCTGCGG	Forward	Genotyping Kumar & Shukla 2005
nCU104	Rv primer for fungal ITS1 with nCU103	TCCTCCGCTTATTGATATGC	Reverse	Genotyping Kumar & Shukla 2005
nCU105	Fw primer for F73 BTUB with nCU106	GGTAACTCGACTGCCATCCAA	Forward	qRT-PCR
nCU106	Rv primer for F73 BTUB with nCU105	AAAGCCTTGCGACGGAACAT	Reverse	qRT-PCR
nCU107	Fw primer for F73 BTUB with nCU108	TCGACCCCAAGAACATGATGG	Forward	qRT-PCR
nCU108	Rv primer for F73 BTUB with nCU107	TTCTGGACGTTGCGCATCT	Reverse	qRT-PCR
nCU109	Fw primer for F73 ITS1 with nCU110	CTTGGTCATTTAGAGGAAGTA	Forward	qRT-PCR Mesny et al. 2021

nCU110	Rv primer for F73 ITS1 with nCU109	GCTGCGTTCTTCATCGATGC	Reverse	qRT-PCR Mesny et al. 2021
nCU111	Fw primer for pCYP79B2::mScarlett genotyping with nCU112	ATGTTCAACGTTGGTGGTGG	Forward	Genotyping
nCU112	Rv primer for pCYP79B2::mScarlett genotyping with nCU111	CTCCATGTGCACCTTGAACC	Reverse	Genotyping
nCU113	Fw primer for pMAM1::NLS::3xmScarlett genotyping with nCU114	TCCCACACTATCTTTCCTCCAC	Forward	Genotyping
nCU114	Rv primer for pMAM1::NLS::3xmScarlett genotyping with nCU113	ACATGAACTGCGGTGAAAGG	Reverse	Genotyping
nCU115	Fw primer for CYP83B1::YFP genotyping with nCU116	TGGACTTCAAGGGCCAAGAT	Forward	Genotyping
nCU116	Rv primer for CYP83B1::YFP or CYP83A1::YFP (binds to YFP sequence) genotyping with nCU115 or nCU117, respectively.	GCTGAACTTGTGGCCGTTTA	Reverse	Genotyping
nCU117	Fw primer for CYP83A1::YFP genotyping with nCU116	ACCCTGATGAGTTTAGGCCC	Forward	Genotyping
nCU118	Fw primer for SPX1 expression with nCU119	CGGGTTTTGAAGGAGATCAG	Forward	qRT-PCR Balzergue et al. 2017

nCU119	Rv primer for SPX1 expression with nCU118	GCGGCAAT GAAAACACACTA	Reverse	qRT-PCR Balzergue et al. 2017
nCU120	Fw primer for PHR1 expression with nCU121	TTGGACGCCAGAGCT TCAC	Forward	qRT-PCR Rodenas et al. 2019
nCU121	Rv primer for PHR1 expression with nCU120	TTCACTACCGCCAAG ACTGTTG	Reverse	qRT-PCR Rodenas et al. 2019
nCU122	Fw primer for PHT1;4 expression with nCU123	TCAATGGCGTTGCCT TCTGT	Forward	qRT-PCR Bari et al. 2006
nCU123	Rv primer for PHR1;4 expression with nCU122	ATCACCAAGCCACCC GAAA	Reverse	qRT-PCR Bari et al. 2006
nCU124	F73RBP1_Fw with nCU125	CTCTCCGTCACCTCC CCTTA	Forward	qPCR on gDNA
nCU125	F73RBP1_Rv with nCU0124	CGCTGGGGAGAGAC AATGTT	Reverse	qPCR on gDNA
nCU126	F73RBP1_Fw with nCU127	AGCTGCCTCTCAACA TCACC	Forward	qPCR on gDNA
nCU127	F73RBP1_Rv with nCU126	GGGGTTTAGACTGCT TCGCT	Reverse	qPCR on gDNA
nCU128 “Primer pair 4”	F73CuATPASE_Fw with nCU129	TCTCGTCGTCCTGGG TACAT	Forward	qPCR on gDNA
nCU129 “Primer pair 4”	F73CuATPASE_Rv with nCU128	ATAGTGCTGGGTCGG TTGTG	Reverse	qPCR on gDNA
nCU130	F73CuATPASE_Fw with nCU131	TTCTTCAGCGTCATG GCCAT	Forward	qPCR on gDNA
nCU131	F73CuATPASE_Rv with nCU130	TTGTCCCTTTGCACG GTTCT	Reverse	qPCR on gDNA

nCU132	AtMYB28_Fw with nCU133	TTTTTCATTATGCGTTTGCAG	Forward	Genotyping
nCU133	AtMYB28_Rv with nCU132	TGTATAAACCAGCTTTTTGGGG	Reverse	Genotyping
nCU134	LBb1 (SALK) with nCU133 & nCU132	GCGTGGACCGCTTGCTGCAACT	Forward	Genotyping
nCU135	AtMYB29_Fw with nCU136	TTGTAGATTGCGATGGGCTA	Reverse	Genotyping
nCU136	AtMYB29_Rv with nCU135	TATGTTTTGCATCATCTCGTCTTC	Forward	Genotyping
nCU137	8409 LB (GABI) with nCU135 & nCU136	ATATTGACCATCATACTCATTGC	Reverse	Genotyping

References

Albert I, Böhm H, Albert M, Feiler CE, Imkampe J, Wallmeroth N, Brancato C, Raaymakers TM, Oome S, Zhang H, Krol E, Grefen C, Gust AA, Chai J, Hedrich R, Van Den Ackerveken G & Nürnberger T (2015) An RLP23-SOBIR1-BAK1 complex mediates NLP-triggered immunity. *Nat. Plants* **1:** 1–9

Anthony MA, Celenza JL, Armstrong A & Frey SD (2020) Indolic glucosinolate pathway provides resistance to mycorrhizal fungal colonization in a non-host Brassicaceae. *Ecosphere* **11:**

Attard A, Gourgues M, Callemeyn-Torre N & Keller H (2010) The immediate activation of defense responses in Arabidopsis roots is not sufficient to prevent Phytophthora parasitica infection. *New Phytol.* **187:** 449–460

Baggs EL, Monroe JG, Thanki AS, O'Grady R, Schudoma C, Haerty W & Krasileva K V. (2020) Convergent loss of an EDS1/PAD4 signaling pathway in several plant lineages reveals coevolved components of plant immunity and drought response. *Plant Cell* **32:** 2158–2177

Balzergue C, Puech-Pags V, Bécard G & Rochange SF (2011) The regulation of arbuscular mycorrhizal symbiosis by phosphate in pea involves early and systemic signalling events. *J. Exp. Bot.* **62:** 1049–1060 Available at: https://academic.oup.com/jxb/article-lookup/doi/10.1093/jxb/erq335 [Accessed April 9, 2018]

Barragán-Rosillo AC, Peralta-Alvarez CA, Ojeda-Rivera JO, Arzate-Mejía RG, Recillas-Targa F & Herrera-Estrella L (2021) Genome accessibility dynamics in response to phosphate limitation is controlled by the PHR1 family of transcription factors in Arabidopsis. *Proc. Natl. Acad. Sci. U. S. A.* **118:**

Bennett AE & Groten K (2022) The Costs and Benefits of Plant-Arbuscular Mycorrhizal Fungal Interactions. *Annu. Rev. Plant Biol.* **73:** 649–672

Berens ML, Wolinska KW, Spaepen S, Ziegler J, Nobori T, Nair A, Krüler V, Winkelmüller TM, Wang Y, Mine A, Becker D, Garrido-Oter R, Schulze-Lefert P & Tsuda K (2019) Balancing trade-offs between biotic and abiotic stress responses through leaf age-dependent variation in stress hormone cross-talk. *Proc. Natl. Acad. Sci. U. S. A.* **116:** 2364–2373

Bhandari DD, Lapin D, Kracher B, von Born P, Bautor J, Niefind K & Parker JE (2019) An EDS1 heterodimer signalling surface enforces timely reprogramming of immunity genes

in Arabidopsis. *Nat. Commun.* **10:** 772 Available at: http://www.nature.com/articles/s41467-019-08783-0 [Accessed May 6, 2019]

Bolger AM, Lohse M & Usadel B (2014) Trimmomatic: A flexible trimmer for Illumina sequence data. *Bioinformatics* **30:** 2114–2120

Böttcher C, Westphal L, Schmotz C, Prade E, Scheel D & Glawischnig E (2009) The multifunctional enzyme CYP71b15 (Phytoalexin deficient3) converts cysteine-lndole-3-acetonitrile to camalexin in the lndole-3-acetonitrile metabolic network of arabidopsis thaliana. *Plant Cell* **21:** 1830–1845

Bozkurt TO & Kamoun S (2020) The plant–pathogen haustorial interface at a glance. *J. Cell Sci.* **133:** jcs237958 Available at: http://jcs.biologists.org/lookup/doi/10.1242/jcs.237958

Bravo A, York T, Pumplin N, Mueller LA & Harrison MJ (2016) Genes conserved for arbuscular mycorrhizal symbiosis identified through phylogenomics. *Nat. Plants* **2:** 15208 Available at: http://www.nature.com/articles/nplants2015208 [Accessed May 26, 2018]

Brundrett MC & Tedersoo L (2018) Evolutionary history of mycorrhizal symbioses and global host plant diversity. *New Phytol.* Available at: http://doi.wiley.com/10.1111/nph.14976

Bustos R, Castrillo G, Linhares F, Puga MI, Rubio V, Pérez-Pérez J, Solano R, Leyva A & Paz-Ares J (2010) A central regulatory system largely controls transcriptional activation and repression responses to phosphate starvation in arabidopsis. *PLoS Genet.* **6:**

Cao Y, Liang Y, Tanaka K, Nguyen CT, Jedrzejczak RP, Joachimiak A & Stacey G (2014) The kinase LYK5 is a major chitin receptor in Arabidopsis and forms a chitin-induced complex with related kinase CERK1. *Elife* **3:** 1–19

Castrillo G, Teixeira PJPL, Paredes SH, Law TF, de Lorenzo L, Feltcher ME, Finkel OM, Breakfield NW, Mieczkowski P, Jones CD, Paz-Ares J & Dangl JL (2017) Root microbiota drive direct integration of phosphate stress and immunity. *Nature* **543:** 513–518 Available at: https://doi.org/10.1038/nature21417

Clark RM, Schweikert G, Toomajian C, Ossowski S, Zeller G, Shinn P, Warthmann N, Hu TT, Fu G, Hinds DA, Chen H, Frazer KA, Huson DH, Scholkopf B, Nordborg M, Ratsch G, Ecker JR & Weigel D (2007) Common Sequence Polymorphisms Shaping Genetic Diversity in Arabidopsis thaliana. *Science (80-.).* **317:** 338–342 Available at: http://science.sciencemag.org/content/317/5836/338.abstract

Clay NK, Adio AM, Denoux C, Jander G & Ausubel FM (2009) Glucosinolate Metabolites Required for an Arabidopsis Innate Immune Response. *Science (80-.).* **323:** 95–101

Available at: https://www.science.org/doi/10.1126/science.1164627

Cui H, Tsuda K & Parker JE (2015) Effector-Triggered Immunity: From Pathogen Perception to Robust Defense. *Annu. Rev. Plant Biol.* **66:** 487–511 Available at: http://www.annualreviews.org/doi/10.1146/annurev-arplant-050213-040012 [Accessed October 16, 2018]

Das D, Paries M, Hobecker K, Gigl M, Dawid C, Lam H-M, Zhang J, Chen M & Gutjahr C (2022) PHOSPHATE STARVATION RESPONSE transcription factors enable arbuscular mycorrhiza symbiosis. *Nat. Commun.* **13:** 477 Available at: https://www.nature.com/articles/s41467-022-27976-8

Delaux P-M, Radhakrishnan G V., Jayaraman D, Cheema J, Malbreil M, Volkening JD, Sekimoto H, Nishiyama T, Melkonian M, Pokorny L, Rothfels CJ, Sederoff HW, Stevenson DW, Surek B, Zhang Y, Sussman MR, Dunand C, Morris RJ, Roux C, Wong GK-S, et al (2015) Algal ancestor of land plants was preadapted for symbiosis. *Proc. Natl. Acad. Sci.* **112:** 13390–13395 Available at: http://www.pnas.org/lookup/doi/10.1073/pnas.1515426112

Deslandes L & Rivas S (2012) Catch me if you can: bacterial effectors and plant targets. *Trends Plant Sci.* **17:** 644–655 Available at: https://www.sciencedirect.com/science/article/pii/S1360138512001495?via%3Dihub#fig0005 [Accessed May 9, 2019]

Durán P, Thiergart T, Garrido-Oter R, Agler M, Kemen E, Schulze-Lefert P & Hacquard S (2018) Microbial Interkingdom Interactions in Roots Promote Arabidopsis Survival. *Cell* **175:** 973–983.e14 Available at: http://www.ncbi.nlm.nih.gov/pubmed/30388454 [Accessed November 7, 2018]

Emonet A, Zhou F, Vacheron J, Heiman CM, Dénervaud Tendon V, Ma KW, Schulze-Lefert P, Keel C & Geldner N (2021) Spatially Restricted Immune Responses Are Required for Maintaining Root Meristematic Activity upon Detection of Bacteria. *Curr. Biol.* **31:** 1012–1028.e7

Feng F, Sun J, Radhakrishnan G V., Lee T, Bozsóki Z, Fort S, Gavrin A, Gysel K, Thygesen MB, Andersen KR, Radutoiu S, Stougaard J & Oldroyd GED (2019) A combination of chitooligosaccharide and lipochitooligosaccharide recognition promotes arbuscular mycorrhizal associations in Medicago truncatula. *Nat. Commun.* **10:** 5047 Available at: http://www.nature.com/articles/s41467-019-12999-5 [Accessed November 23, 2019]

Frerigmann H, Piotrowski M, Lemke R, Bednarek P & Schulze-Lefert P (2021) A network of phosphate starvation and immune-related signaling and metabolic pathways controls the

interaction between arabidopsis thaliana and the beneficial fungus colletotrichum tofieldiae. *Mol. Plant-Microbe Interact.* **34:** 560–570

Frerigmann H, Piślewska-Bednarek M, Sánchez-Vallet A, Molina A, Glawischnig E, Gigolashvili T & Bednarek P (2016) Regulation of Pathogen-Triggered Tryptophan Metabolism in Arabidopsis thaliana by MYB Transcription Factors and Indole Glucosinolate Conversion Products. *Mol. Plant* **9:** 682–695

Gan T, Luo T, Pang K, Zhou C, Zhou G, Wan B, Li G, Yi Q, Czaja AD & Xiao S (2021) Cryptic terrestrial fungus-like fossils of the early Ediacaran Period. *Nat. Commun.* **12:** Available at: http://dx.doi.org/10.1038/s41467-021-20975-1

Gao M, Zhang C, Angel W, Kwak O, Allison J, Wiratan L, Hallworth A, Wolf J & Lu H (2022) Circadian Regulation of the GLYCINE-RICH RNA-BINDING PROTEIN Gene by the Master Clock Protein CIRCADIAN CLOCK-ASSOCIATED 1 Is Important for Plant Innate Immunity . *J. Exp. Bot.***:** 1–13

Gao YQ, Bu LH, Han ML, Wang YL, Li ZY, Liu HT & Chao DY (2021) Long-distance blue light signalling regulates phosphate deficiency-induced primary root growth inhibition. *Mol. Plant* **14:** 1539–1553 Available at: https://doi.org/10.1016/j.molp.2021.06.002

Grigoriev I V., Nikitin R, Haridas S, Kuo A, Ohm R, Otillar R, Riley R, Salamov A, Zhao X, Korzeniewski F, Smirnova T, Nordberg H, Dubchak I & Shabalov I (2014) MycoCosm portal: Gearing up for 1000 fungal genomes. *Nucleic Acids Res.* **42:** 699–704

Gu Z, Eils R & Schlesner M (2016) Complex heatmaps reveal patterns and correlations in multidimensional genomic data. *Bioinformatics* **32:** 2847–2849

Guan R, Su J, Meng X, Li S, Liu Y, Xu J & Zhang S (2015) Multilayered regulation of ethylene induction plays a positive role in arabidopsis resistance against Pseudomonas syringae. *Plant Physiol.* **169:** 299–312

Harbort CJ, Hashimoto M, Inoue H, Niu Y, Guan R, Rombolà AD, Kopriva S, Voges MJEEE, Sattely ES, Garrido-Oter R & Schulze-Lefert P (2020) Root-Secreted Coumarins and the Microbiota Interact to Improve Iron Nutrition in Arabidopsis. *Cell Host Microbe* **28:** 825–837.e6 Available at: https://linkinghub.elsevier.com/retrieve/pii/S1931312820305072

Harun S, Abdullah-Zawawi MR, Goh HH & Mohamed-Hussein ZA (2020) A Comprehensive Gene Inventory for Glucosinolate Biosynthetic Pathway in Arabidopsis thaliana. *J. Agric. Food Chem.* **68:** 7281–7297

Hassani MA, Durán P & Hacquard S (2018) Microbial interactions within the plant holobiont. *Microbiome* **6:** 58 Available at:

https://microbiomejournal.biomedcentral.com/articles/10.1186/s40168-018-0445-0 [Accessed August 13, 2018]

Van Der Heijden MGA, Bruin S De, Luckerhoff L, Van Logtestijn RSP & Schlaeppi K (2016) A widespread plant-fungal-bacterial symbiosis promotes plant biodiversity, plant nutrition and seedling recruitment. *ISME J.* **10:** 389–399 Available at: http://dx.doi.org/10.1038/ismej.2015.120

Hindt MN, Akmakjian GZ, Pivarski KL, Punshon T, Baxter I, Salt DE & Guerinot M Lou (2017) BRUTUS and its paralogs, BTS LIKE1 and BTS LIKE2, encode important negative regulators of the iron deficiency response in Arabidopsis thaliana. *Metallomics* **9:** 876–890

Hiruma K, Fukunaga S, Bednarek P, Piślewska-Bednarek M, Watanabe S, Narusaka Y, Shirasu K & Takano Y (2013) Glutathione and tryptophan metabolism are required for Arabidopsis immunity during the hypersensitive response to hemibiotrophs. *Proc. Natl. Acad. Sci. U. S. A.* **110:** 9589–9594

Hiruma K, Gerlach N, Sacristán S, Nakano RT, Hacquard S, Kracher B, Neumann U, Ramírez D, Bucher M, O'Connell RJ & Schulze-Lefert P (2016) Root Endophyte Colletotrichum tofieldiae Confers Plant Fitness Benefits that Are Phosphate Status Dependent. *Cell* **165:** 464–474 Available at: http://www.ncbi.nlm.nih.gov/pubmed/26997485 [Accessed May 26, 2018]

Hu D, Zhang S, Baskin JM, Baskin CC, Wang Z, Liu R, Du J, Yang X & Huang Z (2019) Seed mucilage interacts with soil microbial community and physiochemical processes to affect seedling emergence on desert sand dunes. *Plant Cell Environ.* **42:** 591–605

Ivanov S, Austin J, Berg RH & Harrison MJ (2019) Extensive membrane systems at the host–arbuscular mycorrhizal fungus interface. *Nat. Plants* **5:** 194–203 Available at: http://www.nature.com/articles/s41477-019-0364-5

Jang G, Yoon Y & Choi Y Do (2020) Crosstalk with jasmonic acid integrates multiple responses in plant development. *Int. J. Mol. Sci.* **21:** 1–15

Kadota Y, Liebrand TWH, Goto Y, Sklenar J, Derbyshire P, Menke FLH, Torres MA, Molina A, Zipfel C, Coaker G & Shirasu K (2019) Quantitative phosphoproteomic analysis reveals common regulatory mechanisms between effector- and PAMP-triggered immunity in plants. *New Phytol.* **221:** 2160–2175 Available at: https://onlinelibrary.wiley.com/doi/abs/10.1111/nph.15523 [Accessed April 29, 2019]

Kaschuk G, Kuyper TW, Leffelaar PA, Hungria M & Giller KE (2009) Are the rates of photosynthesis stimulated by the carbon sink strength of rhizobial and arbuscular

mycorrhizal symbioses? *Soil Biol. Biochem.* **41:** 1233–1244 Available at: http://dx.doi.org/10.1016/j.soilbio.2009.03.005

Kiers ET, Duhamel M, Beesetty Y, Mensah JA, Franken O, Verbruggen E, Fellbaum CR, Kowalchuk GA, Hart MM, Bago A, Palmer TM, West SA, Vandenkoornhuyse P, Jansa J & Bücking H (2011) Reciprocal Rewards Stabilize Cooperation in the Mycorrhizal Symbiosis. *Science (80-.).* **333:** 880–882 Available at: https://doi.org/10.1126/science.1208473

Kim D, Paggi JM, Park C, Bennett C & Salzberg SL (2019) Graph-based genome alignment and genotyping with HISAT2 and HISAT-genotype. *Nat. Biotechnol.* **37:** 907–915 Available at: http://dx.doi.org/10.1038/s41587-019-0201-4

Klein M, Reichelt M, Gershenzon J & Papenbrock J (2006) The three desulfoglucosinolate sulfotransferase proteins in Arabidopsis have different substrate specificities and are differentially expressed. *FEBS J.* **273:** 122–136

Kliebenstein DJ, D'Auria JC, Behere AS, Kim JH, Gunderson KL, Breen JN, Lee G, Gershenzon J, Last RL & Jander G (2007) Characterization of seed-specific benzoyloxyglucosinolate mutations in Arabidopsis thaliana. *Plant J.* **51:** 1062–1076

Koh S, André A, Edwards H, Ehrhardt D & Somerville S (2005) Arabidopsis thaliana subcellular responses to compatible Erysiphe cichoracearum infections. *Plant J.* **44:** 516–529

Kremer JM, Sohrabi R, Paasch BC, Rhodes D, Thireault C, Schulze-Lefert P, Tiedje JM & He SY (2021) Peat-based gnotobiotic plant growth systems for Arabidopsis microbiome research. *Nat. Protoc.* **16:** 2450–2470 Available at: http://dx.doi.org/10.1038/s41596-021-00504-6

Krings M, Taylor TN, Hass H, Kerp H, Dotzler N & Hermsen EJ (2007) Fungal endophytes in a 400-million-yr-old land plant: infection pathways, spatial distribution, and host responses. *New Phytol.* **174:** 648–657 Available at: http://doi.wiley.com/10.1111/j.1469-8137.2007.02008.x

Kuchernig JC, Burow M & Wittstock U (2012) Evolution of specifier proteins in glucosinolate-containing plants. *BMC Evol. Biol.* **12:**

Lahrmann U, Ding Y, Banhara A, Rath M, Hajirezaei MR, Döhlemann S, von Wirén N, Parniske M & Zuccaro A (2013) Host-related metabolic cues affect colonization strategies of a root endophyte. *Proc. Natl. Acad. Sci.* **110:** 13965–13970 Available at: http://www.ncbi.nlm.nih.gov/pubmed/23918389 [Accessed October 16, 2018]

Lahrmann U, Strehmel N, Langen G, Frerigmann H, Leson L, Ding Y, Scheel D, Herklotz S,

Hilbert M & Zuccaro A (2015) Mutualistic root endophytism is not associated with the reduction of saprotrophic traits and requires a noncompromised plant innate immunity. *New Phytol.* **207:** 841–857 Available at: http://doi.wiley.com/10.1111/nph.13411 [Accessed October 16, 2018]

Leek JT, Johnson WE, Parker HS, Jaffe AE & Storey JD (2012) The SVA package for removing batch effects and other unwanted variation in high-throughput experiments. *Bioinformatics* **28:** 882–883

Li C, Zhang Q, Xia Y & Jin K (2021) MaNmra, a negative transcription regulator in nitrogen catabolite repression pathway, contributes to nutrient utilization, stress resistance, and virulence in entomopathogenic fungus metarhizium acridum. *Biology (Basel).* **10:** 1167 Available at: https://www.mdpi.com/2079-7737/10/11/1167

Liang Y, Cao Y, Tanaka K, Thibivilliers S, Wan J, Choi J, Kang C ho, Qiu J & Stacey G (2013) Nonlegumes respond to rhizobial nod factors by suppressing the innate immune response. *Science (80-.).* **341:** 1384–1387 Available at: http://www.ncbi.nlm.nih.gov/pubmed/24009356 [Accessed February 27, 2019]

Liao Y, Smyth GK & Shi W (2014) FeatureCounts: An efficient general purpose program for assigning sequence reads to genomic features. *Bioinformatics* **30:** 923–930

Lipka V, Dittgen J, Bednarek P, Bhat R, Wiermer M, Stein M, Landtag J, Brandt W, Rosahl S, Scheel D, Llorente F, Molina A, Parker J, Somerville S & Schulze-Lefert P (2005) Pre- and postinvasion defenses both contribute to nonhost resistance in Arabidopsis. *Science* **310:** 1180–3 Available at: http://www.ncbi.nlm.nih.gov/pubmed/16293760 [Accessed February 13, 2019]

Liu L, Sonbol FM, Huot B, Gu Y, Withers J, Mwimba M, Yao J, He SY & Dong X (2016) Salicylic acid receptors activate jasmonic acid signalling through a non-canonical pathway to promote effector-triggered immunity. *Nat. Commun.* **7:** 1–10 Available at: http://dx.doi.org/10.1038/ncomms13099

Liu T, Liu Z, Song C, Hu Y, Han Z, She J, Fan G, Wang J, Jin C, Chang J, Zhou JM & Chai J (2012) Chitin-induced dimerization activates a plant immune receptor. *Science (80-.).* **336:** 1160–1164

Love MI, Huber W & Anders S (2014) Moderated estimation of fold change and dispersion for RNA-seq data with DESeq2. *Genome Biol.* **15:** 1–21

Lu Y & Tsuda K (2021) Intimate Association of PRR- and NLR-Mediated Signaling in Plant Immunity. *Mol. Plant. Microbe. Interact.* **34:** 3–14

Luginbuehl LH, Menard GN, Kurup S, Van Erp H, Radhakrishnan G V., Breakspear A,

Oldroyd GED & Eastmond P (2017) Fatty acids in arbuscular mycorrhizal fungi are synthesized by the host plant. *Science (80-.).* **356:** 1175–1176

Luginbuehl LH & Oldroyd GED (2017) Understanding the Arbuscule at the Heart of Endomycorrhizal Symbioses in Plants. *Curr. Biol.* **27:** R952–R963 Available at: http://dx.doi.org/10.1016/j.cub.2017.06.042

Lynch JP (2011) Root phenes for enhanced soil exploration and phosphorus acquisition: Tools for future crops. *Plant Physiol.* **156:** 1041–1049

Ma L, Shi Y, Siemianowski O, Yuan B, Egner TK, Mirnezami SV, Lind KR, Ganapathysubramanian B, Venditti V & Cademartiri L (2019) Hydrogel-based transparent soils for root phenotyping in vivo. *Proc. Natl. Acad. Sci. U. S. A.* **166:** 11063–11068

Ma Z, Guo D, Xu X, Lu M, Bardgett RD, Eissenstat DM, McCormack ML & Hedin LO (2018) Evolutionary history resolves global organization of root functional traits. *Nature* **555:** 94–97 Available at: http://www.nature.com/doifinder/10.1038/nature25783 [Accessed January 31, 2019]

Maciá-Vicente JG, Bai B, Qi R, Ploch S, Breider F & Thines M (2022) Nutrient Availability Does Not Affect Community Assembly in Root-Associated Fungi but Determines Fungal Effects on Plant Growth. *mSystems* **7:**

Meier K, Ehbrecht MD & Wittstock U (2019) Glucosinolate Content in Dormant and Germinating Arabidopsis thaliana Seeds Is Affected by Non-Functional Alleles of Classical Myrosinase and Nitrile-Specifier Protein Genes. *Front. Plant Sci.* **10:** 1–14

Menand B, Yi K, Jouannic S, Hoffmann L, Ryan E, Linstead P, Schaefer DG & Dolan L (2007) An Ancient Mechanism Controls the Development of Cells with a Rooting Function in Land Plants. *Science (80-.).* **316:** 1477–1480 Available at: http://www.ncbi.nlm.nih.gov/pubmed/17556585 [Accessed December 8, 2017]

Meschke H & Schrempf H (2010) Streptomyces lividans inhibits the proliferation of the fungus Verticillium dahliae on seeds and roots of Arabidopsis thaliana. *Microb. Biotechnol.* **3:** 428–443

Mesny F, Miyauchi S, Thiergart T, Pickel B, Atanasova L, Karlsson M, Hüttel B, Barry KW, Haridas S, Chen C, Bauer D, Andreopoulos W, Pangilinan J, LaButti K, Riley R, Lipzen A, Clum A, Drula E, Henrissat B, Kohler A, et al (2021) Genetic determinants of endophytism in the Arabidopsis root mycobiome. *Nat. Commun.* **12:** 1–15

Millet YA, Danna CH, Clay NK, Songnuan W, Simon MD, Werck-Reichhart D & Ausubel FM (2010) Innate Immune Responses Activated in Arabidopsis Roots by Microbe-

Associated Molecular Patterns. *Plant Cell* **22:** 973–990 Available at: https://academic.oup.com/plcell/article/22/3/973/6096733

Mithen R, Bennett R & Marquez J (2010) Glucosinolate biochemical diversity and innovation in the Brassicales. *Phytochemistry* **71:** 2074–2086 Available at: http://dx.doi.org/10.1016/j.phytochem.2010.09.017

Miya A, Albert P, Shinya T, Desaki Y, Ichimura K, Shirasu K, Narusaka Y, Kawakami N, Kaku H & Shibuya N (2007) CERK1, a LysM receptor kinase, is essential for chitin elicitor signaling in Arabidopsis. *Proc. Natl. Acad. Sci.* **104:** 19613–19618 Available at: http://www.ncbi.nlm.nih.gov/pubmed/18042724 [Accessed January 22, 2019]

Newman A, Picot E, Davies S, Hilton S, Carré IA & Bending GD (2022) Circadian rhythms in the plant host influence rhythmicity of rhizosphere microbiota. *BMC Biol.* **20:** 1–15 Available at: https://doi.org/10.1186/s12915-022-01430-z

Ngou BPM, Ahn HK, Ding P & Jones JDG (2021) Mutual potentiation of plant immunity by cell-surface and intracellular receptors. *Nature* **592:** 110–115

Nishiyama T, Sakayama H, de Vries J, Buschmann H, Saint-Marcoux D, Ullrich KK, Haas FB, Vanderstraeten L, Becker D, Lang D, Vosolsobě S, Rombauts S, Wilhelmsson PKI, Janitza P, Kern R, Heyl A, Rümpler F, Villalobos LIAC, Clay JM, Skokan R, et al (2018) The Chara Genome: Secondary Complexity and Implications for Plant Terrestrialization. *Cell* **174:** 448–464.e24 Available at: https://linkinghub.elsevier.com/retrieve/pii/S0092867418308018

Nongbri PL, Johnson JM, Sherameti I, Glawischnig E, Halkier BA & Oelmüller R (2012) Indole-3-Acetaldoxime-Derived Compounds Restrict Root Colonization in the Beneficial Interaction Between Arabidopsis Roots and the Endophyte Piriformospora indica. *Mol. Plant-Microbe Interact.* **25:** 1186–1197 Available at: http://apsjournals.apsnet.org/doi/10.1094/MPMI-03-12-0071-R [Accessed February 7, 2019]

O'Connell RJ & Panstruga R (2006) Tête à tête inside a plant cell: Establishing compatibility between plants and biotrophic fungi and oomycetes. *New Phytol.* **171:** 699–718

Oba H, Tawaray K & Wagatsuma T (2001) Arbuscular mycorrhizal colonization in Lupinus and related genera. *Soil Sci. Plant Nutr.* **47:** 685–694 Available at: http://www.tandfonline.com/doi/abs/10.1080/00380768.2001.10408433 [Accessed May 26, 2018]

Pant B-D, Pant P, Erban A, Huhman D, Kopka J & Scheible W-R (2015) Identification of primary and secondary metabolites with phosphorus status-dependent abundance in

Arabidopsis, and of the transcription factor PHR1 as a major regulator of metabolic changes during phosphorus limitation. *Plant. Cell Environ.* **38:** 172–87 Available at: https://onlinelibrary.wiley.com/doi/10.1111/pce.12378

Parniske M (2008) Arbuscular mycorrhiza: the mother of plant root endosymbioses. *Nat Rev Micro* **6:** 763–775 Available at: https://www.nature.com/nrmicro/journal/v6/n10/full/nrmicro1987.html [Accessed May 22, 2017]

Peng J, Aluthmuhandiram JVS, Chethana KWT, Zhang Q, Xing Q, Wang H, Liu M, Zhang W, Li X & Yan J (2022) An NmrA-Like Protein, Lws1, Is Important for Pathogenesis in the Woody Plant Pathogen Lasiodiplodia theobromae. *Plants* **11:** 2197 Available at: https://www.mdpi.com/2223-7747/11/17/2197

Lo Presti L, Lanver D, Schweizer G, Tanaka S, Liang L, Tollot M, Zuccaro A, Reissmann S & Kahmann R (2015) Fungal Effectors and Plant Susceptibility. *Annu. Rev. Plant Biol.* **66:** 513–545 Available at: http://www.annualreviews.org/doi/10.1146/annurev-arplant-043014-114623

Proust H, Honkanen S, Jones VAS, Morieri G, Prescott H, Kelly S, Ishizaki K, Kohchi T & Dolan L (2016) RSL Class i Genes Controlled the Development of Epidermal Structures in the Common Ancestor of Land Plants. *Curr. Biol.* **26:** 93–99 Available at: http://linkinghub.elsevier.com/retrieve/pii/S0960982215014360 [Accessed December 8, 2017]

Pruitt RN, Locci F, Wanke F, Zhang L, Saile SC, Joe A, Karelina D, Hua C, Fröhlich K, Wan WL, Hu M, Rao S, Stolze SC, Harzen A, Gust AA, Harter K, Joosten MHAJ, Thomma BPHJ, Zhou JM, Dangl JL, et al (2021) The EDS1–PAD4–ADR1 node mediates Arabidopsis pattern-triggered immunity. *Nature* **598:** 495–499

Qin L, Zhou Z, Li Q, Zhai C, Liu L, Quilichini TD, Gao P, Kessler SA, Jaillais Y, Datla R, Peng G, Xiang D & Wei Y (2020) Specific recruitment of phosphoinositide species to the plant-pathogen interfacial membrane underlies Arabidopsis susceptibility to fungal infection. *Plant Cell* **32:** 1665–1688

Rajniak J, Barco B, Clay NK & Sattely ES (2015) A new cyanogenic metabolite in Arabidopsis required for inducible pathogen defence. *Nature* **525:** 376–379

Redecker D (2000) Glomalean Fungi from the Ordovician. *Science (80-.).* **289:** 1920–1921 Available at: https://www.sciencemag.org/lookup/doi/10.1126/science.289.5486.1920

Redkar A, Gimenez Ibanez S, Sabale M, Zechmann B, Solano R & Di Pietro A (2022a) Marchantia polymorpha model reveals conserved infection mechanisms in the vascular

wilt fungal pathogen Fusarium oxysporum. *New Phytol.* **234:** 227–241

Redkar A, Sabale M, Schudoma C, Zechmann B, Gupta YK, López-Berges MS, Venturini G, Gimenez-Ibanez S, Turrà D, Solano R & Di Pietro A (2022b) Conserved secreted effectors contribute to endophytic growth and multihost plant compatibility in a vascular wilt fungus. *Plant Cell* **34:** 3214–3232

Rellán-Álvarez R, Lobet G & Dinneny JR (2016) Environmental Control of Root System Biology. *Annu. Rev. Plant Biol.* **67:** 619–642

Remy W, Taylor TN, Hass H & Kerp H (1994) Four hundred-million-year-old vesicular arbuscular mycorrhizae. *Proc Natl Acad Sci U S A* **91:** 11841–11843 Available at: http://www.ncbi.nlm.nih.gov/pmc/articles/PMC45331/ [Accessed March 12, 2017]

Retallack GJ (1992) Chapter 21 - Paleozoic paleosols. In *Weathering, Soils & Paleosols*, Martini IP & Chesworth WBT-D in ESP (eds) pp 543–564. Elsevier Available at: https://www.sciencedirect.com/science/article/pii/B978044489198350026X

Rich MK, Vigneron N, Liboure C, Keller J, Xue L, Hajheidari M, Radhakrishnan G V., Le Ru A, Diop SI, Potente G, Conti E, Duijsings D, Batut A, Le Faouder P, Kodama K, Kyozuka J, Sallet E, Bécard G, Rodriguez-Franco M, Ott T, et al (2021) Lipid exchanges drove the evolution of mutualism during plant terrestrialization. *Science (80-.).* **372:** 864–868

Rico-Reséndiz F, Cervantes-Pérez SA, Espinal-Centeno A, Dipp-Álvarez M, Oropeza-Aburto A, Hurtado-Bautista E, Cruz-Hernández A, Bowman JL, Ishizaki K, Arteaga-Vázquez MA, Herrera-Estrella L & Cruz-Ramírez A (2020) Transcriptional and morpho-physiological responses of Marchantia polymorpha upon phosphate starvation. *Int. J. Mol. Sci.* **21:** 1–25

Rohart F, Gautier B, Singh A & Lê Cao KA (2017) mixOmics: An R package for 'omics feature selection and multiple data integration. *PLoS Comput. Biol.* **13:** 1–19

Ross A, Yamada K, Hiruma K, Yamashita-Yamada M, Lu X, Takano Y, Tsuda K & Saijo Y (2014) The Arabidopsis PEPR pathway couples local and systemic plant immunity. *EMBO J.* **33:** 62–75

Rouached H, Arpat AB & Poirier Y (2010) Regulation of phosphate starvation responses in plants: Signaling players and cross-talks. *Mol. Plant* **3:** 288–299 Available at: http://dx.doi.org/10.1093/mp/ssp120

Roux M, Schwessinger B, Albrecht C, Chinchilla D, Jones A, Holton N, Malinovsky FG, Tör M, de Vries S & Zipfel C (2011) The Arabidopsis leucine-rich repeat receptor-like kinases BAK1/SERK3 and BKK1/SERK4 are required for innate immunity to

hemibiotrophic and biotrophic pathogens. *Plant Cell* **23:** 2440–2455

Rubio V, Linhares F, Solano R, Martín AC, Iglesias J, Leyva A & Paz-Ares J (2001) A conserved MYB transcription factor involved in phosphate starvation signaling both in vascular plants and in unicellular algae. *Genes Dev.* **15:** 2122–2133

Rush TA, Puech-Pagès V, Bascaules A, Jargeat P, Maillet F, Haouy A, Maës AQM, Carriel CC, Khokhani D, Keller-Pearson M, Tannous J, Cope KR, Garcia K, Maeda J, Johnson C, Kleven B, Choudhury QJ, Labbé J, Swift C, O'Malley MA, et al (2020) Lipo-chitooligosaccharides as regulatory signals of fungal growth and development. *Nat. Commun.* **11:** Available at: http://dx.doi.org/10.1038/s41467-020-17615-5

Schwessinger B, Roux M, Kadota Y, Ntoukakis V, Sklenar J, Jones A & Zipfel C (2011) Phosphorylation-dependent differential regulation of plant growth, cell death, and innate immunity by the regulatory receptor-like kinase BAK1. *PLoS Genet.* **7:** e1002046 Available at: http://dx.plos.org/10.1371/journal.pgen.1002046 [Accessed January 21, 2019]

Singh A, Sharma A, Singh N & Nandi AK (2022) MTO1-RESPONDING DOWN 1 (MRD1) is a transcriptional target of OZF1 for promoting salicylic acid-mediated defense in Arabidopsis. *Plant Cell Rep.* **41:** 1319–1328 Available at: https://doi.org/10.1007/s00299-022-02861-2

Somssich M, Khan GA & Persson S (2016) Cell Wall Heterogeneity in Root Development of Arabidopsis. *Front. Plant Sci.* **7:** 1242 Available at: http://journal.frontiersin.org/Article/10.3389/fpls.2016.01242/abstract [Accessed November 24, 2017]

Sønderby IE, Burow M, Rowe HC, Kliebenstein DJ & Halkier BA (2010) A complex interplay of three R2R3 MYB transcription factors determines the profile of aliphatic glucosinolates in Arabidopsis. *Plant Physiol.* **153:** 348–363

Sun J, Miller JB, Granqvist E, Wiley-Kalil A, Gobbato E, Maillet F, Cottaz S, Samain E, Venkateshwaran M, Fort S, Morris RJ, Ané JM, Dénarié J & Oldroyd GED (2015) Activation of symbiosis signaling by arbuscular mycorrhizal fungi in legumes and rice. *Plant Cell* **27:** 823–838

Tisserant E, Malbreil M, Kuo A, Kohler A, Symeonidi A, Balestrini R, Charron P, Duensing N, dit Frey N, Gianinazzi-Pearson V, Gilbert LB, Handa Y, Herr JR, Hijri M, Koul R, Kawaguchi M, Krajinski F, Lammers PJ, Masclaux FG, Murat C, et al (2013) Genome of an arbuscular mycorrhizal fungus provides insight into the oldest plant symbiosis. *Proc Natl Acad Sci U S A* **110:** 20117–20122 Available at:

http://www.ncbi.nlm.nih.gov/pmc/articles/PMC3864322/ [Accessed March 12, 2017]

Touw AJ, Verdecia Mogena A, Maedicke A, Sontowski R, van Dam NM & Tsunoda T (2020) Both Biosynthesis and Transport Are Involved in Glucosinolate Accumulation During Root-Herbivory in Brassica rapa. *Front. Plant Sci.* **10:** 1–13

Tsuda K, Sato M, Stoddard T, Glazebrook J & Katagiri F (2009) Network properties of robust immunity in plants. *PLoS Genet.* **5:** e1000772 Available at: https://dx.plos.org/10.1371/journal.pgen.1000772 [Accessed February 25, 2019]

Tsuji J, Jackson EP, Gage DA, Hammerschmidt R & Somerville SC (1992) Phytoalexin accumulation in arabidopsis thaliana during the hypersensitive reaction to Pseudomonas syringae pv syringae. *Plant Physiol.* **98:** 1304–1309

Val-Torregrosa B, Bundó M, Chiou T-J, Flors V & Segundo BS (2021) NITROGEN LIMITATION ADAPTATION functions as a negative regulator of Arabidopsis immunity. Available at: https://doi.org/10.1101/2021.12.09.471910

Wang B, Li K, Wu G, Xu Z, Hou R, Guo B, Zhao Y & Liu F (2022) Sulforaphane, a secondary metabolite in crucifers, inhibits the oxidative stress adaptation and virulence of Xanthomonas by directly targeting OxyR. *Mol. Plant Pathol.* **23:** 1508–1523

Wang W, Yang J, Zhang J, Liu YX, Tian C, Qu B, Gao C, Xin P, Cheng S, Zhang W, Miao P, Li L, Zhang X, Chu J, Zuo J, Li J, Bai Y, Lei X & Zhou JM (2020) An Arabidopsis Secondary Metabolite Directly Targets Expression of the Bacterial Type III Secretion System to Inhibit Bacterial Virulence. *Cell Host Microbe* **27:** 601–613.e7 Available at: https://doi.org/10.1016/j.chom.2020.03.004

Wilson MH, Holman TJ, Sørensen I, Cancho-Sanchez E, Wells DM, Swarup R, Knox JP, Willats WGT, Ubeda-Tomás S, Holdsworth M, Bennett MJ, Vissenberg K & Hodgman TC (2015) Multi-omics analysis identifies genes mediating the extension of cell walls in the Arabidopsis thaliana root elongation zone. *Front. Cell Dev. Biol.* **3:** 1–12

Wittstock U & Burow M (2010) Glucosinolate Breakdown in Arabidopsis: Mechanism, Regulation and Biological Significance. *Arab. B.* **8:** e0134

Wittstock U & Gershenzon J (2002) Constitutive plant toxins and their role in defense against herbivores and pathogens. *Curr. Opin. Plant Biol.* **5:** 300–307

Wolinska KW, Vannier N, Thiergart T, Pickel B, Gremmen S, Piasecka A, Piślewska-Bednarek M, Nakano RT, Belkhadir Y, Bednarek P & Hacquard S (2021) Tryptophan metabolism and bacterial commensals prevent fungal dysbiosis in Arabidopsis roots. *Proc. Natl. Acad. Sci. U. S. A.* **118:**

Yamada K, Yamashita-Yamada M, Hirase T, Fujiwara T, Tsuda K, Hiruma K & Saijo Y

(2016) Danger peptide receptor signaling in plants ensures basal immunity upon pathogen-induced depletion of BAK 1 . *EMBO J.* **35:** 46–61

Yamaguchi Y, Huffaker A, Bryan AC, Tax FE & Ryan CA (2010) PEPR2 is a second receptor for the Pep1 and Pep2 peptides and contributes to defense responses in Arabidopsis. *Plant Cell* **22:** 508–22 Available at: http://www.ncbi.nlm.nih.gov/pubmed/20179141 [Accessed February 19, 2019]

Yu P, He X, Baer M, Beirinckx S, Tian T, Moya YAT, Zhang X, Deichmann M, Frey FP, Bresgen V, Li C, Razavi BS, Schaaf G, von Wirén N, Su Z, Bucher M, Tsuda K, Goormachtig S, Chen X & Hochholdinger F (2021) Plant flavones enrich rhizosphere Oxalobacteraceae to improve maize performance under nitrogen deprivation. *Nat. Plants* **7:** 481–499 Available at: http://dx.doi.org/10.1038/s41477-021-00897-y

Zhang B, Wang M, Sun Y, Zhao P, Liu C, Qing K, Hu X, Zhong Z, Cheng J, Wang H, Peng Y, Shi J, Zhuang L, Du S, He M, Wu H, Liu M, Chen S, Wang H, Chen X, et al (2021) Glycine max NNL1 restricts symbiotic compatibility with widely distributed bradyrhizobia via root hair infection. *Nat. Plants* **7:** 73–86

Zhang Y & Li X (2019) Salicylic acid: biosynthesis, perception, and contributions to plant immunity. *Curr. Opin. Plant Biol.* **50:** 29–36 Available at: https://doi.org/10.1016/j.pbi.2019.02.004

Zhao Y, Hull AK, Gupta NR, Goss KA, Alonso J, Ecker JR, Normanly J, Chory J & Celenza JL (2002) Trp-dependent auxin biosynthesis in Arabidopsis: Involvement of cytochrome P450s CYP79B2 and CYP79B3. *Genes Dev.* **16:** 3100–3112

Zhou F, Emonet A, Dénervaud Tendon V, Marhavy P, Wu D, Lahaye T & Geldner N (2020) Co-incidence of Damage and Microbial Patterns Controls Localized Immune Responses in Roots. *Cell* **180:** 440–453.e18 Available at: https://linkinghub.elsevier.com/retrieve/pii/S009286742030060X

Zhou Y, Zhou B, Pache L, Chang M, Khodabakhshi AH, Tanaseichuk O, Benner C & Chanda SK (2019a) Metascape provides a biologist-oriented resource for the analysis of systems-level datasets. *Nat. Commun.* **10:** Available at: http://dx.doi.org/10.1038/s41467-019-09234-6

Zhou Z, Zhao Y, Bi G, Liang X & Zhou JM (2019b) Early signalling mechanisms underlying receptor kinase-mediated immunity in plants. *Philos. Trans. R. Soc. B Biol. Sci.* **374:**

Zhu A, Ibrahim JG & Love MI (2019) Heavy-Tailed prior distributions for sequence count data: Removing the noise and preserving large differences. *Bioinformatics* **35:** 2084–2092

Zipfel C & Oldroyd GED (2017) Plant signalling in symbiosis and immunity. *Nature* **543:** 328–336 Available at: http://www.nature.com/articles/nature22009 [Accessed February 27, 2019]

Zönnchen J, Gantner J, Lapin D, Barthel K, Eschen-Lippold L, Erickson JL, Landeo Villanueva S, Zantop S, Kretschmer C, Joosten MHAJ, Parker JE, Guerois R & Stuttmann J (2022) EDS1 complexes are not required for PRR responses and execute TNL-ETI from the nucleus in Nicotiana benthamiana . *New Phytol.***:** 2249–2264

Erklärung

Ich versichere, dass ich die von mir vorgelegte Dissertation selbständig angefertigt, die benutzten Quellen und Hilfsmittel vollständig angegeben und die Stellen der Arbeit – einschließlich Tabellen, Karten und Abbildungen –, die anderen Werken im Wortlaut oder dem Sinn nach entnommen sind, in jedem Einzelfall als Entlehnung kenntlich gemacht habe; dass diese Dissertation noch keiner anderen Fakultät oder Universität zur Prüfung vorgelegen hat; dass sie noch nicht veröffentlicht worden ist, sowie, dass ich eine solche Veröffentlichung vor Abschluss des Promotionsverfahrens nicht vornehmen werde. Die Bestimmungen der Promotionsordnung sind mir bekannt. Die von mir vorgelegte Dissertation ist von Prof. Dr. Jane Parker betreut worden.

Köln, 17. Dezember 2022

Charles Uhlmann

Erklärung

Ich versichere, dass ich die von mir vorgelegte Dissertation selbständig angefertigt, die benutzten Quellen und Hilfsmittel vollständig angegeben und die Stellen der Arbeit – einschließlich Tabellen, Karten und Abbildungen –, die anderen Werken im Wortlaut oder dem Sinn nach entnommen sind, in jedem Einzelfall als Entlehnung kenntlich gemacht habe; dass diese Dissertation noch keiner anderen Fakultät oder Universität zur Prüfung vorgelegen hat; dass sie noch nicht veröffentlicht worden ist, sowie, dass ich eine solche Veröffentlichung vor Abschluss des Promotionsverfahrens nicht vornehmen werde. Die Bestimmungen der Promotionsordnung sind mir bekannt. Die von mir vorgelegte Dissertation ist von Prof. Dr. Jane Parker betreut worden.

Köln, 17. Dezember 2022

Charles Uhlmann